Department of Mechanical Engineering
University of Canterbury
Te Whare Wānganga o Waitaha
Private Bag 4800
Christchurch 8020, New Zealand

Telephone: +64-3-366 7001
Facsimile: +64-3-364 2078
Website: www.mech.canterbury.ac.nz

UNIVERSITY OF CANTERBURY
Te Whare Wānanga o Waitaha
CHRISTCHURCH NEW ZEALAND

Modelling Jetpack Impact following Emergency Descent

ENME690 Masters Thesis

Student: Duncan Shand
73837346

Supervisors: Academic: A/Prof. Mark Jermy
Co-Supervisor: Kelvin Barnsdale (SERC)

Enrolment Date: 1 Feb 2016

Acknowledgements

Thank you to the following people who offered assistance and advice throughout the project:

Thanks to my supervisors, A/Prof. Mark Jermy and Kelvin Barnsdale, who came to every meeting with an open mind, ready to give advice on the direction of the project and help with road blocks. I thank you both immensely for your support, your feedback and keeping this project on track.

Thanks to Mike Prystie, Thomas Chae, Teresa Schuster and the team at MACL who offered continuing support and assistance. Thank you to MACL for financing this project. It has been a pleasure working with the MACL team.

Thanks to Dr Paul Docherty, Dr Geoffrey Rodgers and Dr Stefanie Gutschmidt for sharing their expertise on statics and dynamics. Their knowledge in these fields greatly helped me to understand possible ways of applying engineering techniques.

Thanks to Henry Dumbleton of Flight Structures, Ltd. for sharing his knowledge and wisdom in detail by explaining aspects of certification and failure rates. This gave me a starting point in a new aspect of aviation. Your help has been greatly appreciated.

Thanks to my parents, Lynne and John, for offering ever present support and checking whether the rest of my life was in some sort of order while I was writing this thesis. I will be ever grateful for your love and kindness.

"Prove your words by your deeds" – Seneca the Younger

"There is the most important thing, and then there is everything else" – Author Unknown

"Ask better questions, […] get better answers" – Tony Robbins

Table of Contents

Disclaimer

The models presented in this report are based on specific and limited inputs. They are ideal models based on assumptions outlined in each respective model section of this thesis. There are many scenarios which are not captured, such as environmental conditions and the terrain of the landing site. The behaviour of the craft in the model will differ to reality because of these reasons.

The description of standards in this thesis are meant for reference only. This document does not give sufficient information for these descriptions to be used in place of standards. When designing a system and conducting safety analyses, the original documents and standards should be used.

Abbreviations and Definitions

FHA – Fault Hazard Analysis. A method of capturing all of the intended functions at an aircraft and system level, and identifying how each of the functions could fail on a conceptual level.

Basic Event – An event such as the failure of a component which can have a failure rate determined and attached to it.

FTA – Fault Tree Analysis. A top down analysis that begins at a top level hazard and asks "what could cause this?" This question is repeated for each cause of failure until a Basic Event is identified. The FTA can be applied as part of the PSSA (Preliminary System Safety Assessment) to determine which failures or combinations of failures can exist (if any) at the lower levels which might cause each failure condition. All of the bottom level events should be Basic Events, the failure rates of which are determined through FMEAs (Failure Mode and Effects Analyses) and FMESs (Failure Mode and Effects Summaries).

Abstract

A single engine twin fan jetpack system (Craft) is modelled to explore its behaviour during emergency descent. This is done using numerical modelling simulations.

Aviation law in relation to the craft is described. There are no specific standards for the civil certification of jetpacks (therefore no jetpacks have been certified under civil law, except as an experimental aircraft). Ways through which a jetpack or other new categories of aircraft may be certified are described.

The behaviour of the craft and parachute are simulated during an emergency descent. The impact velocities for different scenarios are explored and compared to known impact velocity limits. A rudimentary model for the impact of the craft is developed which determines the acceleration on the craft. The pilot is assumed to be rigidly attached to the craft and the peak accelerations that the craft experiences are also compared to known limits.

An automatic deployment system for the parachute is developed. This includes FTAs and failure rates of the selected components within the system.

Background and Literature Review

The Martin Jetpack

The Martin Jetpack "has been designed to be the world's most practical and safest OPHAV: Optionally Piloted Hovering Air Vehicle" [1]. Two versions of the aircraft currently have experimental certification under the NZ Civil Aviation Authority (NZCAA) law, though full type certification is desired [2]. It has potential to be used for search and rescue, military, recreational and commercial applications. It is unique because it has a fly-by-wire flight control system, so is "relatively easy to operate" [3] and has a much longer endurance than other jetpack-like craft. Figure 1 shows the jetpack in flight.

Figure 1: The Martin Jetpack in Flight. Image adapted from [4]

Legalities of Flying

Aircraft certification is a worldwide practice, with certification agencies located in the United Kingdom (UKCAA), New Zealand (NZCAA), Europe (EASA) and USA (Federal Aviation Administration, FAA) to name a few. Each of the certification agencies manages the flight operations in their respective domain and has their own laws governing how aircraft should be registered, certified and flown. However, they frequently accept one another's standards. For example, New Zealand has a Bilateral Aviation Safety Agreement (BASA) with the FAA [5].

An aeroplane may only be flown by an airline if it has had a "type certificate" issued by the aviation authorities of the airline country [6]. In order to do this, the aeroplane must meet the country's aviation rules to show that it is sufficiently safe to fly. Figure 2 shows the Certification Process in New Zealand.

All aircraft operating in NZ are required to have met, and continue to meet, certain standards. These standards are one aspect of aircraft law in New Zealand, which is broken down into sections regarding specific aspects of aviation – the NZ Civil Aviation Rules, or NZCARs. For example, pilot licenses (NZCAR Part 61), flying and certification of drones (NZCAR Part 102), and manufacturing of aircraft parts (NZCAR Part 148). Most parts have a corresponding Advisory Circular (AC). The ACs explain how one can comply with the CAR, puts the CAR into simpler terms to make understanding easier, and gives actions to follow. An AC and quantifies and discusses "terms such as "failure condition" and "extremely improbable"" [6].

When certifying an aircraft, the requirements which have to be complied with depend on the aircraft to be certified and the proposed operations of that aircraft. Other agencies can be "delegated" the task of approving aircraft if that agency is deemed appropriate for doing so. Once compliance is met, a type certificate is granted.

Aircraft can be demonstrated to have met these standards using a combination of analytical and physical testing methods, though flight testing is the "ultimate and indispensable way" of validating a flight control system [6].

Certifying an Aircraft in NZ

A Type Certificate (TC) is CAA approval that a product design meets airworthiness requirements as per the certification basis [7]. A TC can be issued if it meets NZCARs (NZ Civil Aviation Requirements) 21.31 to 21.43 are met and an approved Part 146/148 organization are involved. Figure 2 describes a summary of the type certification process in NZ [7].

The certification of common categories of aircraft such as aeroplanes and helicopters is straightforward compared to the certification of a jetpack, because specific regulations have been made for them. There have been no laws specifically made for the regulation of a jetpack. This means that the certification may include "a lot of Exemptions and Special Conditions – basically a highly customised set of certification requirements which will be agreed between the applicant and CAANZ." [7]

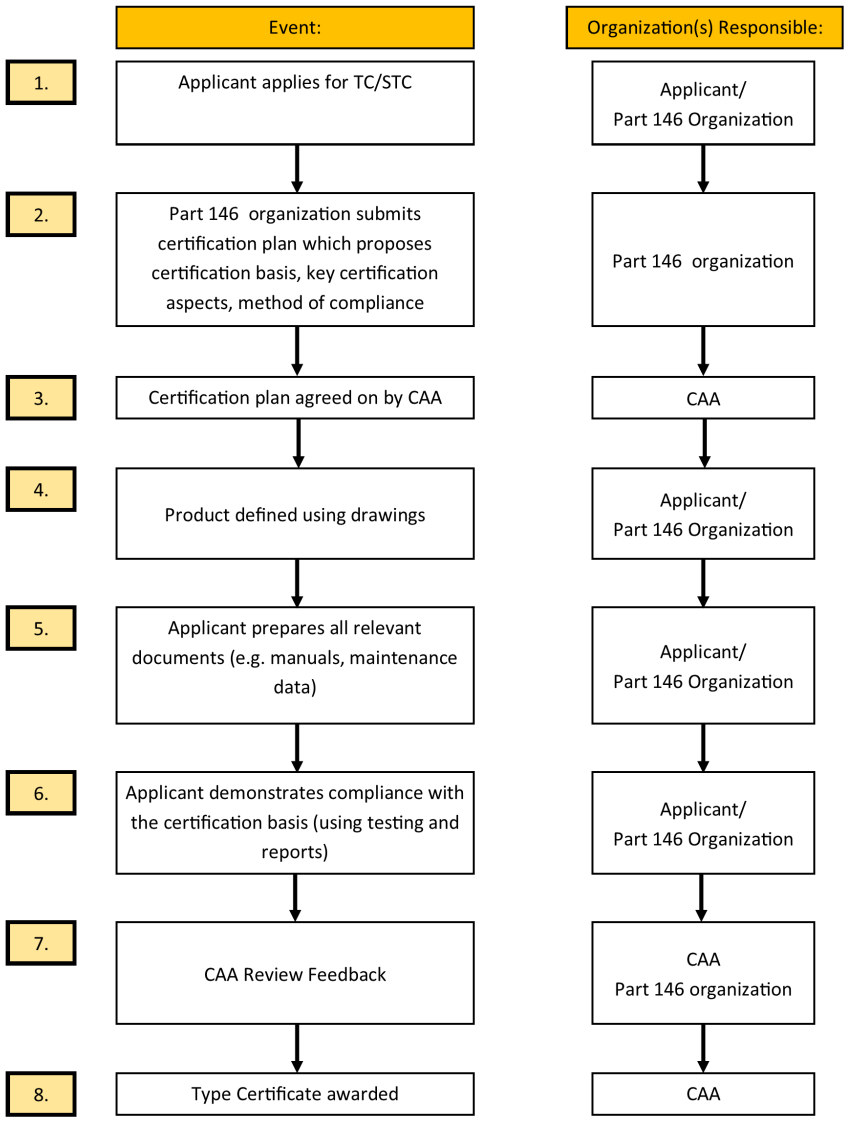

Figure 2: Summary of the Type Certification Process

Types of Aircraft Control Systems

A control system transfers an input command from the pilot to an output change in the position of a control surface. Three ways of doing this are: Mechanical, hydro-mechanical and Fly-by-Wire (FBW).

Hydraulic and Mechanical Control

In a mechanical system the pilot moves the control stick as an input command, and cables and pulleys transfer the force from the control lever through to the control surfaces.

Before the 1980's, the control surfaces of an aircraft were controlled directly by the pilot's input [8]. The mechanical and hydro-mechanical systems require a direct physical connection from the controller in the cockpit to the control surfaces of the aircraft.

A hydraulic system is similar to the mechanical system in that it needs a physical link from the controller to the control surface. The difference is that instead of wires and pulleys operating the entire force transfer, the input command is transferred to a hydraulic circuit which assists the pilot in maneuvering the aircraft. The hydraulic circuit then transfers the command to the actuator, which moves the control surface [9].

Disadvantages of the conventional control system include that the system is heavy due to the cables, pulleys, brackets and supports needed, and periodic maintenance for lubrication and cable stretch (for example) is required. [10]

Fly-by-Wire Control

A FBW system eliminates the need for hydraulic and pulley/cable control systems, as the commands are transmitted electronically from the pilot inputs (e.g., with a joystick) to a flight control computer. The computer then calculates what movements are required and sends the signal to servos and actuators at the control surfaces.

Advantages of FBW

The Aviation Handbook discusses advantages of a FBW control system [10]. Some examples are:

- Integration of several federated systems into a single system
- Superior aeroplane handling characteristics
- Maintenance is made easier
- Manufacture is made easier
- Greater flexibility for including new functionality or changes after initial design and production

Other advantages are:

- The loss rate of FBW aircraft is 10x less than pulley and cable aircraft [11]
- All of the weight of mechanical and hydraulic systems is replaced by electrical wiring.
- Outputs are controlled by computer, resulting in:
    - Pilots are deterred from venturing outside of safety limits [12]
    - Pilots are more situationally aware, meaning a lower risk of accidents related to the pilot not knowing where they are in space [13]
- Autopilot/remote piloting system does not need a set of actuators to interface with the FCS

Challenges and Disadvantages of FBW

- FBW contains software, and therefore cannot be certified through the methods described in AC 25.1309 “because it is not feasible to assess the [details of] software errors … after the completion of system design, development and test” [14].

Certification of FBW to date

Fly-by-Wire systems have been certified in civilian aeroplanes since the early 1970s. The first civilian aircraft with a digital FBW system was the Airbus A320, and as of 2012 there are 8 airlines which have aircraft fitted with FBW control systems [12]. In order to certify the A320 and its new FBW technology,

special conditions which targeted specific issues of the aeroplane (such as flight envelope protection, static stability and lightning interference) were introduced. These special conditions were later integrated into the current standards [6].

No commercial helicopters which have a FBW system have obtained type certification to date, and the Bell 525 Relentless is expected to be the first [13]. It is being certified under modified sections of military standards and is expected to be certified at the end of 2018 [15].

No aircraft has been found that has a type certificate similar to the one needed for the Craft. The certification basis for the Bell 525 Relentless is based on modified military standards [13]. A tiltrotor FBW aircraft, the AW609, is also expecting civil certification in 2018 [16].

Military aircraft with FBW control systems have been around for longer than civilian aircraft with FBW systems [12], however these have not been investigated as the Craft must be certified under civil aviation law.

Certifying the Craft

It is recommended that a certification project which involves the FAA begins with the Partnership for Safety Plan (PSP) and the Project Specific Specification Plan (PSCP) [17]. These outline the standards and requirements which the aircraft has to meet in order for it to be certified, and are very similar to the processes used by the NZCAA [7]. As there are currently no standards for "Jetpack" aircraft it is assumed that the following documents may be used in the certification process:

1. ARP4754A (*system design, verification and validation, configuration management, QA*)
2. ARP4761 (*safety assessment process*) – used to show compliance with 14 CFR 25.1309
3. Advisory Circular AC27-1B
4. Advisory Circular AC23.1309-1E
5. Advisory Circular AC23.1309-1A

ARP4761 and ARP4764A will be used as they are broad in their coverage [18] and are objective based as opposed to prescriptive. There are objectives which the aircraft must meet (described in ARP4754A and ARP4761) but it is completely up to the designer as to how these objectives are met.

Introduction to ARP4754A [18]

ARP4754A is a guideline for the development of civil aircraft systems with an emphasis on safety aspects. The methods in ARP4754A are a way to "provide development assurance for aircraft and systems to minimize the possibility of development errors" [19]. It provides guidelines on how to develop aircraft systems and describes how to identify the Development Assurance Level for systems and items which implement the aircraft functions. ARP4754A is a document intended to act as a guideline for both certification authorities and aircraft manufacturers.

Processes in ARP4754A

Firstly, aircraft functions must be determined. Functions (requirements) may fall into categories such as: safety, operational, customer and performance requirements, which are allocated from the top (aircraft)

level to systems and items. Processes in ARP4754A validate that the requirements are correct and complete.

A safety assessment on the aircraft, each system, and item must be performed to identify failure conditions, modes and probability of failure. This can be done using the techniques outlined in ARP4761.

Each system and item (component) is prescribed a DAL (Development Assurance Level) depending on the consequence of failure. DAL A is the highest level, corresponding to a catastrophic failure if that system fails. DAL E is the lowest, which corresponds to zero safety consequence as a result of failure.

Methods of validation and verification are outlined in ARP4754A. The systems are validated to determine if the system is performing its intended function, and nothing unintended.

A certification plan is then constructed. The plan identifies the certification basis and outlines how the applicant intends to demonstrate compliance.

ARP4754A in this project

The Craft has functions that it needs to perform, and requirements that it must meet in order to fly as intended. ARP4754A explains how to identify these requirements. Once the requirements are identified and allocated systems and items, then that system can be examined for its probability of failure. ARP4761 is used for this examination.

For example, the craft may need safety systems to ensure that it does not impact ground at high velocity if power is lost from significant altitude. One method is the use of a parachute. The requirements of the parachute may be to deploy when it is needed, and to slow the craft down sufficiently before impact. The requirement of deploying the parachute when needed may be achieved with a manual or automatic deployment system. The deployment system will have its own requirements, such as needing to provide the components with power. These will then be allocated to individual items, such as a battery. Once the system and subsystems have been designed, the means and likelihood of potential failure can be identified using ARP4761, such as battery failure. The failure probabilities of individual components can be combined to obtain an overall failure rate for the system.

An industry FHA suggests a parachute system as one means of limiting the veloicty of impact and consequences of propulsion failure. If used, the parachute system will be the critical element to certify to DAL A.

Introduction to ARP4761 [20]

ARP4761 describes the safety assessment methods and techniques necessary to assess an aircraft. These analysis methods include a variety of processes (including, but not limited to FTAs and FHAs). These processes interconnect and are iteratively performed, meaning that every element of every system is quantitatively analyzed.

This standard does not answer the question of "is the function of the system correct?", rather it assumes that the function is correct and instead focuses on quantitatively analyzing the failure rates and modes of the system.

Processes in ARP4761

ARP4761 details how to perform top down (e.g. FTA's) and bottom up (e.g. FMEA) safety analysis processes. The standard considers the aircraft as a whole, before working down to the system and item level.

ARP4761 in this project

This project will utilize the safety processes outlined in ARP4761 to identify the hazards and potential failure causes in the parachute automatic deployment system.

FDAL A Certification

If the parachute system is certified to DAL A, other subsystems may be certified at DAL C. The following is an explanation as to why this is the case, based on page 44 of ARP4754A.

Note: The following procedure is a hypothetical analysis, and the governing certification body (CAA) may see different outcomes from the same situations.

"Functional Failure Set [FFS]: A single member or a specific group of members that are considered to be independent from one another (not necessarily limited to one system) that lead(s) to a top level failure condition." [18]
"Member [of a FFS]: an aircraft system/function or item that may contain an error causing its loss or anomalous behaviour" [18]

Alternatively put, a FFS is a subsystem or group of subsystems whose combined or individual errors can lead to a top level failure condition (e.g. loss of control), and a Member is one of these subsystems. It is possible for a FFS to consist of just one subsystem.

Table 3 in ARP4754A explains the FDAL classifications in relation to the top-level failure conditions as a result of Member errors. The sections of the table which apply to this document are:

- The top level failure condition classification to be analyzed is catastrophic (failure of systems may result in loss of crew member and aircraft)
- In a FFS, one member must be FDAL A. The other members must be given a FDAL according to the most extreme case of their individual failure effect. The most extreme failure condition of other members in the FFS must be below the top-level failure condition being assessed. Additional members in the FFS being assessed must be at least FDAL C.

Process

a. All members contributing to the top level failure condition are identified
b. One of these members MUST be verified to FDAL A
c. The remaining members can be assessed by their INDIVIDUAL failure effects.

d. If the maximum failure condition for any individual Member (not the FDAL A member) is MAJOR (conditions of which are outlined in Figure 2 of [21]), then those members may be verified at FDAL C

Identifying the Top-Level FC and FFS:

Top-Level FC: Aircraft crashes causing death to pilot and/or bystanders and loss of aircraft

FFS: Parachute fails, insufficient structure strength, engine failure, loss of control

Assuming that the parachute is Level A, here follows a brief assessment of the individual systems if they failed individually (not in combination). If the parachute is Level A, then the failure conditions created by the independent failure of other systems cannot exceed Major. Figure 3 defines failure condition classifications.

Classification of Failure Conditions	No Safety Effect	<----Minor----->	<----Major---->	<--Hazardous--->	< Catastrophic>
Allowable Qualitative Probability	No Probability Requirement	Probable	Remote	Extremely Remote	Extremely Improbable
Effect on Airplane	No effect on operational capabilities or safety	Slight reduction in functional capabilities or safety margins	Significant reduction in functional capabilities or safety margins	Large reduction in functional capabilities or safety margins	Normally with hull loss
Effect on Occupants	Inconvenience for passengers	Physical discomfort for passengers	Physical distress to passengers, possibly including injuries	Serious or fatal injury to an occupant	Multiple fatalities
Effect on Flight Crew	No effect on flight crew	Slight increase in workload or use of emergency procedures	Physical discomfort or a significant increase in workload	Physical distress or excessive workload impairs ability to perform tasks	Fatal Injury or incapacitation

Figure 3: Summary of Failure Condition Classification. Image adapted from "FIGURE 2.", AC 23.1309-1E, [21]

1. If the structure cannot endure the impact force of the landing craft (at speed), the engines will be able to control it to the extent required.
   *The maximum classification of this failure condition will be MINOR – if the pilot lands with excessive velocity there will be a slight reduction in safety margins and the crew may experience some physical discomfort (*Figure 3*). This may be as a result of, for example, the structure bending out of expected operational boundaries.*

2. If the engine ceases, then the parachute and structure will save the aircraft after freefall
   This is similar to situation (3), where the pilot voluntarily stops the engine. MAJOR may be the highest failure condition classification if the engine ceases only.
   ➔ ***Note:*** *The landing gear has a maximum height from which it can safely absorb craft impact without a parachute. The parachute will have a lower height limit from where it can deploy and safely decelerate the craft. This failure condition only holds if the lower limit of the parachute is at or below the upper limit of the landing gear structure, such is the case in Figure 4.*

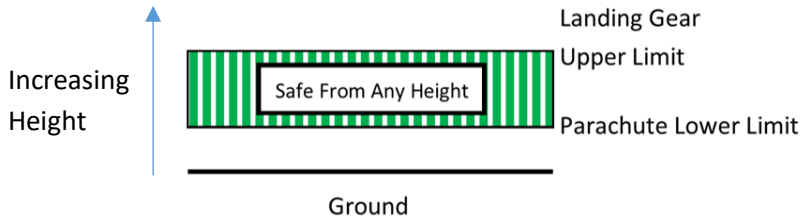

Figure 4: Parachute Lower Limit is lower than Landing Gear Upper Limit

3. If the pilot loses control of the aircraft (vanes or throttle control) then they may cease the engine, requiring the use of the landing gear and/or parachute for a safe impact.
   The maximum failure condition will be MAJOR – there will be reduced functional capabilities of the aircraft. It would be unlikely that the pilot cannot perform tasks "accurately and completely" due to physical distress as they would not have encountered extreme accelerations – this assumes that power loss/gain between fans is even and craft rotation caused by the vanes is such that the craft does not tumble. There would not be a large reduction in safety margins if the parachute was DAL A, and if the scenario in Figure 4 holds true it would be unlikely that the pilot would suffer serious or fatal injury.

The highest failure condition for these is MAJOR, under the conditions that the "***Note"*** in (2) and assumptions in (3) hold true. If this is the case, all other members in this FFS can be assessed with FDAL C.

AC 23.1309-1E [21]

This standard specifies that it may be used for the initial approval of a new type design (§ 2). It "provides guidance and information for an acceptable means, but not the only means, for showing compliance with the requirements of Section 23.1309 … for part 23 airplanes" (§ 1.a.)

Table 2 in AC 23.1309-1E classifies aircraft in 4 categories (Classes I – IV). The Martin Jetpack is likely Class I, as it is a single engine aircraft weighing less than 6000 lbs. However, airplanes in Class I are usually well tested and well known/have lots of industry experience among them – "The probability standards are based on historical accident data, systems analyses, and engineering judgment for each class of airplane." (§ 15.b.) The probability of a catastrophic failure condition occurring must be $<10^{-6}$ per flight hour in Class I aircraft, though the lack of historical data in jetpacks in comparison to other Class I aircraft may mean that the probability of a catastrophic failure condition occurring must compare to failure rates in Class II, III or IV aircraft; $<10^{-7}$, $<10^{-8}$ or $<10^{-9}$, respectively.

AC 23.1309-1E and an Automatic Parachute Deployment System

For hazardous and catastrophic failure conditions, such as high velocity impact, a thorough safety assessment is necessary. A detailed safety analysis for each failure condition specified in the FHA must be completed. (§ 17.d.) "No catastrophic failure condition … should result from the failure of a single component, part, or element of a system." (§ 17.d.(3)). The analysis may range from a report which

compares the similarity of two systems or interprets test results, “to a detailed analysis that may or may not include estimated numerical probabilities” (§ 19.a.).

A probability analysis such as an FTA may be constructed, which includes numerical probability information (§ 19.b.). “Information concerning unsafe system operating condition(s) must be provided in a timely manner to the crew to enable them to take appropriate corrective action.” [22] The possibility of crew errors must be minimized so that additional hazards are minimized, and the operating procedure must be included in the Aircraft Flight Manual.

It is assumed that the proper maintenance is carried out. Actions for maintenance should be included in the instructions for continued airworthiness.

The Role of Aircraft Certification in this Project

The relevance of certification is relevant to two areas in this thesis: the modelling of the craft and its parachute system during the emergency descent phase of flight, and automatic deployment system of the parachute.

The behaviour of the Craft and parachute during emergency descent needs to be better understood in order for impact conditions to be predicted (e.g., craft velocity and orientation upon impact). This data can be used as inputs to an impact model to determine how the pilot will be affected. From this it will be possible to determine the parameters and initial conditions which will create unsafe landing scenarios, and if necessary, alter the emergency descent system or the operating limits of the Craft.

The automatic parachute deployment system needs to be analyzed quantitatively and qualitatively. ARP4761 and ARP4764A provide specific guidelines and procedures for system development and analysis.

System Safety Assessment

One potential means of catastrophic failure is high velocity impact. Two systems related to this means of failure are assessed: the automatic deployment system and the parachute system.

The automatic deployment system is developed and analyzed with quantitative data. It is assumed that a parachute is required to prevent high velocity impact. The validity of the parachute as a system to prevent high velocity impact must be verified. The failure conditions for the parachute are not assessed.

Objective 1 – Numerical Modelling

Numerical modelling was used to simulate how the parachute and craft would behave during descent and determine the impact state of the Craft. The objective of numerical modelling was to set up a basic model of the parachute to see how it would perform under a few selected scenarios. These different scenarios were simulated using MATLAB. The aim of the model is to determine a range of heights from which, if the craft loses power, the parachute would be able to decelerate the Craft to a safe impact velocity.

There are a range of heights from which if the craft loses power it will impact the ground at an unsafe velocity. This range is the Unsafe Deployment Zone (UDZ). The lower limit of the UDZ is the highest fall

height from which the landing gear is assumed to safely absorb impact. The upper limit is the height below which the parachute cannot decelerate the craft to a safe velocity before impact. The extent to which certain conditions affect the UDZ are identified.

Previous Modelling in Literature

Previous models simulate the descent of a parachute-payload system. The White-Wolf model is commonly used for analytical studies [23]. Wolf [24], Doherr, et al. [25], Gao [26] and Guglieri [27] consider the independent movement of the parachute and payload. Models which do not consider independent movement are those of Tory [28] and Dobrokhodov [29].

There has been "a lack of accurate dynamic modelling of apparent mass effects and nonlinear aerodynamics of distorted canopies" [29]. The same paper states that in existing models "the only aerodynamics considered are those of a fully deployed and symmetric canopy", as of 2003. Since then at least one model has been developed which integrate parachute opening dynamics with a multi-body dynamic model [26]. Guglieri [27] includes the modelling of riser forces and a drogue chute.

The inflation curve model, where an assumed drag area growth profile is used, and the apparent mass model, where the physics of the model are improved by accounting for the effects of the air mass were shown to produce similar responses [30].

Parachute Modelling

Parachute inflation has been modelled [31], although no modeling of ballistic parachute deployment was found. Methods which have been used to simulate a parachute in a fluid include FEM [32, 33], CFD[34] and numerical simulation [35]. Most of these models consider the parachute either already inflated or a steady inflation.

Methodology

3 models were set up in MATLAB. Each model simulates a part of the craft's emergency descent stage. The first model simulates the fall profile of the craft through space, with assumptions such as that the parachute is either completely deployed or packed, and that both the craft and parachute can only travel in the vertical direction.

The second model is similar to the first in that it simulates the descent of the parachute-craft system. In this model the parachute and craft can move vertically and horizontally, i.e. it is a 2-D model.

The third model simulates the impact of the craft into the ground. This model is limited in that it only simulates the Craft landing in an upright position onto even, flat, infinitely hard and infinitely slippery terrain.

Differences in 1D and 2D Models

The 1D model simulates the parachute and Craft as one entity. The 2D model by allows the craft and parachute to rotate and move independently in 2D space, and wind effects are included.

Department of Mechanical Engineering
University of Canterbury
Te Whare Wānganga o Waitaha
Private Bag 4800
Christchurch 8020, New Zealand

Telephone: +64-3-366 7001
Facsimile: +64-3-364 2078
Website: www.mech.canterbury.ac.nz

UNIVERSITY OF CANTERBURY
Te Whare Wānanga o Waitaha
CHRISTCHURCH NEW ZEALAND

1D Mathematical Modelling of a Parachute System

Abstract

A mathematical model of the operation of the craft-parachute system was created. This was done by using force balances to iteratively determine the acceleration, speed, and change in altitude of the craft through time. A first order Euler's method was used to determine acceleration, speed and altitude at each time step, and the drag equation was used to determine the drag force on the Craft at each iteration.

Results showed that using an estimated pilot reaction time of 3s, there are a range of altitudes within which it is unsafe to deploy the parachute (5-91m if the craft is already descending). Within this zone ("Unsafe Deployment Zone") there is insufficient altitude for the parachute to be effective, and the Craft is above the safe fall zone from which the Craft structure will be able to absorb the impact.

The Unsafe Deployment Zone (UDZ) can be eliminated if the time from the Craft losing power upon descent to when the signal is sent (from the manual or automatic pilot module) within 0.249 seconds. The allowable reaction time increases to 0.453s if the craft is at a hover before losing power, and again to 0.656s if the Craft is ascending at 2m/s at the time of loss of power.

Variables and Values

Variable	Description	Value	Source/comments (if applicable)
F_d	Drag force on the Craft	(varies)	-
F_w	Weight force on the Craft	3139.2 N	-
$m_{aircraft}$	Combined weight of Craft and payload. Assumed to always be at maximum	330 kg	[36]
g	Acceleration due to gravity	9.81 m/s^2	-
ρ	Density of air. Assumed constant	1.2 kg/m^3	-
v	Velocity of craft	(varies)	-
Cd_{craft}	Drag coefficient of craft (Rhombus)	1.1	[37]
Cd_{para}	Drag coefficient of parachute	1.03	Based on industry data
A_{craft}	Effective area of craft	1 m^2	Assumed based on industry estimates

A_{para}	Area of parachute (based on ø8.4m)	55.4m^2	Assumed based on best diameter estimates
t	Time step used for MATLAB simulation	1x10^{-4} s	-
Δt	Time step used for test data	0.005 s	-
SF	Drag Area Ratio	Varies from zero to 1 over Deployment Interval	-
μ	Dynamic Viscosity of air	1.73 x10^{-5} [kg/ms]	[38]

Introduction and Objectives

Ballistic Parachutes

Ballistic parachutes are one way to ensure the fall speed of an aircraft remains controlled in an unpowered descent. A rapid deployment of the parachute becomes increasingly critical to an aircraft's survival the closer to the ground operations are – this includes takeoff and landing phases of flight.

The aim of this simulation was to test the altitudes at which the parachute will be effective, and find limits (if any) where the parachute will be ineffective. This was done by mathematically modelling the Craft and parachute system in MATLAB, consistent with the assumptions outlined in "Assumptions". This paper describes the parachute system and how it was modelled.

Assumptions

- The system has an initial state, transition state, and final state. Figure 5 and Figure 6 show the final and initial states, respectively.
- During the transition state, the drag area ratio was assumed to follow an "S" shape as best estimated by industry data.
- The inflation time of a ballistic parachute was assumed to be 0.63 seconds in a purely vertical fall [39].
- A force is transferred from the parachute to the Craft from the moment of detonation.
- The Craft is carrying the maximum allowable load (total mass = 330kg [36]). This gives the highest estimate for impact velocity as the parachute has to bear more weight.
- The deployment system is manual, meaning that the pilot's reaction time is considered.
- The pilot reaction time is 3 seconds
- The Craft has an effective "frontal area" of 1m^2 (A_{craft}) and has a drag coefficient of 1.1 (Cd_{craft})
- The system remained in the upright position for the duration of the simulation

- The drag coefficient of the Craft was constant, though in reality it would change with Reynolds Number and velocity.
- The Craft was either in descent, hover, or ascent at the beginning of the simulation – i.e. it had a vertical velocity of -2m/s, 0m/s or +2m/s, respectively.
- Wind velocity is zero – the craft only has a vertical velocity component
- The mass used for drop testing was assumed to have zero drag
- The Craft structure will save the Craft from a fall of up to 6m
- Environmental factors such as weather and bird strike have not been considered.

Methodology

Terminal Velocity Calculation

At an vertical impact velocity of 10m/s, the human body is in the "zone of certain survival" [40]. See Appendix 1 for a range of survivable and fatal impact velocities. The survivable impact velocity is closer to 11.8m/s if purely vertical, however 10m/s is used for conservative purposes.

The terminal velocity of the craft with the parachute deployed was calculated to show that the Craft will fall at less than 10m/s after deployment. The terminal velocity of the craft without the parachute deployed was also calculated for comparison.

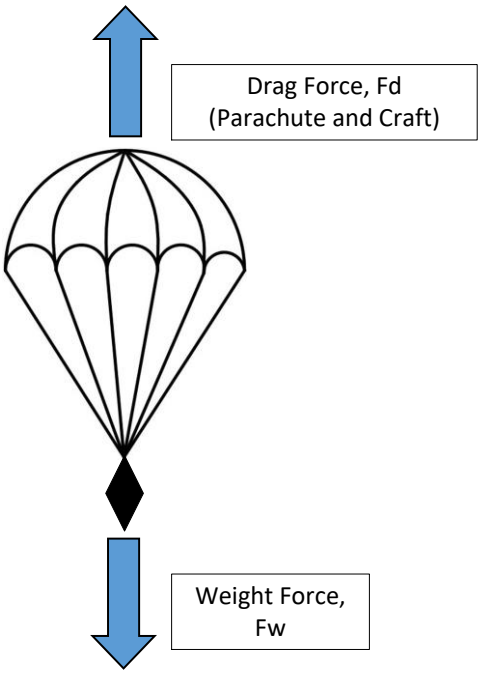

Figure 5: The model with the parachute deployed and relevant forces

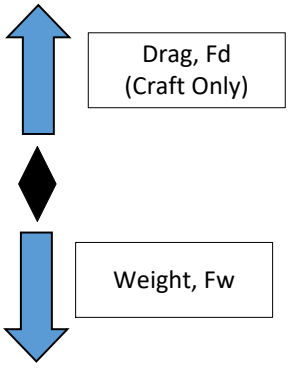

Figure 6: The model with parachute packed and relevant forces

Relevant Equations:

The terminal velocity is reached when the weight force and the drag force on the Craft are equal, i.e.

$$F_d = F_w \tag{1}$$

The weight force on the Craft can be expressed by:

$$F_w = m_{aircraft} g \tag{2}$$

The drag force of the Craft can be expressed by:

$$F_d = \frac{1}{2}\rho v^2 CdA \tag{3}$$

Rearranging (3) for v and substituting (1) and (2):

$$v = \sqrt{\left(\frac{m_{aircraft} g}{\frac{1}{2}\rho CdA}\right)} \tag{4}$$

Table 1 summarizes the terminal velocities.

Configuration	Terminal Velocity (m/s)
Parachute Deployed (Parachute and Craft)	9.6
Craft Only	228.7

Table 1: Expected Terminal Velocity of the Craft with and without the parachute

An industry test report determines the terminal velocity of the combined craft and parachute as 8-9.3 m/s. These terminal velocities require Cd values ranging from 1.12-1.52, or parachute diameters ranging from 8.8-10.2m. This discrepancy may mean that the parachute tested has a higher drag coefficient than predicted in Table 3, or that the test results used to predict the coefficients in Table 3 are not the same test results that industry tests use.

Simulation

The simulation was split into 2 phases: freefall and parachute. A parachute transition was incorporated into the parachute phase, to allow for the transition of the parachute from its packed to deployed state. These were combined to create the model.

The initial velocity was set, as well as the estimated delay time between the loss of power and when the parachute is fully deployed. The delay time consisted of the variables described in Table 2.

Delay Factor	Delay Time (s)	Reason/Source
Pilot Reaction Time (estimated)	3	Minimum allowable reaction time based on industry estimates
Deployment Time	0.63	Deployment time as advertised by a parachute manufacturer [39]
Deployment System Latency	0.114	Based on industry estimates
TOTAL	**3.744**	

Table 2: Delay Times

The pilot reaction time (i.e. total response time from loss of power through to initiating the parachute) was estimated to be 3s. The average total response time for a helicopter pilot to detect and respond to a loss of power is 4.13s [41]. The systems on a helicopter may be more complicated and therefore a faster reaction time on the Craft may be valid.

Calculation of the Drag Coefficient of the Parachute

The drag coefficient was calculated from experimental test data. The tests involved releasing a mass (equipped with the parachute) from a crane. The distance fallen and vertical velocity were recorded at increments of 0.005 seconds. The data points used to calculate the drag coefficient were those between the time of full inflation and ground impact.

A combination of force balances, the drag equation and Newton's 2nd law were used to determine the drag coefficient at each time step.

The layout is the same as that in Figure 5, noting that in this case the net forces acting on the Craft may not be zero. F_{NET} is upwards, in the direction that the parachute exerts a force on the craft.

$$F_{NET} = F_d - F_w \tag{5}$$

Substituting the forces with Newton's 2nd law and the drag equation into (5) gives:

$$ma_{tot} = \frac{1}{2}\rho v^2 Cd_{para} A_{para} - mg \ * \tag{6}$$

Where:

$$a_{tot} = \frac{v_2 - v_1}{\Delta t} \tag{7}$$

v_2 and v_1 were taken from the experimental data, Δt =0.005s

* Note g is positive. It is accounted for in the force balance

Rearranging for Cd_{para} gives:

$$Cd_{para} = \frac{2 \times (ma_{tot} + mg)}{\rho v^2 A} \tag{8}$$

The drag coefficients calculated were then averaged over the 3 tests – "Test 2", Test 4" and "Test 5". These were the only tests available. The results are summarized in Table 3.

Test	2	4	5	TOTAL AVERAGE
Drag Coefficient Average	0.93	1.09	1.06	1.03

Table 3: Drag Coefficient Values as Calculated from Drop Test Data

This closely matches the drag coefficient value of ~1.00 for a hemispherical parachute canopy in Reynolds Numbers above 10^5 [42] which equates to a craft vertical velocity of 0.17m/s with the parachute deployed, using Eq. 9.

$$Re = \frac{\rho v D}{\mu} \tag{9}$$

Equations for Simulation

Force balances and a first order Euler's Method were used for the simulation of the Craft and parachute.

The following method was iteratively used to simulate the velocity and altitude as the Craft descended.

The drag force equation (10) was used to determine the drag force of the parachute and Craft. For the freefall phase of descent the parachute terms were ignored. The velocity in the previous iteration or the initial velocity was used.

$$F_d = \frac{1}{2}\rho\, V_{n-1}^2 (Cd_{craft}A_{craft} + Cd_{para}A_{para}) \tag{10}$$

Equation 11 was used during the transition state to account for the drag area ratio of the parachute. The drag area is the drag coefficient multiplied by the area. The ratio of instantaneous drag area (drag area at a point in time during inflation) to drag area at full inflation increases over time from zero at the point of parachute initiation, to 1 when the parachute is fully inflated. The drag which would have been created if the parachute had been fully inflated is multiplied by the drag area ratio. This gives a continuous opening profile for the chute.

$$F_d = \frac{1}{2}\rho\, V_{n-1}^2 (Cd_{craft}A_{craft} + \mathrm{SF} * Cd_{para}A_{para}) \tag{11}$$

The drag coefficient of the parachute was assumed to increase over time according to the S-shaped plot in Figure 7. This is based on industry data. The beginning of this curve begins when the detonator activates the parachute and ends at the time the parachute is assumed to be fully deployed (0.63s later).

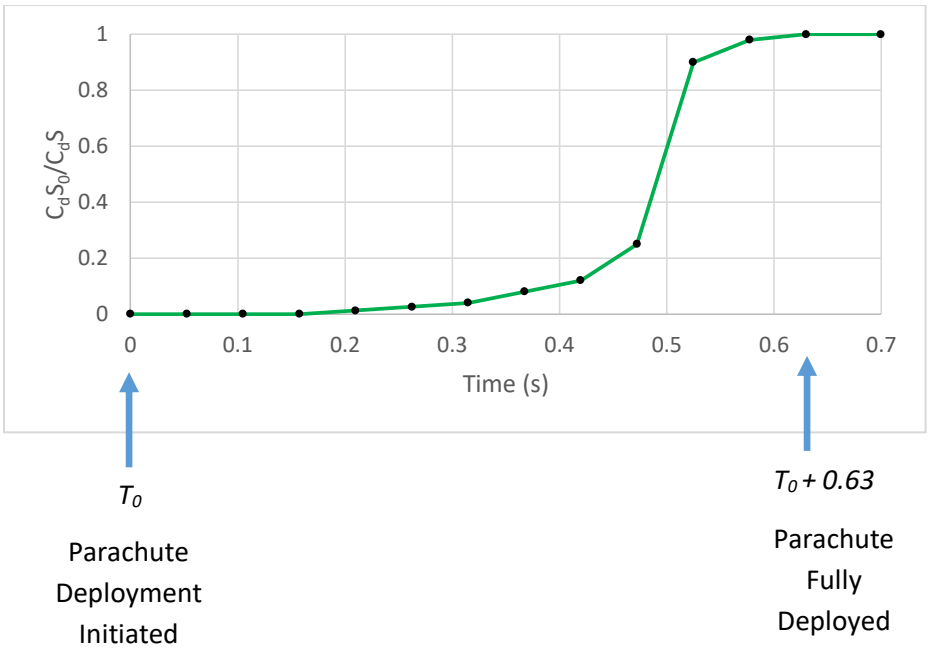

Figure 7: Drag Area Ratio

Equation (12) is the force balance equation. This describes the difference in the drag force and the weight force:

$$F_{diff} = F_{drag} - Fw \tag{12}$$

Newton's 2nd law, Equation (13), was used to calculate the acceleration that the Craft was experiencing as a result of the forces upon it:

$$a = \frac{F}{m} \tag{13}$$

Equations (14) and (15) were used to calculate the simulated velocity of the Craft and its position in vertical space as it fell:

$$V_n = V_{n-1} + at \tag{14}$$

$$D_n = D_{n-1} + V_n t \tag{15}$$

Figure 8 outlines the solving process for the simulation.

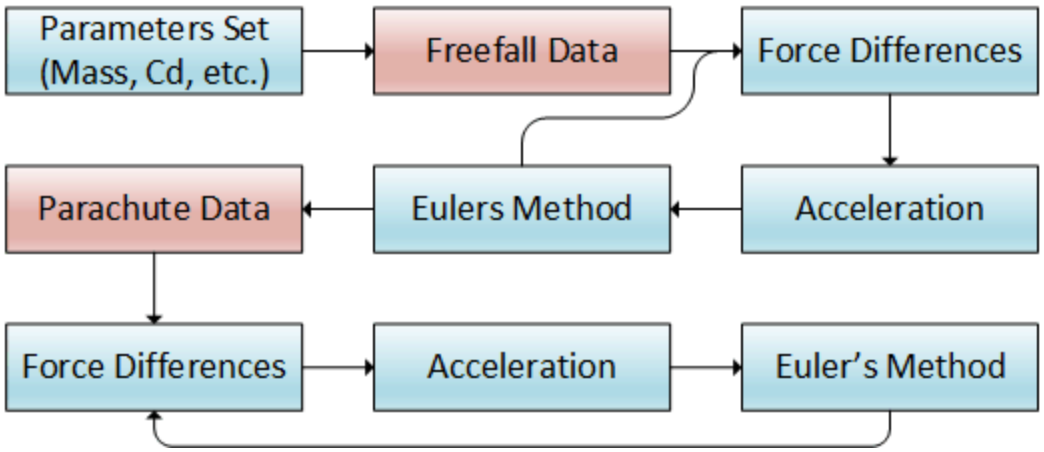

Figure 8: Flow Chart of the Solving Process

The process between "Freefall Data" and "Parachute Data" was iterated for the freefall phase of descent until 1 of 2 conditions had been met:

1. The time it had been falling met the time that the parachute had taken to deploy, or:
2. The height the Craft had fallen met or exceeded the altitude the Craft had fallen from, indicating it had impacted the ground.

If the Craft had not impacted the ground by the time that the parachute had been deployed, then the iteration process would break and move on to a section which iterated through the same equations as previously, only this time the drag of the parachute was accounted for. The velocity profile was tracked until the craft impacted with the ground.

The process in Figure 8 was performed for altitudes of 0.125m -100m in steps on 0.125m. The impact velocity which resulted from each altitude was recorded and compared with the maximum allowable impact velocity (Refer Figure 11).

The required reaction time of the pilot to maintain below a velocity of 10m/s was then determined. This required estimating a reaction time, and simulating an unpowered Craft descent from the altitude where the highest impact velocity occurred. The estimated required reaction time was decreased until the Craft did not exceed 10m/s for the entirety of the descent.

Results

Table 4 summarizes the limits of the Unsafe Deployment Zone and the maximum pilot reaction time allowed to launch the parachute before the Craft gains a velocity of 10m/s at any stage of the descent. Figure 12 shows the simulated velocity profile of the Craft if the maximum reaction times are satisfied.

Initial vertical velocity	UDZ Lower Limit (m)	UDZ Upper Limit (m)	Max impact velocity (m/s)	Max impact velocity drop height (m)	Required Pilot Reaction time to Eliminate UDZ (s)
-2m/s (descending)	4.9	90.2	32.4	62.3	0.249
0 m/s (hovering)	5.2	83.2	30.8	56.6	0.453
2 m/s (ascending)	4.9	76.0	29.3	50.8	0.656

Table 4: The Unsafe Deployment Zones for different Initial Vertical Velocities.
Note: UDZ lower limit based on capabilities of parachute only, not landing gear.

For power lost in the 5m and 91m altitude range, the impact velocity is simulated to be larger than 10m/s if the Craft is initially descending when power is lost.

The remainder of the analysis assumes that the Craft is in its descent phase prior to power loss, as this is the most dangerous scenario of the 3 in Table 4.

The profile of Figure 9 and Figure 10 consists of 3 curves. These represent the freefall, transition and parachuting phases of descent respectively. The craft is in freefall phase for as long as it takes the pilot to launch the parachute, and for the parachute system to respond and completely deploy the parachute. Figure 9 shows that the craft falls 52.1m before chute deployment is initiated.

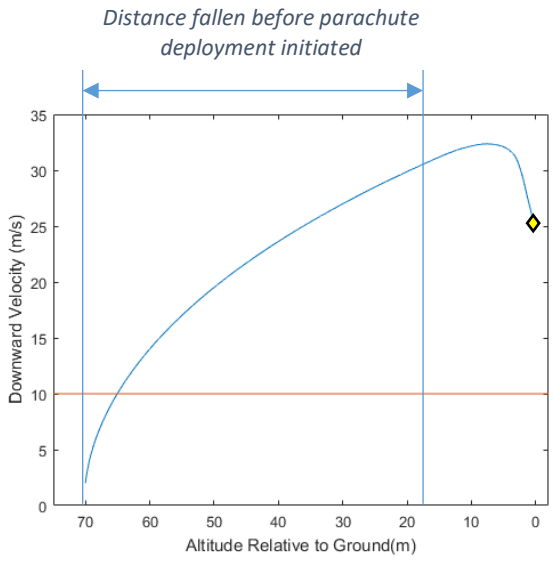

Figure 9: The Velocity Profile for when the Craft loses power at 70m - Pilot Reaction = 3s, Initial Velocity = -2m/s

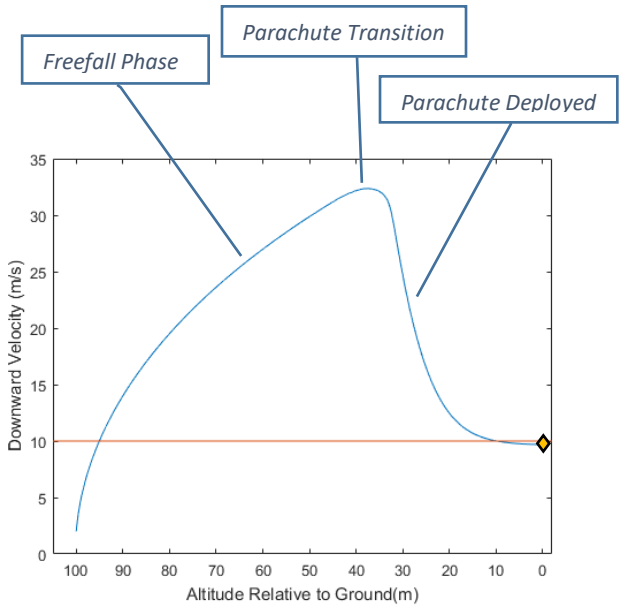

Figure 10: The Velocity Profile for when the Craft loses power at 100m - Pilot Reaction = 3s, Initial Velocity = -2m/s

This process was repeated for a range of altitudes. The downward velocity at ground level is the impact velocity. The impact velocity was recorded for each initial altitude tested (Figure 11). The diamonds in Figure 9 and Figure 10 correspond to those in Figure 11.

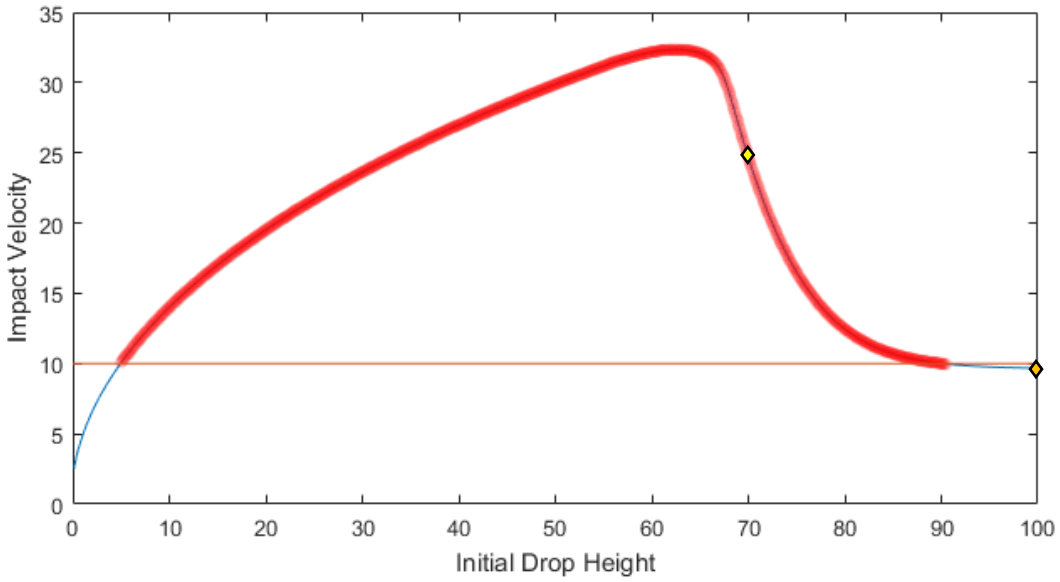

Figure 11: The Impact Velocity dependent on which height the Craft loses power - Pilot Reaction = 3s, Initial Velocity = -2m/s

Figure 12 shows that it is possible to prevent an impact speed from any altitude providing that the reaction time is below 0.24s.

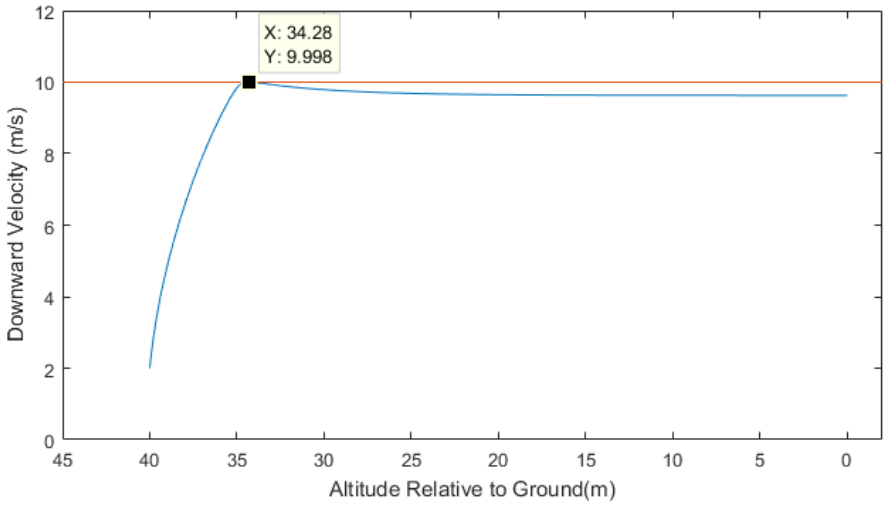

Figure 12: Vertical Velocity Profile if Pilot/System reaction time is below 0.24s – Initial Altitude = 40m, Initial Velocity = -2m/s

It is assumed that the Craft structure can absorb an impact from a height of 6m based on industry estimates. If the parachute is fully deployed within 0.99 seconds of losing power – the total time to full deployment assuming that the pilot reaction time is 0.24s – it will begin opening after 1.4m of freefall and completely open after the craft has lost 6.6m of altitude. The UDZ will be eliminated in this instance, as shown in Figure 13.

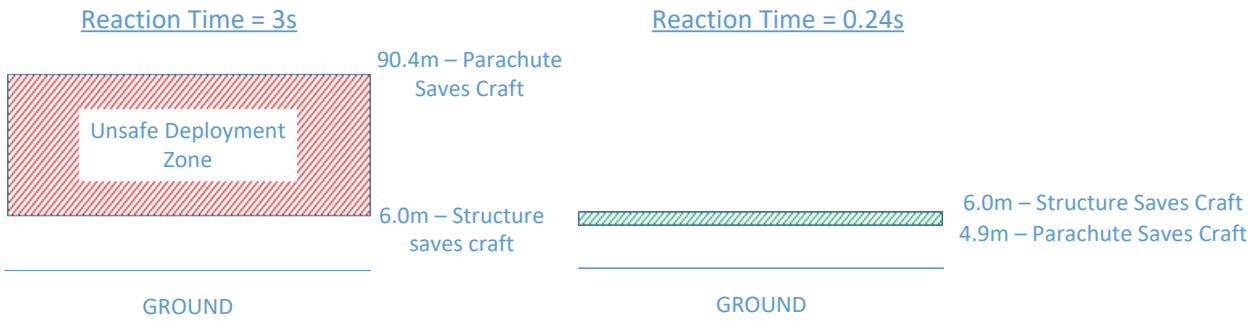

Figure 13: A Pilot Reaction Time of 3s vs. 0.24s

Discussion

The maximum permissible impact velocity of a helicopter under autorotation may exceed the limits discussed in this document, and impact forces may be absorbed elsewhere (e.g. in the seats or elsewhere in the structure).

The UDZ lower limit is based purely on the parachute capabilities and does not consider how the Craft structure will absorb impact.

It is unlikely that a pilot will be able to deploy the parachute in the time required to maintain a descent rate of less than 10m/s. An automatic deployment system will likely be needed to ensure that this descent rate is kept within this boundary.

The terminal velocity of the combined parachute and Craft was determined to be 9.6m/s, which is the velocity the model approached.

A force from the parachute is assumed to be transferred to the Craft from the moment of parachute detonation. One way to more accurately represent this in future is to assume that a certain distance or time passes before the parachute begins acting on the Craft. Distance may be more difficult to model (though possibly more accurate) as this model assumes that the parachute and Craft are 1 entity.

A change from a PRT of 2s to 3s means that the upper limit of the UDZ increases. This is expected because the craft is in freefall for a longer time period, and therefore the effects from the parachute are not present until the craft is at a higher freefall velocity.

The allowable PRT which ensures that the Craft never exceeds a vertical velocity of 10m/s increases from 0.07s in a model which does not have a transition period, to 0.24s in this model in which such a period is present. This is because it is assumed that the drag from the parachute, even though it is scaled, acts on the craft before the transition stage is complete in a model which includes the transition.

Conclusions

A 1D mathematical model of the craft in emergency descent was created. A simulation of how the parachute and craft would act based on their aerodynamic properties was performed.

The velocity profile from a range of altitudes was recorded, and the impact velocity of the Craft was recorded at different altitudes given a time interval of 3.75s between the power loss and full parachute inflation. This gave a zone of altitudes where deployment would be unsafe because the Craft exceeded 10m/s upon impact. It is possible to eliminate an unsafe deployment zone by ensuring the parachute is completely deployed within 0.99s.

A manual deployment system will not be sufficient reliably open the parachute in the time required between an altitude of 5m and 91m if the Craft is descending. It is therefore likely that an auto-deploy system will be required for low altitudes.

Department of Mechanical Engineering
University of Canterbury
Te Whare Wānganga o Waitaha
Private Bag 4800
Christchurch 8020, New Zealand
Telephone: +64-3-366 7001
Facsimile: +64-3-364 2078
Website: www.mech.canterbury.ac.nz

UC UNIVERSITY OF CANTERBURY
Te Whare Wānanga o Waitaha
CHRISTCHURCH NEW ZEALAND

2D Mathematical Modelling of a Parachute System

Summary

A mathematical model simulates the motion of the Craft during emergency descent. This is split into 2 stages: when the Craft is in freefall (before parachute deployment has been initiated) and post parachute initiation. The freefall stage ends after a combination of reaction time (3s in these simulations) and system delay time (0.114s), after which the effects of the parachute are also simulated.

It is assumed that the parachute follows a transient deployment curve, where the drag area of the parachute increases from 0% to 100% during deployment. After the parachute has been deployed, the Craft will change orientation as the tension in the cord applies a force and torque.

This model takes an initial flying velocity and reaction time of the pilot/system as inputs, and also takes on Craft and parachute mass, drag, area, inertial properties, and other variables outlined in "*Variables and Values*". The model outputs the Craft velocity and orientation on impact, as well as an altitude from above which the impact will be "safe". This is based on vertical and horizontal velocity limits.

The motion of the parachute and Craft is determined by adding the forces on each of the 2 entities, coupled by the tension in the cord attaching them. From the forces, the acceleration, velocity and position in space is determined using a first order Euler's method approximation.

The cord connection between the Craft and parachute was modelled as a spring, with the exception that when the distance between the Craft and the parachute was less than the length of the cord, the tension was zero.

This report explores several initial states of the Craft and compares simulated data such as peak acceleration and tension force to experimental data.

Variables and Values

Variable	Description	Value	Source/Notes (if applicable)
	Stage 1 Simulation		
θ_{abs}	Angle between Craft velocity vector and Craft orientation	*Varies* [degrees°]	-
θ_p	Angle between Craft orientation and vertical	*Varies* [degrees°]	-
θ_m	Angle between Craft velocity vector and vertical	*Varies* [degrees°]	-
α_{abs}	Craft drag factor	*Varies* [kg/m]	Refer Eq. (5)
α_1	[Drag force of Craft from the vertical] ÷ [velocity of Craft]	0.66 [kg/m]	Refer Eq. (1)

α_2	[Drag force of Craft in the horizontal] ÷ [velocity of Craft]	1.2 [kg/m]	Refer Eq. (2)
$Cd_{jp-vert}$	Drag coefficient of top/bottom of Craft	1.1 [unitless]	[37]
$Cd_{jp-face}$	Drag coefficient of face/rear of Craft	2 [unitless]	[37]
$A_{jp-vert}$	Area of Craft from top view	1 m^2	Assumed based on industry estimates
$A_{jp-face}$	Area of Craft from frontal view	1 m^2	Assumed based on industry estimates
$\boldsymbol{Fd_{craft}}$	Drag force on the Craft	*Varies* [N]	-
$\boldsymbol{F_{jp}}$	Total force on the Craft	*Varies* [N]	-
m_{TOT}	Combined weight of Craft and payload. Assumed to always be at maximum	330 kg	[36]
g	Acceleration due to gravity	9.81 m/s^2	-
$\boldsymbol{vel_g}$	Vector of Craft velocity relative to ground [x y]	*Varies* [m/s]	-
	Stage 2 Simulation		
θ_{jp}	Angle of Craft to positive vertical	*Varies* [degrees]	-
θ_{diff}	Angle between θ_{jp} and θ_{GLOBAL}	*Varies* [degrees]	-
$\dot{\theta}_{jp}$	Angular velocity of Craft	*Varies* [degrees/s]	-
$\ddot{\theta}_{jp}$	Angular acceleration of Craft	*Varies* [degrees/s^2]	-
$\theta_{diff,pc}$	Angle between parachute orientation to vertical and parachute velocity vector	*Varies* [degrees]	-
θ_{GLOBAL}	Angle of parachute to positive vertical	*Varies* [degrees]	-
α_{pc}	Parachute drag factor	*Varies* [kg/m]	-

SF	Drag Area Ratio	*Varies* [unitless]	-
$\boldsymbol{F_{TRANS}}$	Translational component of tension force Craft subjected to	*Varies* [N]	-
F_{ROT}	Rotational component of tension force Craft subjected to	*Varies* [N]	-
$\boldsymbol{FT}$	Tension force applied to the Craft from the parachute and vice versa	*Varies* [N]	-
du	Length of extension of parachute cord	*Varies* [m]	-
d	Distance between Craft COM and top/bottom of Craft	1.1 m	Assumed half total height of Craft
$Cd_{para,vert}$	Drag coefficient of parachute (vertical)	1.03	Refer Previous Chapter
$Cd_{para,hori}$	Drag coefficient of parachute (horizontal)	2	Assume parachute side is shaped like a rectangle with semi-spheres attached to its ends. [37]
$A_{para,vert}$	Planform area of parachute (based on ø8.4m)	55.4m^2	Assumed based on best diameter estimates
$A_{para,hori}$	Area of side of parachute	8.4m^2	Assume h=1m
Cd_{plate}	Drag coefficient of plate for rotational drag	1.28 [unitless]	[43]
A_{plate}	Area of plate for rotational drag	1.1m^2	
m_{jp}	Mass of Craft	320.5 kg	Based on best industry data estimates
m_{pc}	Mass of parachute	9.5 kg	Assumed, based on industry estimates
$\boldsymbol{wind_g}$	1x2 vector describing the wind velocity relative to ground $[x, y]$	[8 0] m/s	Assumed, based on industry estimates
$\boldsymbol{u_{pc}}$	1x2 vector describing the position coordinates of the parachute $[x, y]$	*Varies* [m]	-

$\dot{\boldsymbol{u}}_{\boldsymbol{pc,g}}$	Translational velocity of parachute relative to ground	*Varies* [m]	-
$\boldsymbol{u}_{\boldsymbol{jp}}$	1x2 vector describing the position coordinates of the Craft $[x, y]$	*Varies* [m]	-
$\dot{\boldsymbol{u}}_{\boldsymbol{jp,g}}$	1x2 vector describing Craft velocity relative to ground [x y] $[x, y]$	*Varies* [m/s]	-
$\boldsymbol{u}_{\boldsymbol{jp2}}$	1x2 vector describing the position coordinates of the parachute connection point $[x, y]$	*Varies* [m]	-
$\Sigma \mathrm{M}_{\mathrm{COM,jp}}$	Total moment about Craft COM	*Varies* [Nm]	-
M_{drag}	Moment as a result of rotational drag	*Varies* [Nm]	-
I	Moment of Rotational Inertia of Craft about central diameter	153.7 kgm^2	Ref Eq. 16
D_0	Assumed diameter of Craft if assumed cylindrical	1m	Assumed, based on image of Craft
ρ	Density of air. Assumed constant	1.2 kg/m^3	-
L	Length of parachute lines	10 m	Assumed, based on test photos
$\boldsymbol{F}_{\boldsymbol{pc}}$	Total force on the parachute	*Varies* [N]	-
$\boldsymbol{Fd}_{\boldsymbol{pc}}$	Total drag force on the parachute	*Varies* [N]	-
k	Spring constant of the parachute cord	250 KN/m	Assumed 550 Paracord [44]
$\boldsymbol{cv}_{\boldsymbol{end}}$	Unit vector of Craft velocity at end of freefall	*Varies* [unitless]	-
t	Time step used for MATLAB simulation	1x10^{-5} s	-

Values Recommended for Review:

Several of the values used are based on estimates. Area of the Craft is estimated visually, as well as the shape of the parachute and length of the parachute cords. The type of parachute cord is assumed. Because of these estimations, it is recommended the following values are reviewed:

$L, m_{jp}, m_{pc}, k, A_{parahori}, Cd_{parahori}, d, Cd_{jpvert}, Cd_{jphori}, A_{jpvert}, A_{jphori}, D_0, \boldsymbol{Wind}$

Variables to change whether simulating hover or horizontal cruise speed scenarios:

Variable	Value if Horizontal Cruise Simulation	Value if Hover Simulation
θ_{jp0}	10°	0°
vel_{x0}	23.6 m/s (with wind in direction of Craft)	0m/s
DT	1.2s	0.63s

Introduction and Objectives

The objective of this model is to simulate the Craft during the emergency descent phase. This model accounts for the dynamic movement of the parachute and Craft as separate entities coupled by a cord. The movements of the Craft and parachute are based on parameters such as the spring constant of the parachute line (outlined in “Table of Variables”) and assumptions outlined in “Assumptions”.

This model does not account for the events which occur on impact as the simulation operates only until the Craft reaches ground level.

The goal of the simulation is to explore how the Craft descends with a parachute in an emergency (i.e. when there is a power loss). This is done by modelling the fall profile of the Craft, assuming an initial horizontal (forward) velocity, Pilot or System Reaction Time (PRT) and parachute deployment angle before simulating to find the impact velocity from each initial height above ground. The velocity profile of the Craft can also be compared to velocity limits [40]. The velocity limit is the upper limit of survivable impact velocity.

The minimum height above ground at which the Craft can fly horizontally at cruise speed can be determined. Below this height it may be safe to ascend and descend vertically, however if the Craft is travelling horizontally, it must be at a higher initial height at the time of power loss to be slowed down to acceptable velocity than if it was in a hover. This is because the swinging motion of the Craft caused by the parachute results in extra vertical velocity during the emergency descent phase. This extra vertical velocity must be damped out, and therefore the Craft must be at a higher height above ground when it is at cruise speed to be decelerated to an allowable descent velocity. Increasing the horizontal velocity of the Craft also decreases the safe impact velocity in the vertical direction. If the horizontal impact speed of the Craft is 0m/s, the edge of the survival certainty zone for the vertical velocity is 12m/s. If the horizontal impact speed is 10m/s, the edge of this zone for the vertical velocity decreases to 11m/s.

Different values for the minimum height (Upper Limit of the Unsafe Deployment Zone – UDZ) are obtained based on differing assumed pilot/system reaction times and whether the Craft is simultaneously in the Ascent, Hover, or Descent phase of flight.

Assumptions

- The air is incompressible, inviscid and irrotational.
- The drag area of the parachute increases according during deployment follows an "S" shape (refer Figure 23)*
- The parachute reaches full inflation 1.2s after initiation. *
- Wind speed assumed to be a constant 8m/s at all heights, based on intended operation limits.
- It is assumed that the Craft has a maximum cruising airspeed of 15.6 m/s at the time of power loss. This is based on intended operation limits. The maximum allowable wind speed is added to this airspeed to obtain a maximum initial groundspeed of 23.6 m/s.
- The total system mass is 330kg. This is based on intended operation limits and therefore gives the highest estimate for impact velocity as the parachute must bear more weight.
- The parachute remains completely inflated after inflation process is complete. *
- Drag and tension are the only forces on the parachute at all times. The ballistic nature of the parachute is not accounted for.
- Due to the large mass ratio of the Craft and parachute, the ballistic release of the parachute is assumed to have negligible effect on the Craft motion.
- The parachute is launched at the same speed as the Craft from an assumed connection point at the top of the Craft. i.e. it has zero velocity relative to the Craft on launch, and gains relative velocity due to drag *
- The Parachute is assumed to deploy in the opposing direction to the Craft velocity
- The attachment point of the parachute is 1.1m above the Craft COM when the Craft is vertical. This is estimated based on a scale diagram of the Craft.*
- The attachment point of the cords to the parachute is the parachute COM*
- The time taken to deploy the parachute includes Pilot (or auto deploy) Reaction Time (PRT), the time in which the parachute system takes to fully deploy (1.2s) and the total firing system latency (0.114s). These values are based on industry estimates.
- The area of the frontal and plan forms of the Craft ($A_{jp-vert}$ and $A_{jp-face}$) are each assumed to be 1m^2. This is estimated based on a scale diagram of the Craft.*
- The Craft is the shape of a rhombus, orientated vertically.
- The drag coefficients of the Craft front and planform are assumed to be 2 and 1.1 [37], respectively. The Reynolds Number is assumed to always be above 10^5, meaning that the drag coefficients remain constant throughout the simulation.
- The parachute cord is 10m in length. This is estimated from test report photos.*
- The parachute cord is assumed to be 550 Paracord.*
- The parachute cord spring constant, k, is 250 KN/m [44]. *
- Data for ballistic parachutes suggests that there are 28 parachute lines [45], and so a total spring constant of 28*k was used for the simulation.*
- All cords are loaded with equal force when in tension.
- The drag coefficient of the Craft is the same from the top direction as from the bottom.
- The drag coefficient of the Craft is the same from the front direction as from the rear.

- The Craft only changes in pitch, not roll nor yaw. That is to say, the pilot only tilts forward and backward, not sideways. This is a result of the limitations of a 2D model. The initial Craft velocity only includes forward and vertical motion.
- The Craft has no lateral movement. A limitation of the 2D model is that this the motion of the Craft always remains in the same plane.
- The Craft has an initial orientation of 10° clockwise to the vertical for the freefall phase of descent. Craft orientation is only variable after parachute initiation.
- Any wind is only in the horizontal plane. There is no upward or downward air motion.
- The Craft is assumed to maintain the same orientation during freefall before parachute deployment is initiated. In reality this will change depending on where the crafts Centre of Pressure (COP) and Centre of Mass (COM) are located. *
- The forces on the parachute, including the drag force, act through the COM of the parachute at all times. The COP remains in the same location as the COM, and does not vary with parachute angle.
- The parachute does not collapse under a side wind.*
- The inertia of the Craft can be estimated assuming that the Craft is a cylinder with uniform density rotated about its central diameter.
- The parachute cord never exceeds its elastic limit.
- The spring constant of the parachute cord is constant and does not change with elongation
- Drop tests were performed from a crane with zero horizontal or initial velocity.
- All parachute cords have equal tension and are at the same angle relative to the Craft-parachute axis
- Environmental factors such as weather and bird strike have not been considered.
- The apparent mass (mass of air under the parachute canopy during and after inflation) is not considered.

* Recommended assumptions to check and refine

Free Body Diagrams and Reference Frames:

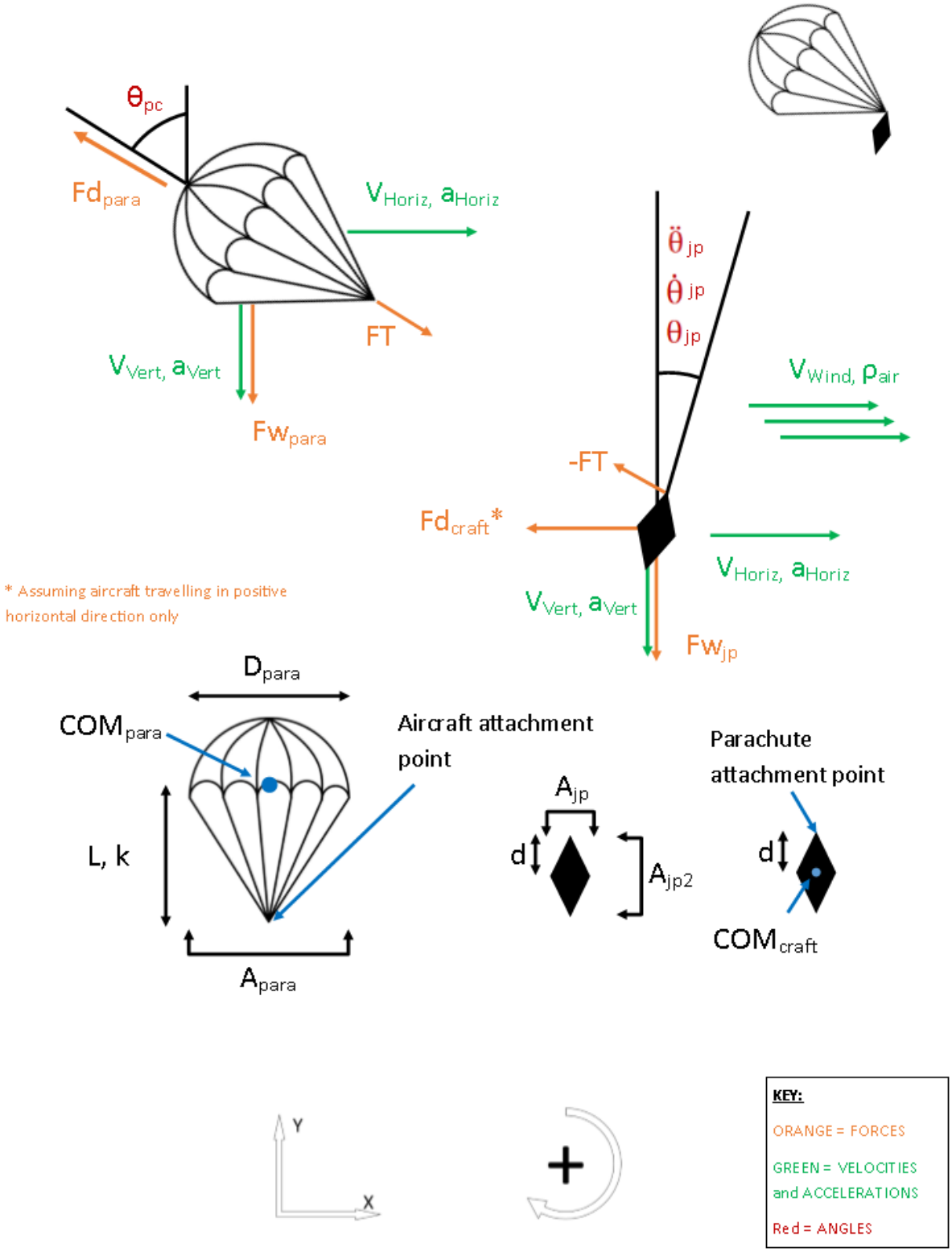

Figure 14: Free Body Diagrams and Reference Frames

Methodology

This section of modelling includes two stages – the initial freefall (Stage 1) and the descent of the Craft and parachute as a coupled system (Stage 2). The freefall stage of the Craft was performed similarly to that in the model in the previous chapter, "*Mathematical Modelling of the Parachute of the Martin Jetpack*", with differences as outlined in *Stage 1 Simulation*. In order to account for the tension force of the parachute cord, the combined parachute-Craft system was modelled as outlined in *Stage 2 Simulation.*

Figure 15 shows the Craft with the parachute deployed.

Figure 15: Craft with Parachute Deployed

Stage 1 Simulation

The inputs for Stage 1 are the frontal orientation of the Craft (10° in this simulation), the initial height above ground, and the horizontal and vertical velocities.

If the Craft is not travelling directly parallel or directly perpendicular to the wind, the drag force on the Craft will be a combination of air resistance on the top/bottom and front/rear faces of the Craft. This is outlined in Figure 16.

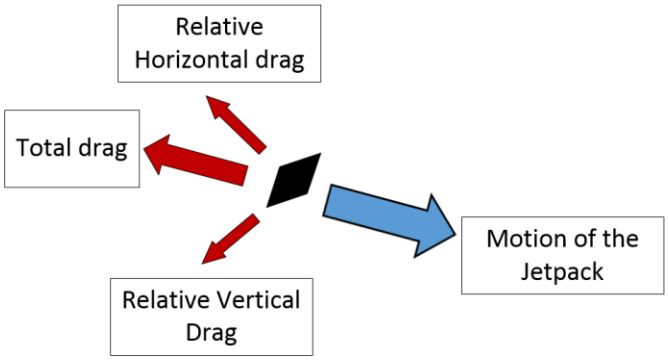

Figure 16: Drag on the Craft as a result of its Motion

The drag force on the Craft is always in the opposite direction to the velocity vector of the Craft. The amount of drag force that the Craft experiences is dependent on the ratio of the frontal and bottom drag areas of the Craft exposed to the velocity. For example, if the Craft was travelling at 45° to the wind velocity vector, then an equal ratio of drag from the relative horizontal and vertical directions would be combined to obtain a value for the total drag.

The drag force caused by an object moving through a fluid is determined by the density of the fluid, ρ, the velocity of the object, vel, the drag coefficient of the object, Cd, and the frontal area of the object, A. If all of these except for the velocity are constant for the duration of a time dependent simulation, as is the case with the horizontal and vertical motion of the Craft through the air, then the factors excluding velocity can be combined to form a "drag factor". Refer Eq's 1 and 2.

The total drag factor on the Craft changes depending on θ_{abs} (Eq. 4). In order to obtain a value for the overall drag factor, ratios of the drag factor resulting from a vertical (α_1) and horizontal (α_2) headwind on the Craft are taken (Refer Eq. 3). α_1 and α_2 are calculated using Eq's 1 and 2.

$$\alpha_1 = \frac{1}{2}\rho Cd_{jp-vert}A_{jp-vert} \tag{1}$$

$$\alpha_2 = \frac{1}{2}\rho Cd_{jp-face}A_{jp-face} \tag{2}$$

The orientation of the Craft relative to the direction that the Craft is travelling is calculated. This is done by obtaining the angle of the Craft velocity vector relative to the wind (θ_m) and the orientation angle of the Craft axis (θ_{jp}) to the vertical. This is outlined in Figure 17.

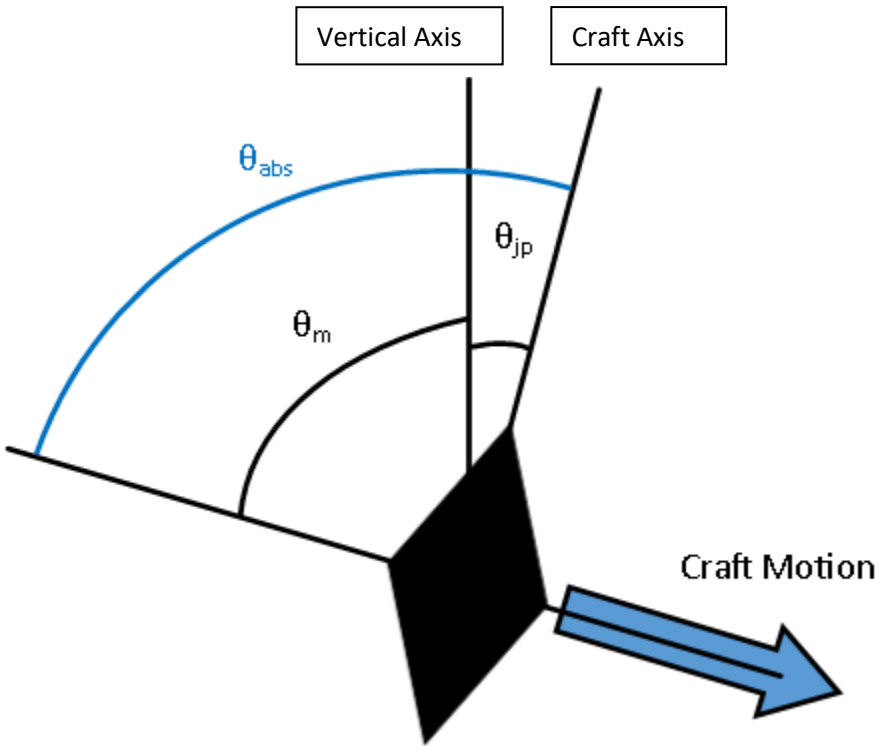

Figure 17: The Angle between the Motion of the Craft and its Absolute Orientation Angle

In Figure 17, θ_{jp} is positive and θ_m is negative because the positive vertical is the datum. If the Craft was to be tilted 90° anticlockwise from the position in Figure 17, θ_{jp} would be negative, however unless the motion of the Craft changed direction, θ_m would remain the same. If the Craft motion (but not the Craft orientation) changed anticlockwise by 90°, then θ_m would be positive because both $vel_{g,x}$ and $vel_{g,y}$ would be positive.

Obtaining the angle between Craft orientation and the velocity vector:

The angle of the relative velocity of the Craft to the air with respect to the vertical is calculated using Equation 3. Wind speed is subtracted from the ground speed of the Craft in order to obtain the speed of the Craft relative to the air.

$$\theta_m = \tan^{-1} \frac{vel_{g,x} - wind_{g,x}}{vel_{g,y} - wind_{g,y}} \quad (3)$$

Where $vel_{g,x}$ and $vel_{g,y}$ are the velocities of the Craft in those respective directions relative to ground, and likewise for the wind components.

θ_{jp} is assumed at the beginning of the simulation. The difference between the two angles is calculated. Refer Equation 4.

$$\theta_{abs} = \theta_{jp} - \theta_m \tag{4}$$

Drag Force on the Craft

The total drag factor based on the angle of the Craft to the air (including wind speed) is calculated using Equation 5. This accounts for drag from the front/rear and top/bottom of the Craft.

$$\alpha_{abs} = \sqrt{(\alpha_1 \cos(\theta_{abs}))^2 + (\alpha_2 \sin(\theta_{abs}))^2} \tag{5}$$

Equation 6 is then used to calculate the total drag force on the Craft. This multiplies the drag factor by the square of the absolute velocity to obtain an absolute force. This is then multiplied by a unit vector of the Craft's velocity relative to the wind to scale the force into x and y components. Again, the wind velocity is subtracted from the Craft ground velocity to obtain the Craft velocity relative to the air.

$$\boldsymbol{Fd_{craft}} = -\alpha_{abs} \times norm\left(\boldsymbol{vel_g} - \boldsymbol{wind_g}\right)^2 \times \frac{\boldsymbol{vel_g} - \boldsymbol{wind_g}}{norm\left(\boldsymbol{vel_g} - \boldsymbol{wind_g}\right)} \tag{6}$$

Where $\boldsymbol{vel_g}$ and $\boldsymbol{wind_g}$ are 1x2 vectors containing the x and y components of the Craft and wind velocity relative to ground, respectively.

Equations 3-6 were used to calculate the drag on the Craft in all stages of simulation

Total Force on the Craft

The total force on the Craft is then calculated (Equation 7). The two forces acting on the Craft are the weight of the Craft and the drag resulting from its motion.

$$\boldsymbol{F_{jp}} = \boldsymbol{Fd_{craft}} + m_{TOT}\boldsymbol{g} \tag{7}$$

Newton's 2nd law is then used to calculate the acceleration on the Craft. The velocity and position are then calculated using a first order Euler Method. This iterates as per the first model until 1 of 2 events occurs:

1. The Craft impacts the ground
2. The amount of time necessary to initiate parachute deployment has passed

If Event (2) occurs, the parachute has deployed and Stage 2 Simulation commences.

Stage 2 Simulation

The parachute and Craft were considered as independent entities, coupled only by the parachute cord. The cord was modelled as a spring between the 2 masses.

The connection point from the Craft to the parachute is assumed to be a frictionless pin joint. This is the point through which the cord can apply a force or torque to the Craft. A pin joint was chosen because it allows the Craft to rotate independently of the parachute, while allowing the parachute to apply a translational force.

Figure 18 and Figure 22 show the free body diagrams of the parachute and Craft which were considered for this simulation:

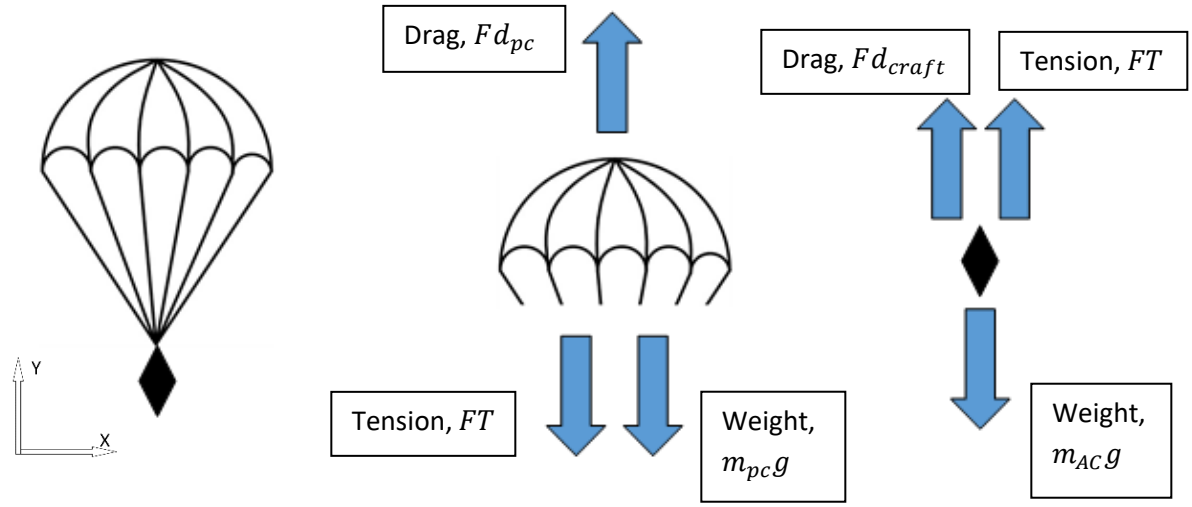

Figure 18: The Forces on the Parachute and Craft

When the coupled system is on an angle, the angle of some of the forces change and some do not. This is outlined in Figure 22. Figure 22 assumes that the motion of the Craft is directly downwards, hence the drag in the positive vertical.

The Addition of Parachute Dynamics

The Craft is assumed to maintain the same orientation during freefall. In reality this will change depending on where the crafts Centre of Pressure (COP) and Centre of Mass (COM) are located. The initial position and velocity vectors of the Craft in Stage 2 were the final vectors which were calculated during Stage 1.

After freefall the Craft was assumed to have the ability be rotated or translated by the parachute. The extent to which the Craft was rotated or translated depends on the relative angle of the Craft and parachute, and whether there is tension in the cord.

The relative angle of the Craft and parachute was calculated using Eq. 8

$$\theta_{diff} = \theta_{jp} - \theta_{pc} \tag{8}$$

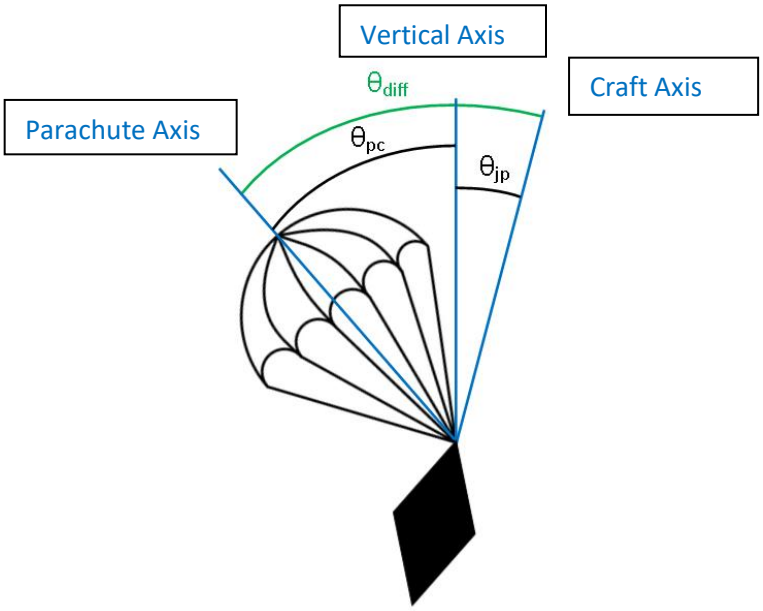

Figure 19: Angle of Craft and Parachute

The proportion of the force which acts to translate and rotate the Craft can be calculated using Eq's 9 and 10 respectively. Eq 9 calculates the proportion of the tension force modelled as acting through the Craft COM, and then distributes that force into global X and Y coordinates.

$$\boldsymbol{F_{trans}} = |\boldsymbol{FT}| \cos(\theta_{diff}) \left[\sin(\theta_{jp}) \ \cos(\theta_{jp})\right] \tag{9}$$

$$F_{rot} = |\boldsymbol{FT}| \sin(\theta_{diff}) \tag{10}$$

Figure 20 shows how the total tension force is split into the translational and rotational components.

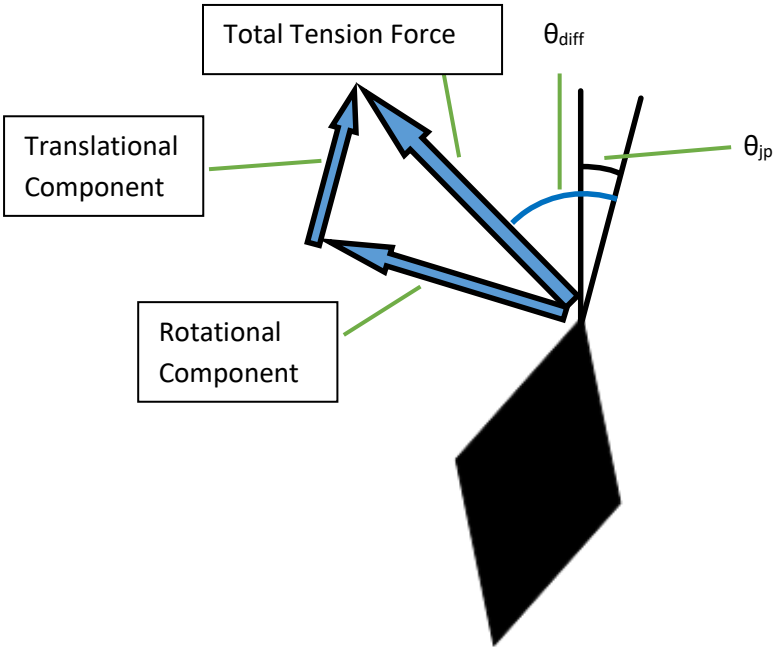

Figure 20: Tension Force Result on Craft

When there is tension in the cord, the total force on the Craft then becomes:

$$\boldsymbol{F_{jp}} = \boldsymbol{F_{trans}} + m_{jp}\boldsymbol{g} + \boldsymbol{Fd_{craft}} \quad (11)$$

2 forces were assumed to be acting on the Craft which result in its rotation about its COM (Centre of Mass):

1. The tension force in the cord perpendicular to the Craft, and
2. The drag on the Craft caused by its rotational velocity.

The rotation of the Craft is accounted for by modelling the connection point of the parachute to the Craft. It is assumed that this point is 1.1m above the crafts COM, approximately half the height of the Craft based on best industry data estimates.

The rotational drag on the Craft was considered by assuming that the Craft was a flat plate, and that the rotational drag encountered by the Craft could be modelled half way between the COM and the top/bottom-most point on the Craft, although a more accurate COP position would be $d/\sqrt{2}$. Figure 21 shows the assumed details relevant to modelling the rotational drag. The moment due to rotation can be calculated using Eq 12.

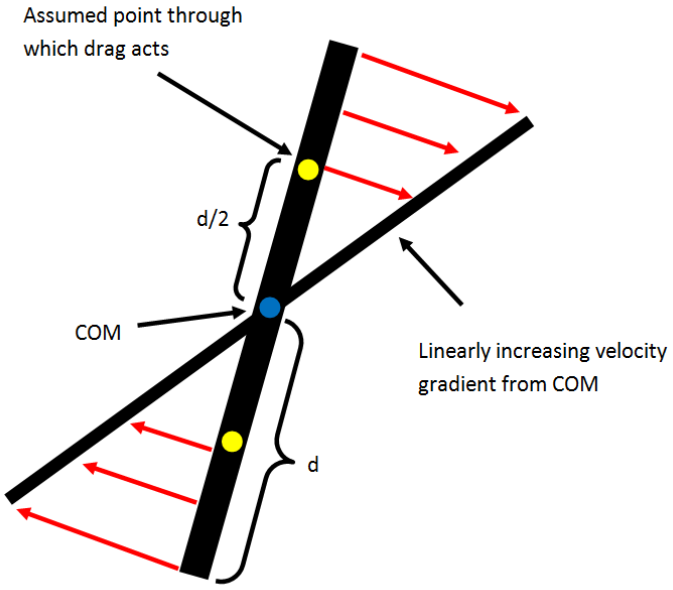

Figure 21: Rotational Drag on Craft

$$M_{drag} = 2 \times \frac{1}{2}\rho\left(\dot{\theta}_{jp}\frac{\pi}{180}\frac{d}{2}\right)^2 Cd_{plate}A_{Plate} \times \frac{d}{2} \tag{12}$$

Where $\dot{\theta}_{jp}$ is in degrees, and the coefficient of 2 represents the 2 plates modelled from the points on the Craft above and below the COM. The $\pi/180$ term converts the velocity from degrees to the radians required. The bracketed term is the tangential velocity at $\frac{d}{2}$. The final $\frac{d}{2}$ is the moment arm.

When there is tension in the cord perpendicular to θ_{jp}, a moment will be applied to the Craft. The lever arm through which the moment acts to crate this moment is assumed to be the assumed distance from the Craft COM to the connection point, d. A new rotational position of the Craft can be determined using the following set of equations and Euler's Method in rotational coordinates:

$$\Sigma M_{COM,jp} = F_{rot}d - M_{drag} \tag{13}$$

$$\ddot{\theta}_{jp,rad} = \Sigma M_{COM,jp}/I \tag{14}$$

$$\ddot{\theta}_{jp} = \frac{\ddot{\theta}_{jp,rad}}{\pi \times 180} \tag{15}$$

The Craft inertia, I, is modelled as a solid cylinder of uniform density rotating about its central diameter. The inertia can be calculated using Eq. 16, where the central diameter, D_0, is assumed to be 1m and the length of the cylinder is the height of the Craft, $2d$, or 2.2m.

$$I = \frac{1}{4} m_{jp} \left(\frac{D_0}{2}\right)^2 + \frac{1}{12} m_{jp} (2d)^2 \tag{16}$$

The angle at which the parachute is released is assumed to be in the opposite direction to the velocity vector of the Craft relative to the wind. It is assumed to have the same velocity as the Craft. This is calculated using Equation (17) to define a unit vector for the desired direction of deployment:

$$\boldsymbol{cv_{end}} = -\left(\frac{\boldsymbol{vel_g}}{norm(\boldsymbol{vel_g})}\right) \tag{17}$$

The vector, cv_{end}, was used as a multiplier to give an initial position of the parachute. The model breaks if the parachute and its attachment point to the Craft are in the same location because θ_{GLOBAL} is calculated using the relative positions of the 2 entities (Eq (21)). If the simulation detects that the relative positions of the entities are the same, then an error message will be presented and the simulation will end.

The final position and velocity of the Craft COM at the end of Stage 1, u_{jp} and u_{jp2}, respectively, were the values used at the beginning of Stage 2.

$$\boldsymbol{u_{jp2}} = \boldsymbol{u_{jp}} + \left[dsin(\theta_{jp}) \quad dcos(\theta_{jp})\right] \tag{19}$$

$$\boldsymbol{u_{pc}} = \boldsymbol{u_{jp2}} + 0.0001\ \boldsymbol{cv_{end}} \tag{20}$$

The angle of the parachute is calculated using Equation 21.

$$\theta_{GLOBAL} = \tan^{-1} \frac{u_{pc,x} - u_{jp,x}}{u_{pc,y} - u_{jp,y}} \tag{21}$$

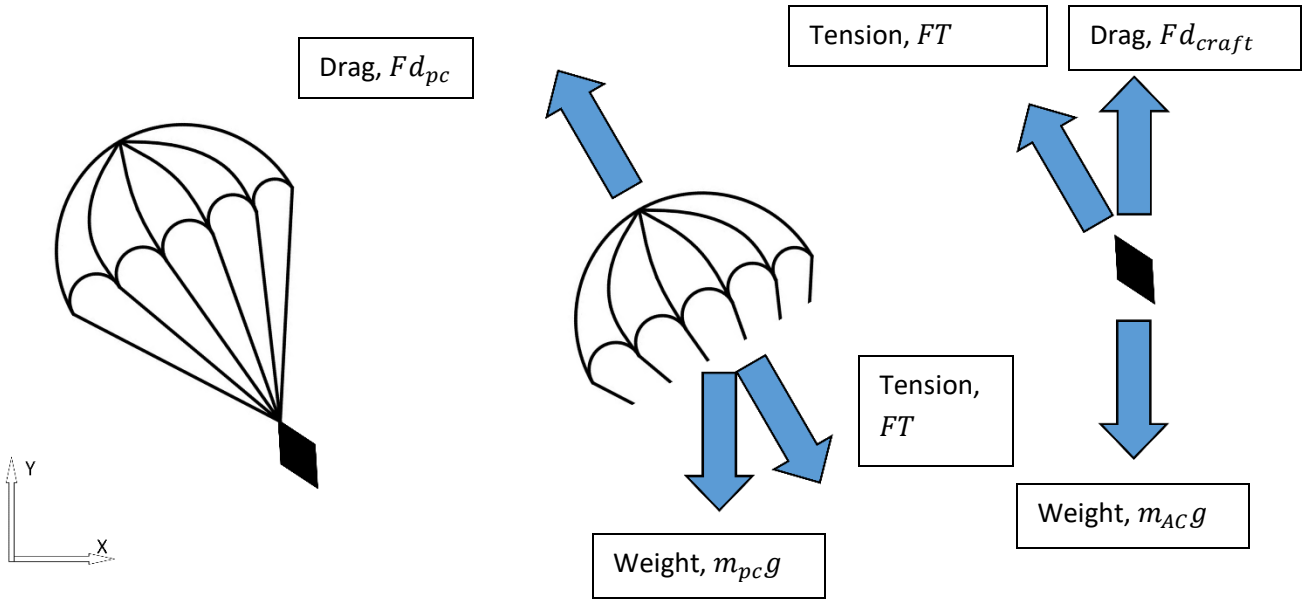

Figure 22: Forces on Angled System

The drag area ratio is used as in the 1D model, with the exception that the deployment time is assumed to be 1.2s, instead of 0.63s.

Figure 23 shows the best available estimate of the drag area ratio from industry data. This closely matches the trend for drag area shown in Figure 24. Poole [46] uses an exponential function to simulate canopy growth. The function can be used to calculate canopy drag force during inflation. Full inflation is assumed to occur after 1.2s.

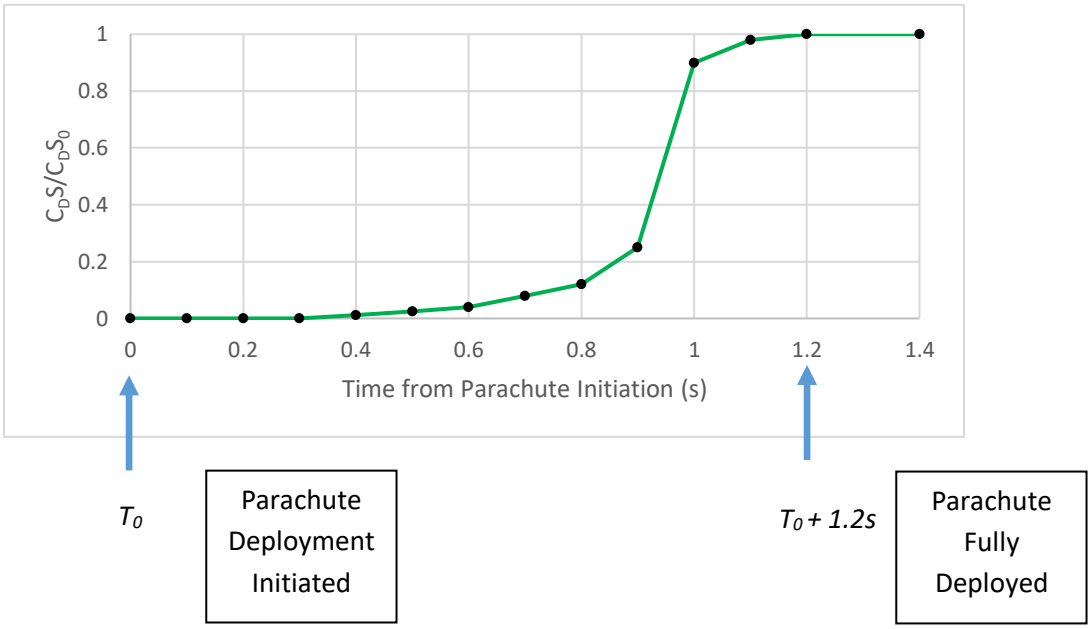

Figure 23: Drag Area Growth in Simulated Parachute

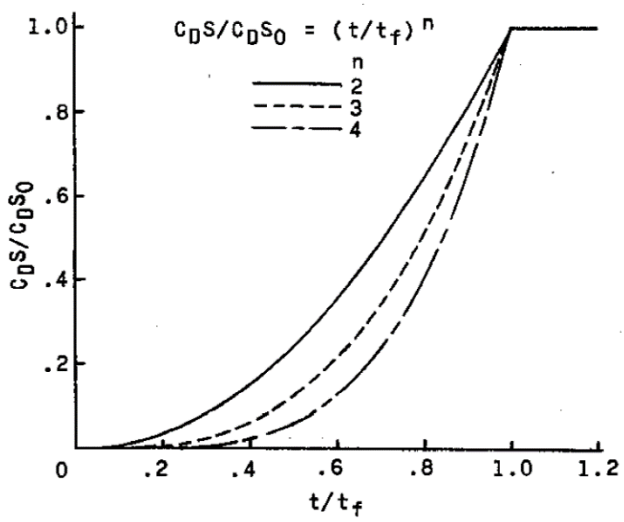

Figure 24: Canopy Drag Area Growth Functions [46]

Where:

C_DS is the instantaneous drag area of parachute canopy during full inflation
C_DS_0 is the drag area of the parachute canopy at full inflation
t is the time from bag strip
t_f is the filling time (from bag strip to inflation)
n is an exponential power, dependent on the system being explored

The distance between the parachute and the Craft is determined by taking the difference of the position vectors of the parachute COM and the attachment point of the parachute to the Craft in space. In the case that there is no tension in the cord, the extension is considered to be zero. The extension in the cord is calculated using Eq. 22:

$$du = \max(0, norm(\boldsymbol{u_{pc}} - \boldsymbol{u_{jp2}}) - L) \tag{22}$$

Where u_{pc} and u_{jp2} are 1x2 vectors which describe the position (in x,y coordinates) of the parachute and where the parachute cord attaches to the Craft, respectively. It is assumed that the cord attachment point on the parachute is the parachute COM. du is the extension in the cord. This extension is the difference between the actual length (including extension) and the no-load length, L (no extension).

The tension force between the parachute and Craft is calculated using Eq. 23.

$$\boldsymbol{FT} = k \times du \times \frac{(\boldsymbol{u_{pc}} - \boldsymbol{u_{jp2}})}{du + L} \tag{23}$$

Eq. 23 uses Hooke's Law, $F = k \times du$, and then gives the force a direction by multiplying it by a unit vector which accounts for the relative positions of the Craft and parachute. The direction of the tension force on the parachute is therefore towards the Craft, and the tension force on the Craft is directed towards the parachute. The tension force on the Craft is of equal magnitude and opposite direction to the tension force on the parachute.

Equation 24 adds the tension, drag and weight forces on the Craft.

$$\boldsymbol{F_{jp}} = \boldsymbol{FT} + \boldsymbol{Fd_{craft}} + m_{jp}\boldsymbol{g} \tag{24}$$

The drag force on the parachute is calculated using Eq. 25. The methodology of calculating the drag factor on the parachute, α_{pc}, is the same as calculating that of the Craft (Eq's 1-6, areas and drag coefficients of the parachute used in place of the crafts.)

$$\boldsymbol{Fd_{pc}} = SF \times \alpha_{pc} \times norm(\dot{\boldsymbol{u}}_{\boldsymbol{pc,g}} - \boldsymbol{wind_g})^2 \times \left(\frac{\dot{\boldsymbol{u}}_{\boldsymbol{pc,g}} - \boldsymbol{wind_g}}{norm(\dot{\boldsymbol{u}}_{\boldsymbol{pc,g}} - \boldsymbol{wind_g})}\right) \tag{25}$$

Where:

$$\alpha_{pc} = \sqrt{\left(\left(\frac{1}{2}\rho C d_{para,vert} A_{para,vert}\right)\cos(\theta_{diff,pc})\right)^2 + \left(\left(\frac{1}{2}\rho C d_{para,hori} A_{para,hori}\right)\sin(\theta_{diff,pc})\right)^2}$$

$\dot{\boldsymbol{u}}_{\boldsymbol{pc,g}}$ is a 1x2 vector containing the velocity of the parachute in x and y.

Equation 26 adds the tension, drag and weight forces on the parachute.

$$\boldsymbol{F_{pc}} = -\boldsymbol{FT} - \boldsymbol{Fd_{pc}} + m_{pc}\boldsymbol{g} \quad (26)$$

Newton's Second Law is then used to calculate the acceleration on each the parachute and Craft given the forces. Euler's method was then used to determine the new velocity and position of the Craft and parachute. From these new positions, a new du can be determined, and so the cycle repeats.

Convergence Study

Each iteration in this model relies on information from the previous iteration. A convergence study was performed to determine the maximum time step which can be used. The study relied on 2 main parameters, the spring constant of the cord, k, and the time step, dt. The higher the spring constant of the cords, the lower the value of the maximum timestep could be. If the time step was too low and the k value too high, then the cord would oscillate between being in tension and being slack over one timestep. This is shown in Figure 25 where the timestep is 0.001s. The system is not stable in this scenario. Figure 26 shows the tension force for the same simulation using a timestep of 0.00002s.

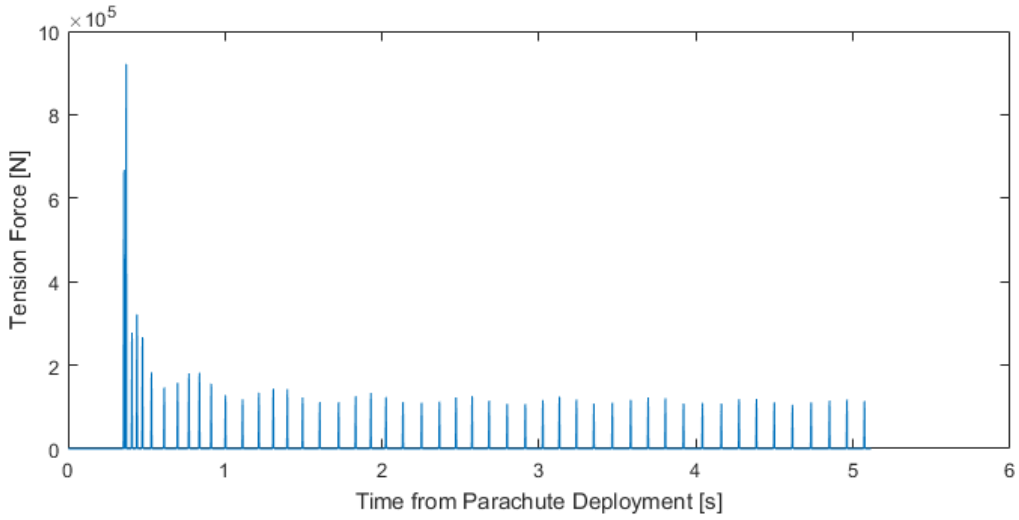

Figure 25: Unstable Simulation, dt = 0.001s

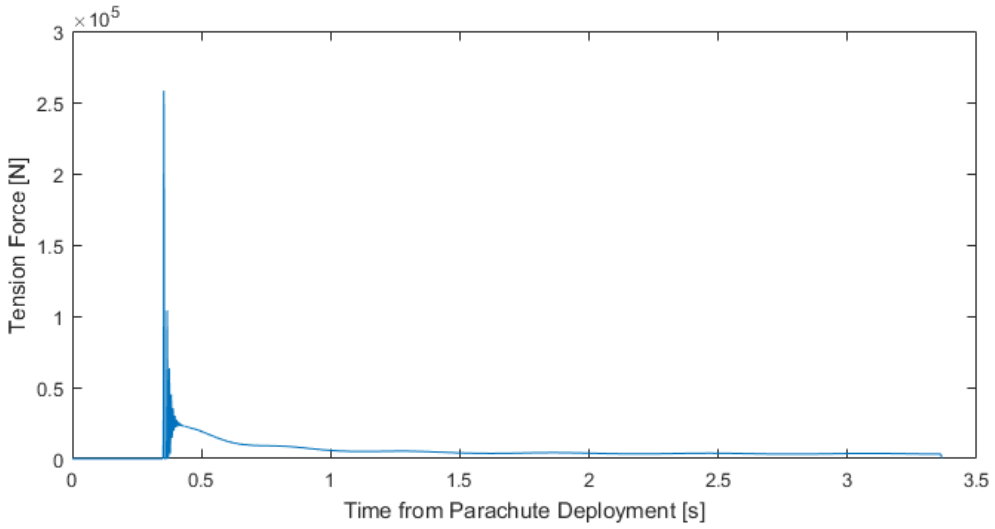

Figure 26: Stable Simulation, dt = 0.00002s

Table 12 (Appendix 2) shows the comparison of time step values and k values which were measured. For a k value of 7 x10^6 N/m, a timestep of dt = 0.0001s will capture parameters such as the position vectors to within 0.2% of the value which would be obtained if a timestep of 0.00005s was used. Capturing the maximum tension force in the cord requires a value for dt of 0.00001s. Simulations showed that this will produce values ± 0.6% of the maximum tension force obtained if a time step of 0.000005 was used.

Parachute Rotation

In this model it is assumed that the parachute COM is the same point as where the cord attaches to on the parachute. The drag factor of the parachute varies with its rotation in the same way as the crafts: the angle to the oncoming air velocity determines the total drag factor on the parachute. If the oncoming velocity is side-on to the parachute, then the side of the parachute will be the only area producing drag. Conversely, if the oncoming velocity towards the parachute is solely in its vertical direction, then the entirety of the drag force produced by the parachute will be in the vertical direction relative to the parachute.

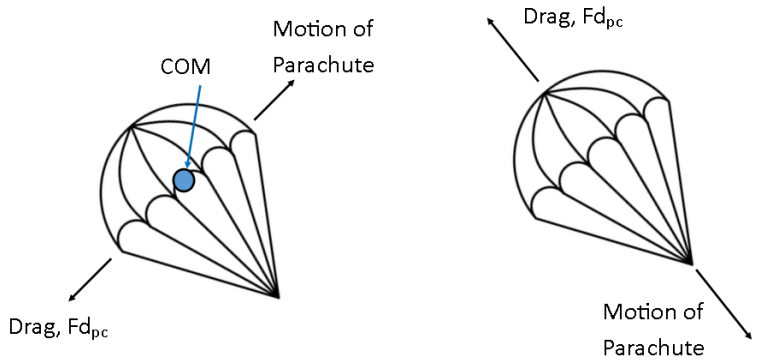

Figure 27: Drag Force on the Parachute as a Result of its Motion in its relative horizontal (Left) and vertical (Right) Planes

A limitation with the model is that if the parachute happens to be travelling inverted, it is assumed that the top of the parachute will provide as much drag as the underside, and any scenario which may cause the parachute to collapse is not captured in the model.

Results

Descent Profile

Figure 28 shows the profile of the descent of the parachute and Craft for initial groundspeeds of 0 and 15.6m/s. Both instances assume 8m/s constant wind in the same direction as groundspeed. Groundspeed is plotted as opposed to airspeed. This is because if the Craft is hovering relative to the ground and the wind speed is 8m/s, then the airspeed of the Craft is 8m/s, but the groundspeed is 0.

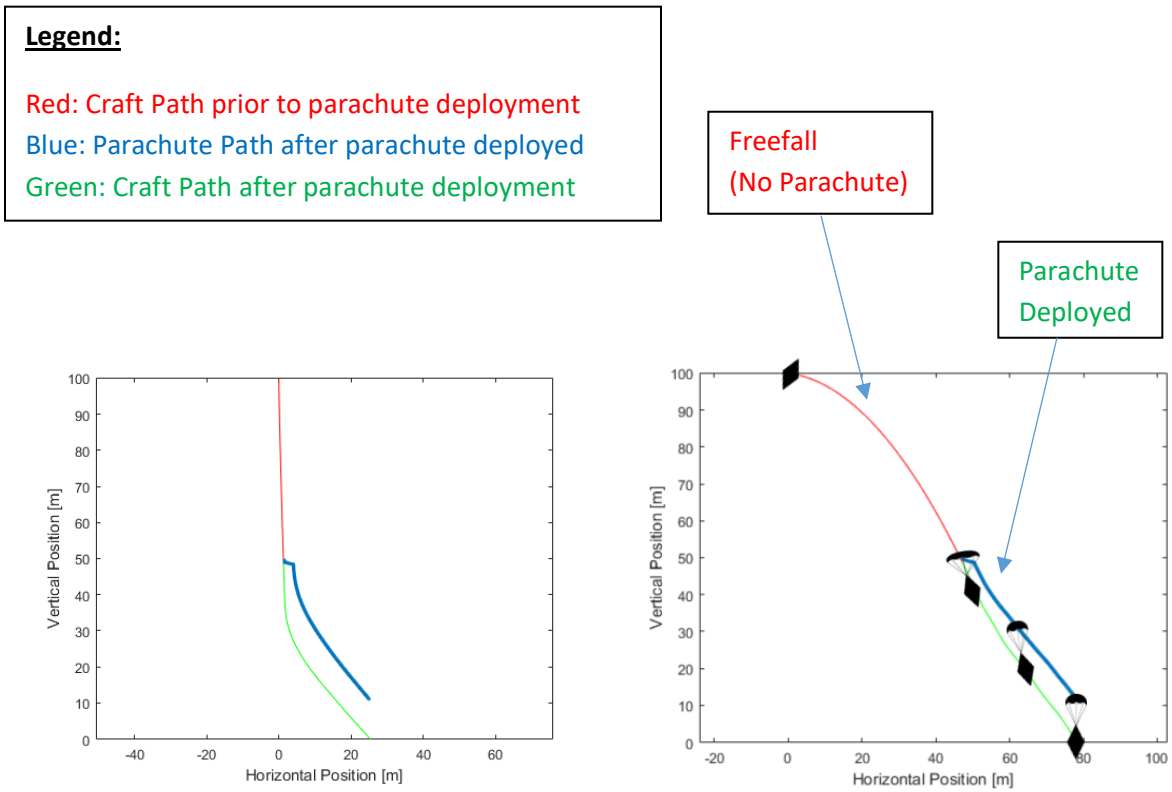

Figure 28: Descent Path of Parachute and Craft System for Initial Groundspeeds of 0m/s (Left) and 15.6m/s (Right)

Both plots in Figure 28 have the following initial conditions:

- Vertical Velocity: 2m/s downwards
- Height at power loss: 100m
- Reaction Time to Deploy parachute: 3s
- Wind velocity: +8m/s

Calculating the Upper Limit of the UDZ (Unsafe Deployment Zone)

The UDZ is a range of fall heights from which the Craft will impact the ground at an unsafe velocity. The lower limit of the UDZ is determined by the landing gear of the Craft. There will be a maximum height above which the landing gear will not safely absorb the impact. The upper limit is determined by the parachute system. The parachute system requires time to deploy and decelerate the Craft, so there will be a fall height below which the parachute cannot deploy and decelerate the Craft to a safe velocity before impact. If the upper limit of the UDZ can be eliminated, or made to be below the lower limit, then the Craft will impact the ground at a safe velocity from any fall height. Figure 29 shows the UDZ in the case where the parachute lower limit is higher than the landing gear upper limit (Left), and the UDZ eliminated (Right).

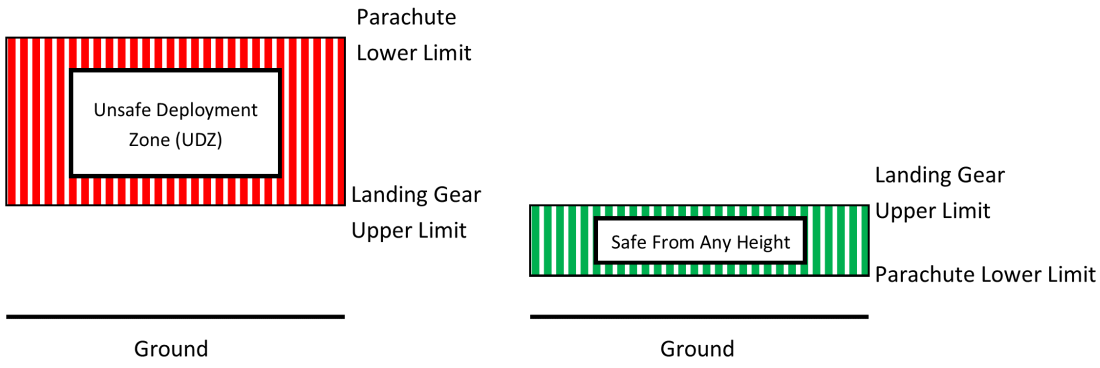

Figure 29: Diagram of UDZ, Present (Left) and Eliminated (Right)

NASA [40] states that a tolerable impact speed for a human is 10m/s in the vertical and 10m/s in the horizontal directions, simultaneously. However, in the current model the Craft oscillates around 10m/s in the vertical, and takes time to settle below this limit. With the Craft oscillating as it does, it is not possible to gather accurate data for the upper limit of the UDZ, as observations of parachuting objects [47-49] reveal that in reality the oscillatory motion of the Craft in this model relative to the parachute (refer Figure 30) is excessive. These observations of parachuting objects show that the motion of the parachute and object are observed to be the same; after the alignment of the object and parachute, they tend to oscillate together.

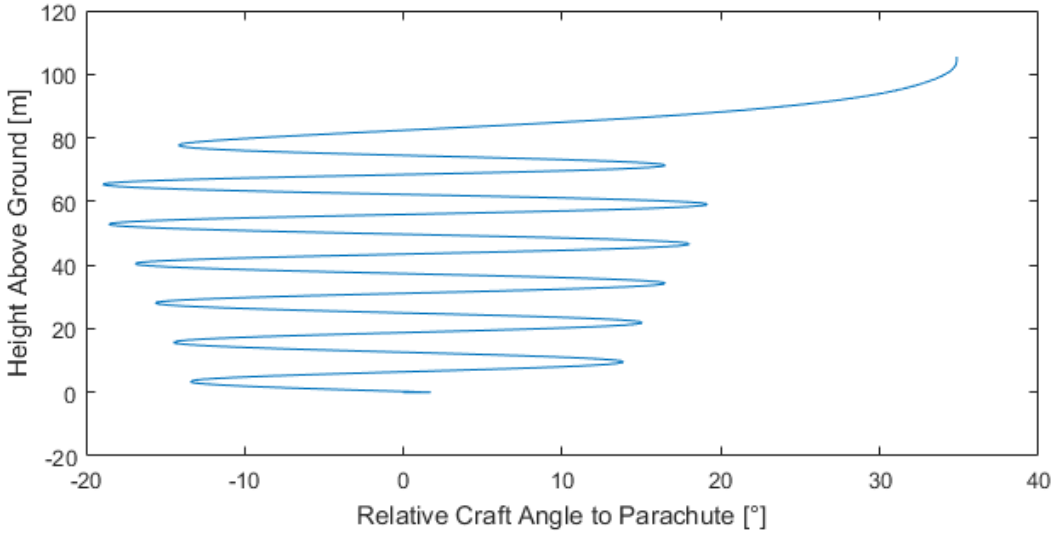

Figure 30: Craft Oscillations with Wind Included

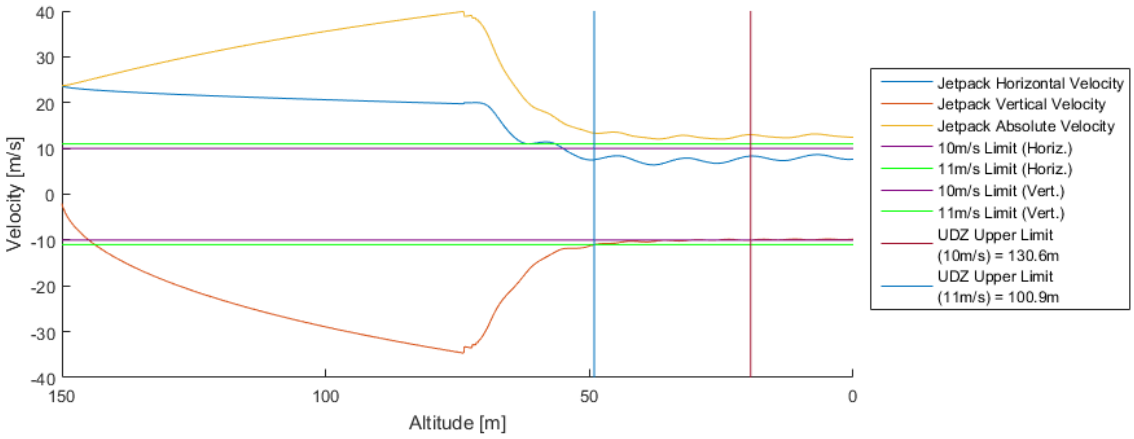

Figure 31: Velocities of the Craft if Undamped

Figure 31 shows that with these oscillations, the horizontal velocity is quickly decelerated to below the 10m/s threshold, while the vertical velocity oscillates above and below this threshold for 11m before settling below it.

The simulation can be altered to reduce the observed effects of the Craft oscillations on the upper limit of the unsafe deployment zone. Three ways which this can be achieved are:

1. Increase the permissible vertical impact velocity to 11m/s. Figure 31 shows that with the Craft oscillations the vertical velocity to settles below 11m/s considerably faster than below 10m/s. Increasing the limit of the vertical velocity to 11m/s is plausible, however a limit of 10m/s in the

horizontal and 11m/s in the vertical is no longer within the bounds of certain survival, but on the border of certain and marginal survival. The safe zone of the NASA plot suggests that up to ~12m/s is acceptable if in the vertical only.

2. Add a damping factor to damp out the oscillations of the Craft about the parachute attachment point.
3. Replacing the pin-jointed assumption with a more accurate model of how the parachute connects to the Craft. This model assumes that there is a sole parachute attachment point on each the Craft and parachute. In reality the cords could connect to different parts of each entity. This could change the damping properties, though it is currently unknown how these properties would change and to what extent.

Permissible Impact Velocity of 11m/s

Increasing the permissible vertical impact velocity to 11m/s is only valid in situations where the horizontal velocity is below 10m/s on impact. If the Craft is not travelling below this horizontal limit, then the edge of the zone of human survival is exceeded.

Figure 32 shows that the 11m/s limit is valid for power loss heights above 27.6, 53.0 and 95.0m for a PRT of 0, 1.5 and 3 seconds, respectively, because from these heights the parachute is able to decelerate the Craft to 10m/s in the horizontal before the Craft impacts the ground. These heights are calculated by: [initial height at power loss] – [height at which both horizontal and vertical velocity remain below limits].

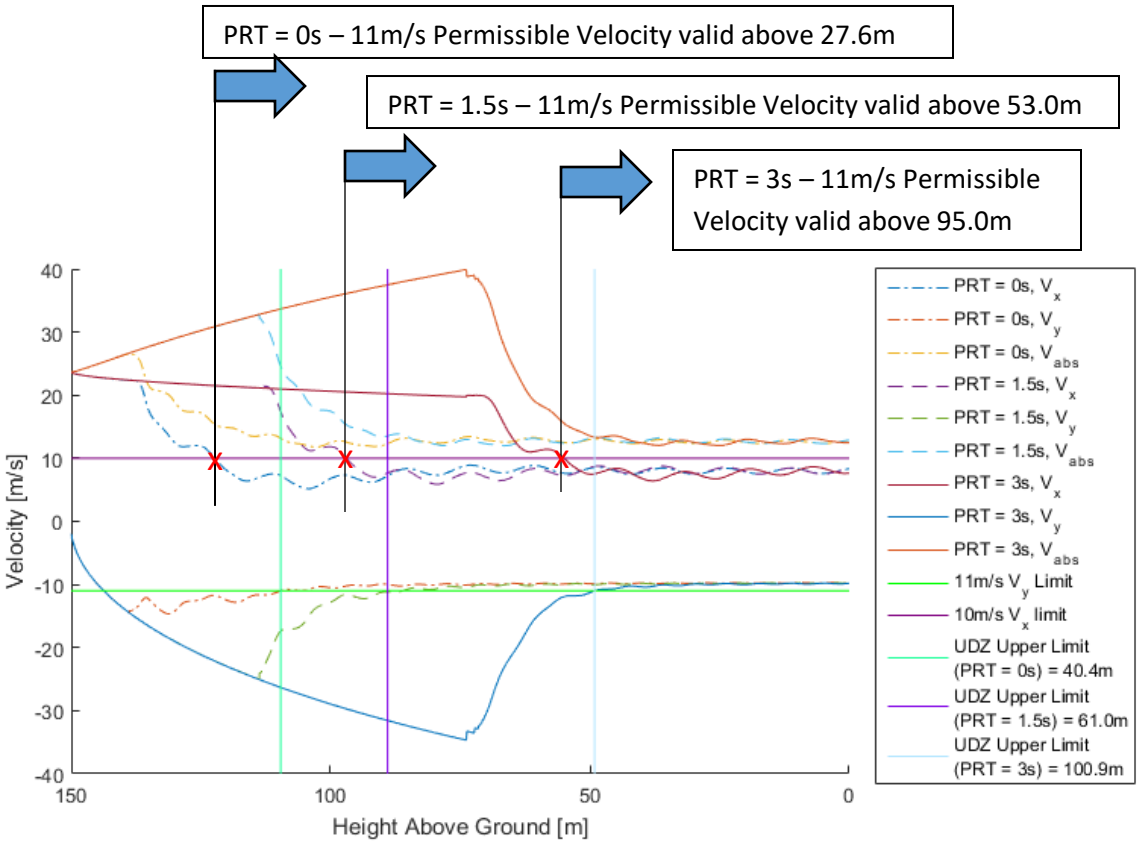

Figure 32: Horizontal, Vertical and Absolute Craft velocities during descent for a PRT of 0, 1, 2, and 3 seconds for the undamped system

At a height of 74m for PRT = 3s, there is a discontinuity in the velocity. This suggests that the Craft is subjected to a large acceleration at the moment of deployment.

The upper limit of the UDZ increases with increasing PRT at an increasing rate. This is expected as at larger PRTs the Craft in in freefall for a longer time. The Craft falls further at a larger velocity each passing moment the parachute is not deployed, due to gravity.

Altering the permissible velocity upon impact can be dangerous as it is no longer a conservative estimate. Changing the permissible impact velocity to 11m/s is plausible, though this method only applies above certain fall heights and is therefore not usable in all cases.

Artificial Damping

A damping factor of was added into the model to damp out the Craft oscillations. Different damping constant values were tested, and a damping constant of 20 Nms/radian more closely emulates what is observed in [47-49] than an undamped model. A value of 20 Nms/radian is approximately 20x the damping of a human knee joint when at 40° and 105° [50].

Figure 33 describes the velocity profile of the Craft when its oscillations are artificially damped. This is compared to the velocity profile of the Craft when there is no damping and the Craft is free to oscillate like a pendulum around the connection point of the parachute. The damped oscillations cross the threshold of -10m/s in the vertical within 31.6m altitude loss after parachute initiation. The parachute requires 2.26s from initiation to decelerate the Craft to -10m/s, as shown in Figure 34.

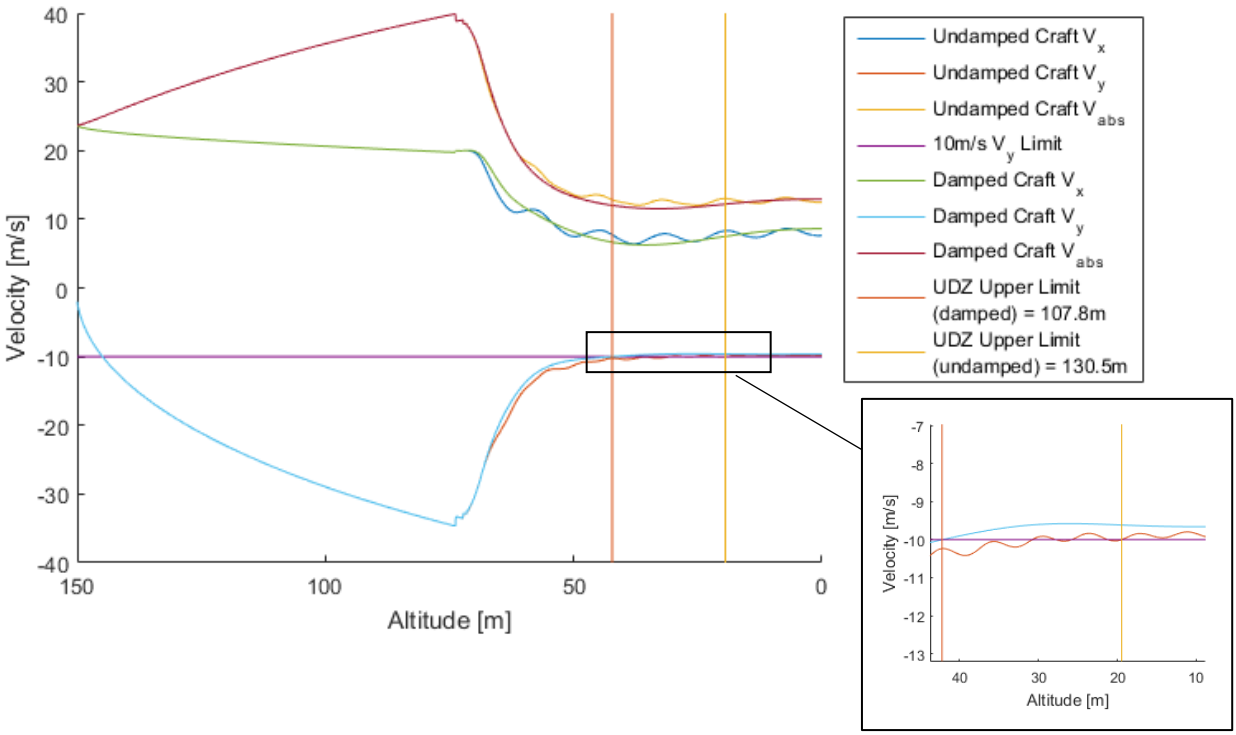

Figure 33: Velocity Profile With and Without Damping
PRT = 3s, Height at Power Loss = 150m, Wind = +8m/s, V_{y0} = -2m/s

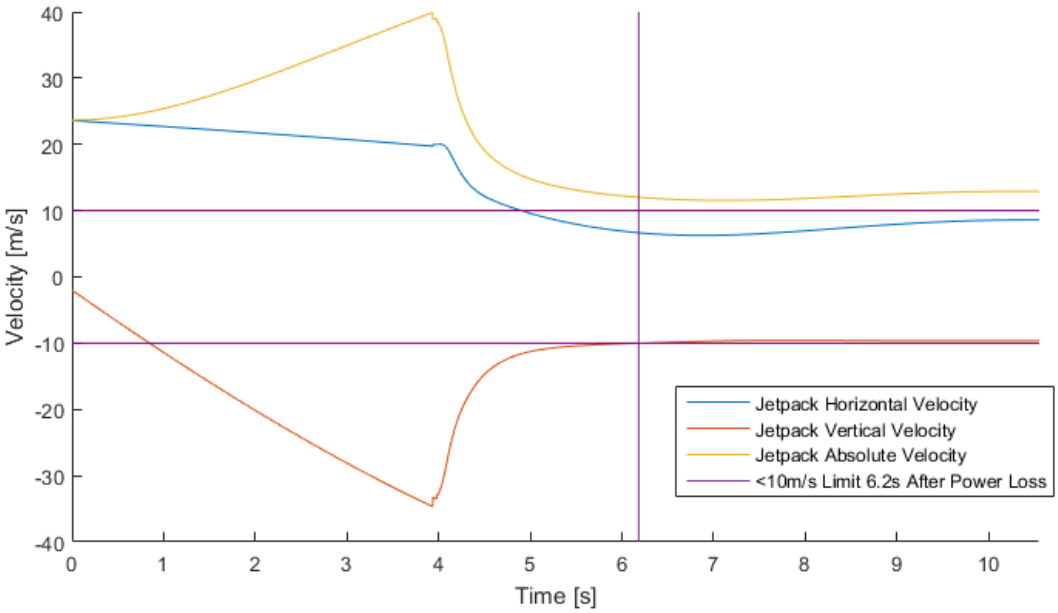

Figure 34: Velocity Profile with Damping over time
PRT = 3s, Height at Power Loss = 150m, Wind = +8m/s, V_{y0} = -2m/s

The method of adding artificial damping has been used for future simulations. Adding artificial damping is a realistic estimate of Craft behavior because it closely matches the observed oscillations of objects under a parachute. This method has no known limiting cases.

Comparison of Cruise Speed and Hover as Initial Condition

Figure 35 shows the upper limit of the UDZ for the Craft in hover and cruising speed cases. The upper limit is calculated for a range of reaction times for when the Craft is travelling at cruise speed and when it has zero initial ground speed. When the Craft is travelling, the UDZ increases for each successive reaction time. A higher initial velocity means that the parachute must decelerate the Craft more, increasing the time in which the Craft slows to a safe velocity and in turn the height needed to reach this velocity.

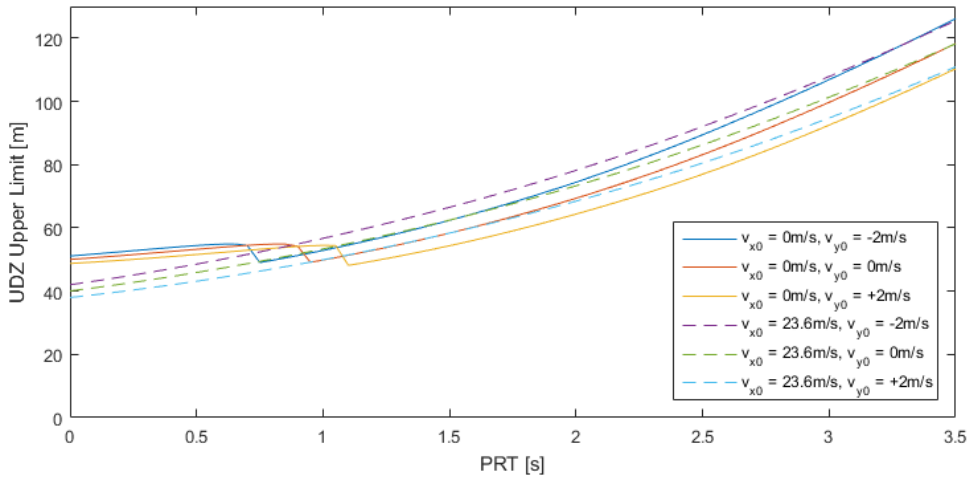

Figure 35: Cruise Speed and Hover as Initial Horizontal Velocity Conditions, DT = 1.2s in both cases, $V_{x, lim}$ = 10m/s, $Vy_{, lim}$ = 10m/s

At PRTs of approximately 1s and under, the hover condition results in a higher upper limit for the UDZ. There is a discontinuity at PRTs of ~1s. This is because at PRTs of ~1s and below, the parachute decelerates the Craft in the vertical direction to $V_{y, lim}$ before decelerating the Craft to $V_{x, lim}$ in the horizontal. This makes $V_{x, lim}$ the critical velocity, which is why the UDZ is higher for a hover than at cruising speed for lower PRTs.

The horizontal velocity of the Craft with zero initial airspeed exceeds the horizontal limit by 0.3m/s in Figure 36. The horizontal limit is increased to 12m/s for some of the following cases. This is no longer conservative as this limit lies on the border of certain survival and marginal survival [40].

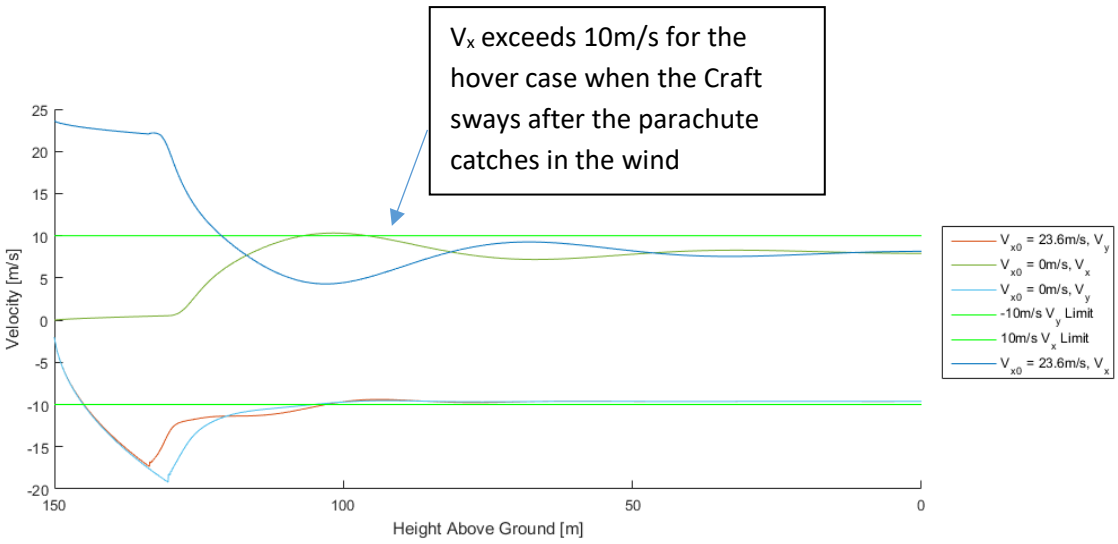

Figure 36: Velocity of Craft – Hover vs. Cruise Speed Scenario, PRT = 0.5, Artificial Damping Included

Comparison of Wind Conditions

Figure 37 shows a comparison of UDZs with and without the effects of an 8m/s (groundspeed) wind in the direction of the Craft motion. Craft assumed travelling 0m/s initial groundspeed in both cases.

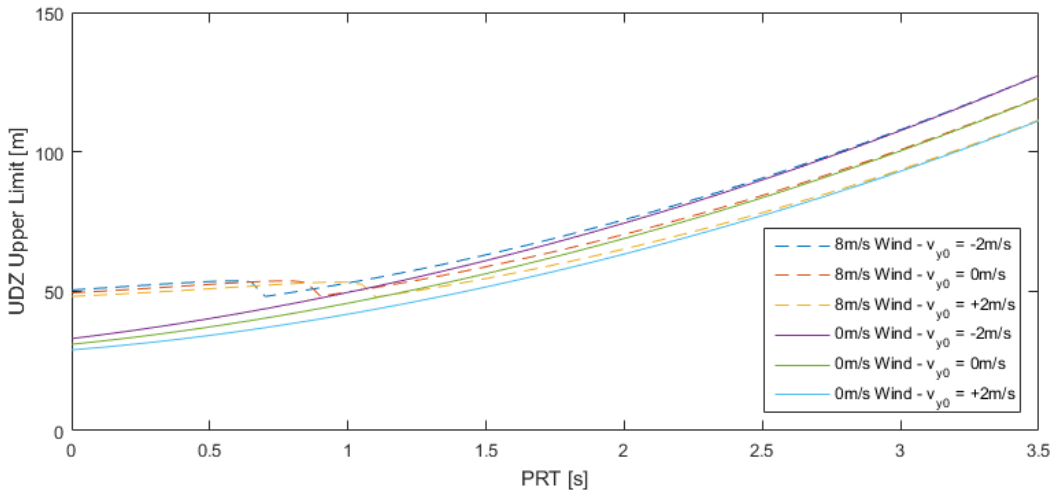

Figure 37: Craft Oscillations Damped, with and without Wind Effects
$V_{x,\,lim}$ = 10m/s, $Vy_{,\,lim}$ = 10m/s

The effects on the upper limit of the UDZ caused by the addition of wind are similar to the effects seen in the comparison of the cruise speed and hover initial conditions. This makes sense because both scenarios compare changes in Craft velocity relative to the wind.

The UDZ upper limit has a range of 5.5m and averages approximately 50m for PRTs under 1s independent of the initial vertical Craft velocity. The effects of wind increase the upper limit of the UDZ for all cases, although the UDZ upper limit converges as the PRT increases.

If the Craft is descending at the point of power loss, the UDZ upper limit is higher than if the Craft was stationary or ascending. This is expected behaviour as if the Craft has a higher initial velocity at power loss one would expect the parachute require more time to decelerate the Craft.

The addition of an 8m/s wind increases the UDZ upper limit by 17.4, 18.4 and 19.2m for the descending, hover and ascending cases respectively for PRT = 0s.

Parachute Size Comparison – ø8.4m vs. ø12m

The current parachute design was compared to a hypothetical parachute which has a diameter of 12m. Figure 38 compares how the two sizes affect the UDZ Upper Limit.

Assuming that the mass of the parachute scales with D^2, the mass of the ø12m parachute would be twice that of the ø8.4m. This increase is only 1/33 of total Craft mass, so the ø12m parachute is assumed to have the same mass as the ø8.4m.

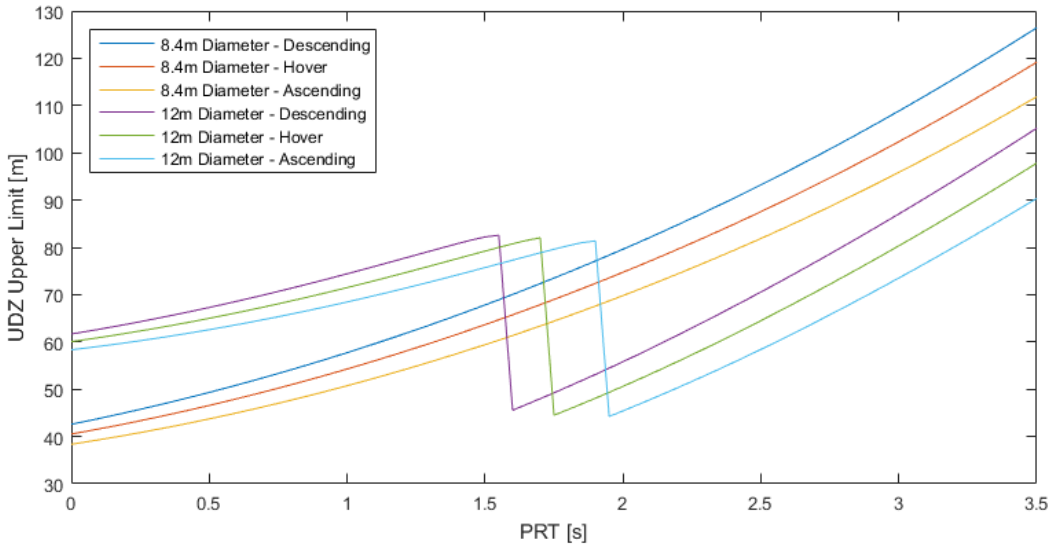

Figure 38: Comparison of UDZ as a result of Different Parachute Diameters, Horizontal Velocity Limit: 10m/s, Vertical Velocity Limit: 10m/s, Wind: +8m/s

Assuming a PRT of 3s and zero vertical velocity at power loss, the UDZ upper limit for the 8.4m parachute is 102.4m, compared to 80.3m for the 12m parachute. If the PRT is reduced to zero, the UDZ upper limit for the 8.4m parachute decreases to 40.5m and the 60.1m for the 12m parachute. Reducing the PRT from 3s to zero reduces the UDZ upper limit by 61.9m and 20.2m for the 8m and 12m parachute, respectively.

An initial vertical velocity of +2m/s results in a UDZ upper limit of 95.9m, compared to 108.8m if the Craft is travelling at -2m/s under the same conditions – a difference of 12.9m. If the PRT is decreased to zero, this difference changes to 4.2m.

The 12m parachute gives a higher UDZ upper limit than the 8.4m parachute at PRTs below 1.60, 1.75 and 1.95s for the descending, hover and ascending cases respectively. At each of these PRTs the 12m parachute gives a UDZ upper limit of 24.5m less than the 8.4m parachute. This is the maximum difference in UDZ upper limit between the two parachutes at comparable PRTs. This difference results because the amplitude of oscillation of the system is higher with a 12m parachute, as suggested by the larger oscillations of the system in the horizontal plane (V_x) in Figure 40.

Figure 39 shows the results if the permissible horizontal impact velocity was increased to 12m/s, the border of the survivable impact zone in [40]. Under this permissible velocity, the oscillations of the velocity in the horizontal are negligible and the vertical velocity remains the critical limit for most of the simulation.

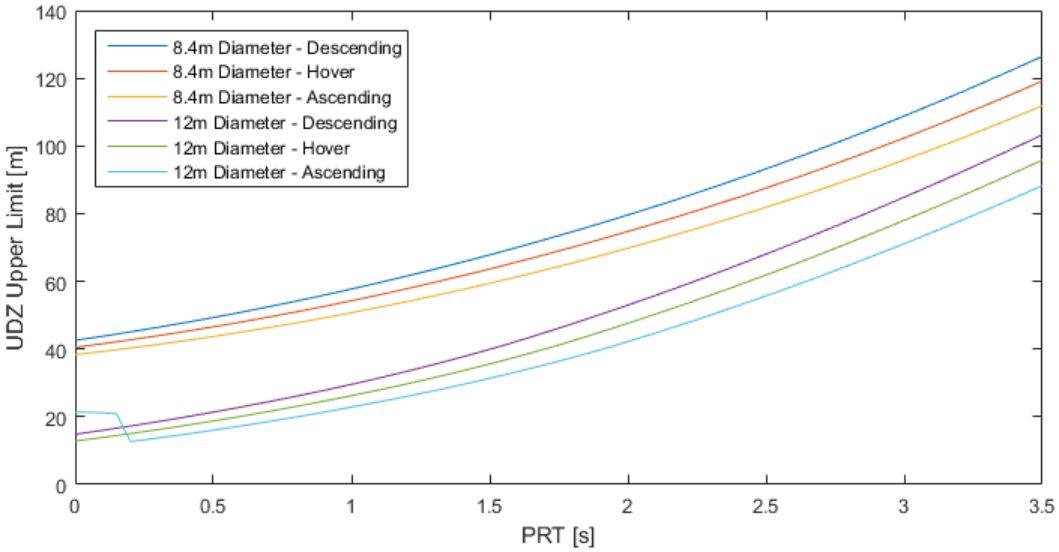

Figure 39: Comparison of UDZ as a result of Different Parachute Diameters, Horizontal Velocity Limit: 12m/s, Vertical Velocity Limit: 10m/s, Wind: +8m/s

The discontinuity in the curve for the 12m diameter ascending case represents a change in the critical velocity direction. For example, the critical velocity (the final velocity, horizontal or vertical, to reach below 10 m/s or 12m/s, respectively) for a PRT of 0.15s is the horizontal, but at PRT = 0.20s the vertical velocity is the critical limit.

This discontinuity occurs in the ascending case only as a longer time interval is required for the cords to be pulled taut in the ascending case. The Craft is initially travelling upwards when the parachute is deployed, and the parachute initially deploys downwards (as in Figure 55) because the drag is in the opposite direction to the Craft. This travel in the opposite direction means that the parachute takes longer to deploy and therefore requires a larger height to decelerate the Craft.

For lower PRT's, the 12m diameter is noticeably better at decelerating the Craft. In the descending case, the 8.4m parachute requires a height of 42.6m to decelerate the Craft to a safe velocity. The 12m parachute only requires a height of 14.8m to safely slow the Craft in comparison, a difference of 27.8m. This difference decreases with increasing PRT, though at PRT = 3s the difference in the descending case is still 23.9m in favour of the 12m parachute.

One possible downside of the larger parachute which will need further research is that the opening shock may be larger, as an increased area will result in more drag force and in turn an increase in the acceleration experienced by the Craft (and pilot).

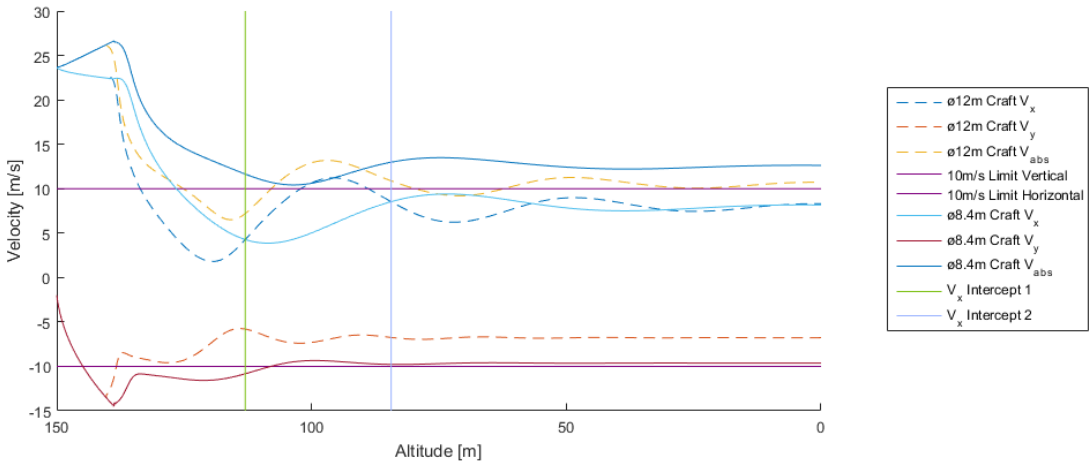

Figure 40: Craft velocity profile as a result from an 8.4m vs. 12m Diameter parachute.
PRT = 0s, Wind = +8m/s, V_{x0} = +23.6m/s, V_{y0} = -2m/s, $V_{x,\,lim}$ = 10m/s, $Vy_{,\,lim}$ = 10m/s

Figure 40 shows the velocity profile of the 8.4m vs. 12m diameter parachute when subjected to the same initial conditions. The 12m parachute initially slows the Craft more efficiently in both the vertical and horizontal directions than the 8.4m parachute: a larger parachute area results in a larger drag force. The Craft slows down in the vertical 30.3m earlier when the 12m parachute is simulated.

Whether the horizontal velocity of the Craft simulated with the ø12m and ø8.4m parachute has the higher horizontal velocity depends how much the Craft has fallen. If the Craft impacted the ground from a power loss height of 37.0 – 65.6m (between "V_x Intercept 1" and "V_x Intercept 2" in Figure 40) then the 12m parachute would impact with a higher velocity. If the power loss height was, for example, 27 or 75m then the 8.4m parachute would result in a higher velocity impact.

Figure 41 shows that when the Craft falls while descending and no with no initial horizontal velocity an 8m/s wind has very similar effects on a Craft with an ø8.4 and ø12m diameter. If the horizontal limit is the critical limit, then the drag of the parachute may not have as large an influence on the UDZ.

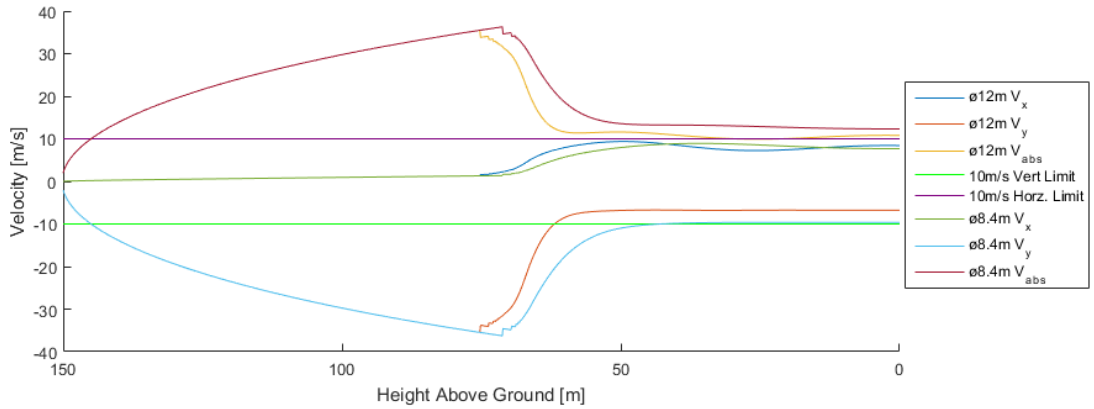

Figure 41: Parachute Diameter Effects on Craft Velocity
PRT = 3s, Wind = +8m/s, V_{x0} = 0m/s, V_{y0} = -2m/s, $V_{x,\,lim}$ = 10m/s, $Vy_{,\,lim}$ = 10m/s

Opening Shock – Max Craft Acceleration

The maximum opening shock is compared to the maximum acceleration measured in drop test data. The drop test data is recorded in increments of 5ms, so the acceleration in the model is also taken over intervals of 5ms. The acceleration is calculated using the change in speed between each time interval.

The maximum Craft acceleration converges to 539m/s^2 (54.9 g's) over and for the time interval dt = 0.00001s. The maximum opening shock over 5ms is simulated to be 239m/s^2 (24.4 g's). If the head experienced an acceleration of this magnitude, it is likely that brain injury will occur as this peak exceeds the limit of 80m/s^2 (8.2 g's) for 3ms [51]. If the assumption that the parachute is initiated at a distance, L, from the Craft (Refer "*Initiation Point of the Parachute*", following section), then the maximum acceleration over 5ms is 61m/s^2 (6.2 g's). This value underestimates the peak accelerations obtained from drop test data shown in Table 5.

Test Number:	Maximum Opening Shock (m/s^2)	Maximum Opening Shock (g's)	Time Interval Used (s)
1	21.3	2.2	0.0025
2	79.5	8.1	0.005
3	146.9	15.0	0.00333
4	89.1	9.1	0.005
5	79.6	8.1	0.005
[Report Results]	155.3	15.8	-
[Report Results]	149.4	15.2	-
AVERAGE:	**129.3**	**13.2**	**-**

Table 5: Drop Test Maximum Opening Shock

The velocity measured for tests 1-5 may not be accurate at every data point, particularly tests 1 and 3, as there are periods where the data shows no change in the velocity for intervals of up to 80ms. Additionally, the setup for each test is unknown and the parameters used (e.g. test mass, initial velocity, reaction time) may differ widely between the tests. This would explain the discrepancies between tests 1 and 3, for example.

Test report acceleration data are more consistent then data derived from the excel sheets (tests 1-5). The reports give peak force and mass values which can be used to calculate maximum acceleration. It was possible that the force values in the test reports were obtained using strain gauges between the parachute

and the Craft. If this was the case, the exclusion of pilot harness damping in simulations matches experiment conditions. The difference in test report data and data derived from excel sheets may be that the mass used in the test reports is heavier (320 and 330 kg), or that the instruments used in tests 1-5 did not have a sufficient response time.

Shocks of 3-6g's are a standard opening shock that a skydiver travelling at terminal velocity is subjected to when under a sport canopy, and at 9-12 g's the opening shock has been documented as "hard (fast) and painful" [52]. Based on this, the test data shows that the opening shock of the parachute is likely to subject the pilot to high but tolerable accelerations.

The simulations estimate a higher peak acceleration. This may be because there is at least one compliant element in the real system which is assumed to be rigid in the model. It is possible that the spring constant of the parachute cords is less than the predicted value. This would result in increased flexibility and the tension force may decrease as a result.

The model may not be reliable for predicting opening shock in its current set up.

Initiation Point of Parachute

The model currently accounts for the opening of the parachute by multiplying the drag force on the parachute by the ratio of an assumed instantaneous drag area to total drag area ("Drag Area Ratio"). This is possible because the drag force is directly proportional to the instantaneous drag area. The instantaneous drag area to total drag area is zero at the moment of deployment and 1 at the moment of full inflation.

The instantaneous drag area of the Craft is based on data of the tension force in the cord. This means that when the Drag Area Ratio is a non-zero value, the force on the Craft through the tension in the cord changes as well as parachute area. Therefore, the instant the instantaneous drag area becomes non-zero, the tension in the cord should also be non-zero. This is only possible if the cord is at full extension when the drag becomes a non-zero value.

Since the Drag Area Ratio data has been derived from tension forces in the cord, then it would be correct to assume that when the parachute initiates, it is already 10m from the Craft, i.e. it instantaneously appears in midair.

If the initial parachute location is assumed to be at the attachment point, u_{jp2}, then increasing the Drag Area Ratio will increase the parachute drag force, but the tension force will remain zero because the parachute is still at a distance less than the length of the cord, L, from the Craft.

The cord must be at full extent to apply a force on the Craft. Refer Figure 42a. If parachute initiation is assumed to occur at the Craft attachment point, then when the Drag Area Ratio is initially non-zero (near the beginning of initiation) the tension in the cord will still be zero (Figure 42b).

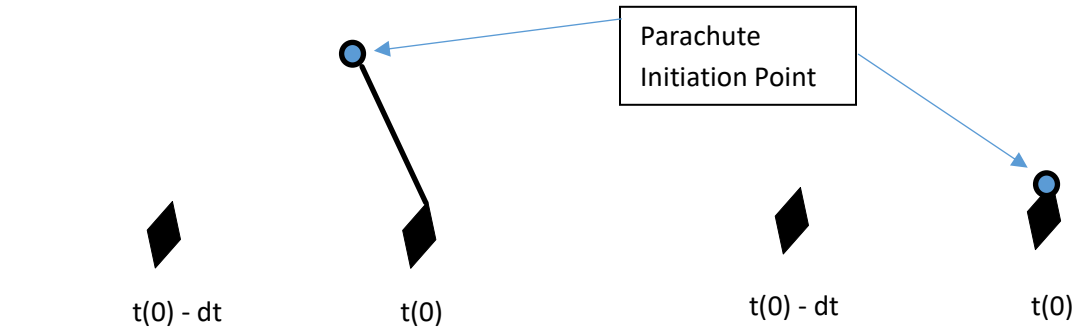

(a) Parachute and Craft the Moment Before and at Parachute Deployment Initiation– Parachute launched at distance, L, from Craft. t(0) is the instant of deployment

(b) Parachute and Craft the Moment Before and at Parachute Deployment Initiation – Parachute launched from attachment point. t(0) is the instant of deployment

Figure 42 (a-b): Comparison of Different Assumed Parachute Initiation Points

Figure 43 shows the effects of the initiation point on the UDZ upper limit. Launching from the attachment point is consistently more conservative as the parachute cords have to reach full extension before applying a force, which takes time.

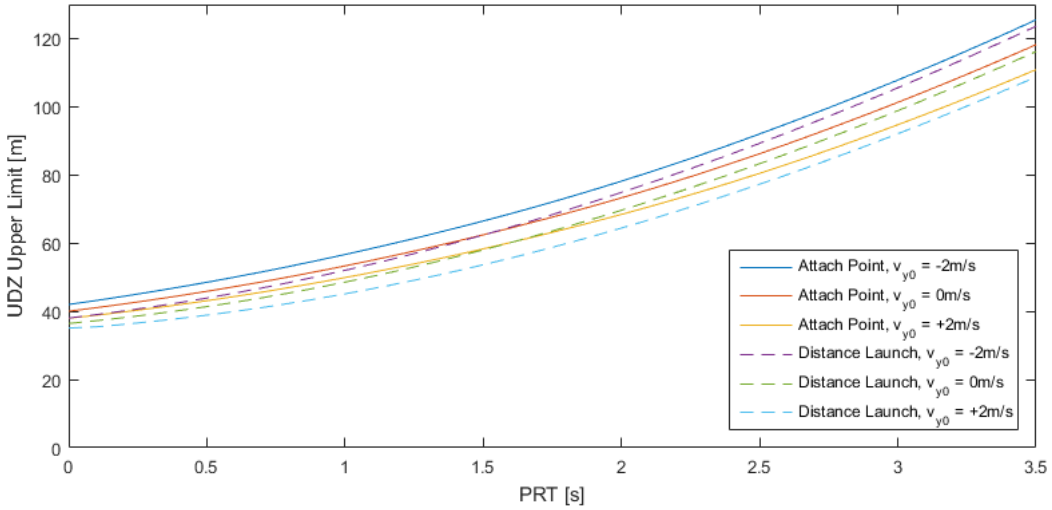

Figure 43: The Effects of the Deployment Location on the Upper Limit of the UDZ

Figure 44 shows that the maximum tension changes by an order of magnitude depending on the initiation point of the parachute. This is because the Craft and parachute will be travelling away from one another at a larger velocity when the parachute is initiated at the attachment point. The shape of how the tension in the cord changes with time also differs between the different assumed initiation points.

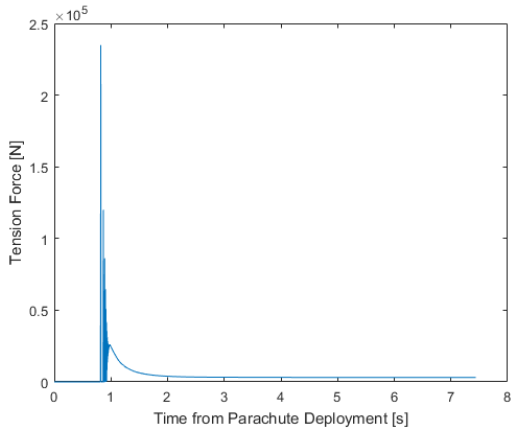

(a): Tension Force over Time for initiation at ujp2 norm[ujp-ujp2] → 0)

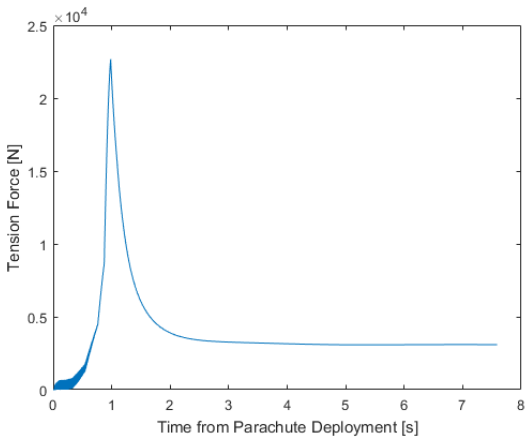

(b): Tension Force over Time for initiation at full extent (norm[ujp-ujp2] = L)

Figure 44 (a-b): Tension Force Comparison between Different Initiation Point Assumptions

The beginning of Figure 44b appears unstable, however this is with a timestep of $2x10^{-6}$s, and the simulated maximum tension changes less than 0.5% between this timestep and $1x10^{-5}$s. The computer ran out of memory at timesteps lower than this.

Figure 45 shows an overlay of scaled drag area ratio and the tension force in the cord. The right hand figure shows that the drag area ratio much more closely matches the tension force profile when the parachute is assumed to be initiated at full extension.

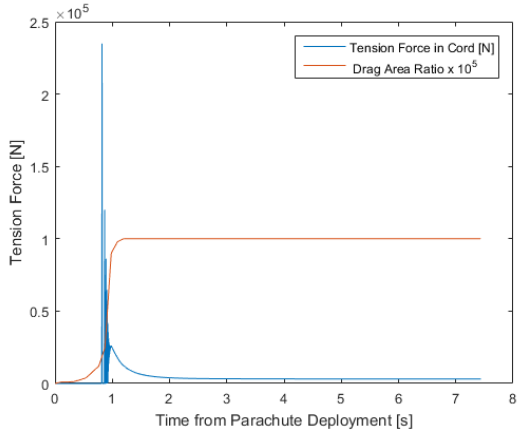

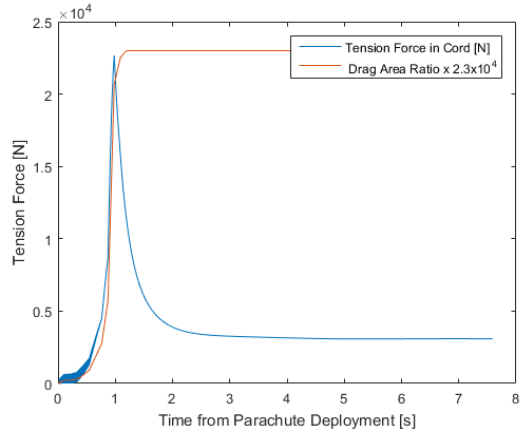

Figure 45: Overlay of Drag Area Ratio and Tension Force for initiating the parachute from the attachment point (Left) and from full cord extension (Right)

Initiating at the attachment point is consistently more conservative for UDZ predictions, although the difference in the UDZ upper limit is small (4.1m at PRT = 1.5s for descending case).

Comparison of Tension Force to Drop Test Results

Figure 46 shows a comparison of the measured tension force and drag force through time for one of the drop tests. Air resistance on the Craft is shown to be negligible, and the tension force is therefore calculated assuming zero drag on the Craft in the experimental data using Eq. 27. The mass used in each drop test is assumed to be 330kg.

$$FT = m_{jp}\ddot{u}_{jp} - m_{jp}g \tag{27}$$

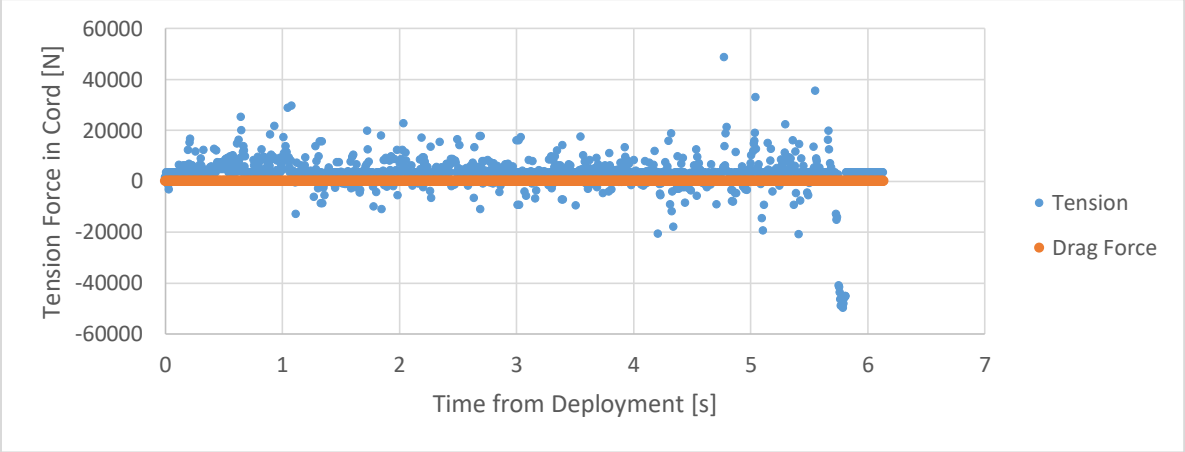

Figure 46: Experimental Force Comparison as per test data

It is not clear why a negative value is occasionally obtained for the tension force, however it is noted that the largest negative values for tension are towards the end of the test, likely near the time of impact.

Table 6 shows the experimental results for the peak tension force calculated by Eq. 27. The maximum tension force is taken as the peak tension force calculated through the descent. This means that the values in Table 6 may not be the result of the opening shock as they could occur at any stage during the descent. This is particularly true for drop tests 1 and 3, as the stages of parachute deployment through time are not marked on these as they are for the other tests.

Drop Test Number:	Maximum Tension Force (kN)
1	10.3
2	16.8 (-23.0)
3	51.7
4	44.2
5	29.5
[Test Report]	49.7
[Test Report]	49.3
Average	**43.0 (43.6)**

Table 6: Maximum Tension Force for Drop Test Data

The simulated tension force is much closer to the maximum measured tension force in testing when the parachute is initiated from a distance. The maximum tension force in the experimental data changes a large amount between each drop test. More tests may need to be performed and analyzed to obtain a more consistent tension value.

There are negative values for the tension force. It is unclear exactly what this represents, however if the absolute value is taken then it produces a higher average maximum tension force. It has therefore been included in brackets in Table 6.

Test reports show a peak tension force of 45.5kN. Results from tests 3 and 4 show maximum forces within 12% of this. The tension force may have been directly measured or accounted for assumptions not yet apparent in the model. The conditions under which the experimental tests were conducted are an area of uncertainty.

While the initiation at full extension more accurately simulates the profile of the tension force through time, neither setup accurately predicts the maximum value of the tension force compared to experimental data. The maximum values predicted and their error to the experimental data are summarized in Table 7. As the report data is directly measured using strain gauges, it is likely that the model is over/underestimating depending on the assumed attachment point – possibly because of the overestimated rigidity of components. Initiating the parachute from the attachment point gives almost 5x the reported value of 50kN. Initiating at full extent produces an estimate 55% of the 50kN value.

	Attachment Point	Full Extension	Experimental Average/ Report Average
Value	**234.9 kN**	**22.7 kN**	**29.9/49.5 kN**
Difference to Experimental Average (29.9 kN)	**7.9x** experimental average	**0.8x** experimental average 25% Difference	-/-
Difference to Test Report (49.5 kN)	**4.7x** experimental average	**0.5x** experimental average 55% Difference	-/-

Table 7: Maximum Tension Force as Predicted by Simulations and in Testing.

These inaccuracies suggest that the model may not be reliable at predicting the maximum tension force in the current setup. The model assumes the worst case: that all of the cords have equal tension and are pulled taut simultaneously. In reality they may pull taut one after another over a few milliseconds. This would mean that the peak acceleration and force would be distributed over a larger time interval, and would explain why the model gives a larger value for the tension force. This more unevenly distributed force also explains why the test results vary from test to test.

Simulation results which more closely match experimental data may be obtained through changing the initial conditions to match test conditions, though in addition assumptions must be checked and the model improved. Refer "*Future Modelling Work*" section in this thesis for suggestions on the subject.

Discussion

Comparison of Damping Method and Fixed Orientation

Another way of "damping" out the oscillations of the Craft is to "lock" the Craft and parachute together after they align. Figure 47 shows how the Craft rotates after the deployment of the parachute. The "locked" assumption assumes that once alignment has been reached (Far Right) the two entities remain aligned until ground impact, and the Craft can no longer rotate relative to the parachute.

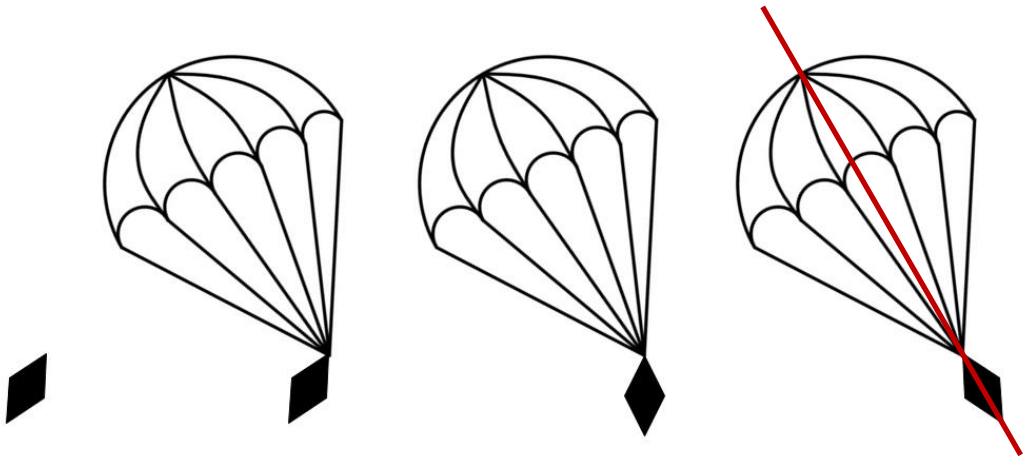

Figure 47: Craft Rotation after Parachute Initiation

This assumption has the problem that the Craft has rotational energy which is suddenly lost from the system, and there is a discontinuity in the angle and rate of change of the angle of the Craft, as shown in Figure 48. This is because the angle of the Craft suddenly stops being an independent value and is instead based on the relative position of the Craft and parachute – the value of the angle of the Craft is suddenly taken as θ_{GLOBAL} as opposed to θ_{jp}.

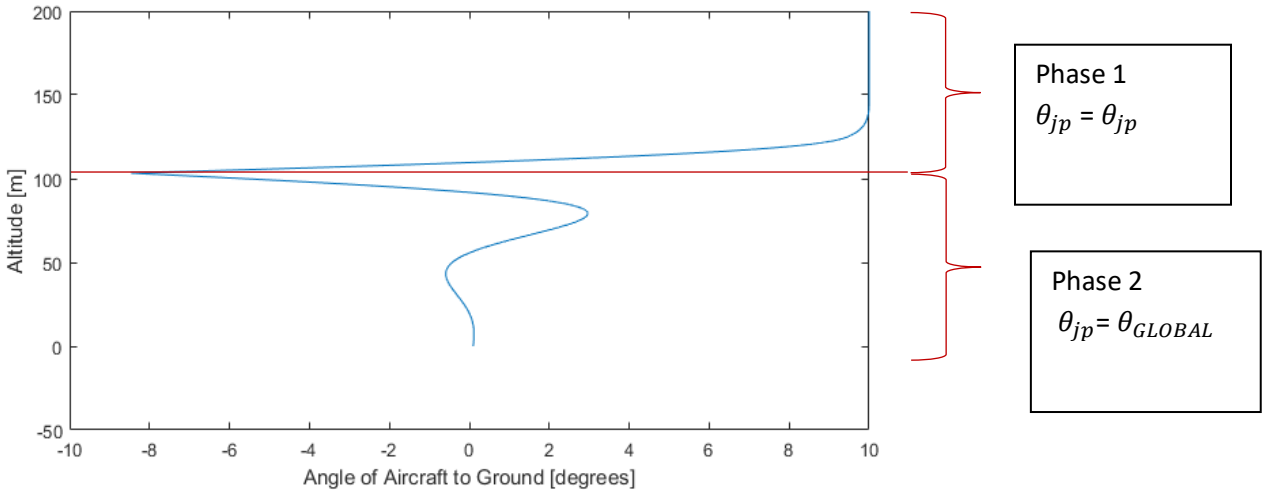

Figure 48: Discontinuity of Angle of Craft between Phases 1 and 2

The angle of the Craft through the emergency descent phase is shown in Figure 48, assuming that the fixed assumption is used. There is a discontinuity in the rate of change of the angle. Therefore this assumption may accurately predict the positions of the Craft and parachute through space, though the simulated angle will not be accurate at all stages of descent.

Figure 49 shows that there is little difference in the upper limit of the UDZ between the assumptions of "Craft is locked after alignment" and "Craft oscillations are damped" are used. There is a ~0.9m difference in the upper limit at PRT = 0s, and a 1.1m difference at PRT = 3.5s for all initial V_x scenarios. The damped assumption is marginally more conservative from PRT = 2.2s and above as it predicts a higher upper limit for the UDZ.

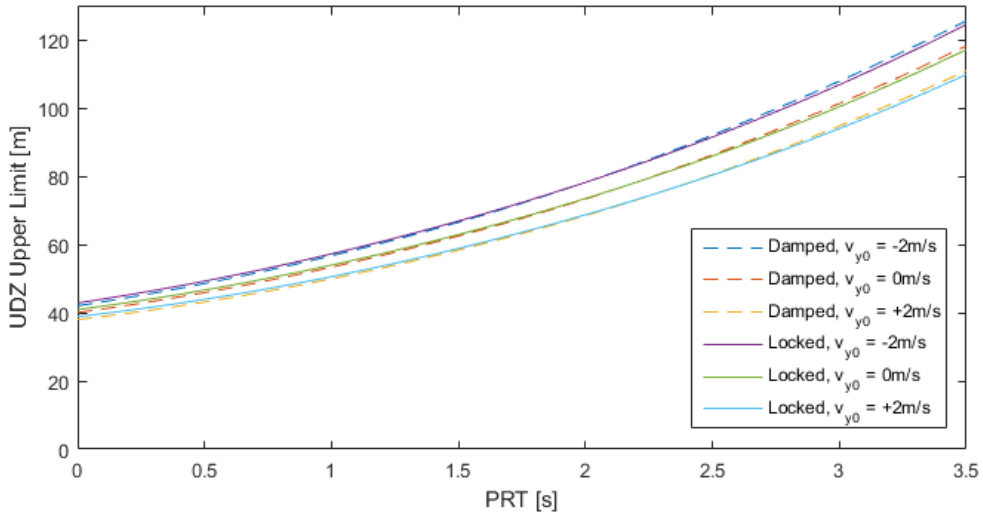

Figure 49: Effect of Locked and Damping Assumptions on UDZ Upper Limit
V_{x0} = 23.6 m/s, Wind = +8m/s

The assumption that a pin joint is the sole attachment point of the parachute to the Craft may be an oversimplification. More information on the geometry of the Craft-parachute system will need to be known in order to represent the system more accurately in simulation, such as the location of cord attachment points on the Craft and parachute. The oscillations of the Craft relative to the parachute may change with a less simplified and more accurately modelled parachute connection point. For example, it is possible that the parachute lines will not only be attached to just 1 point on the Craft as assumed in this model, which may affect the damping properties.

3D Oscillations and Vertical Wind

Figure 50 shows the observed oscillations for a parachute in 3D space.

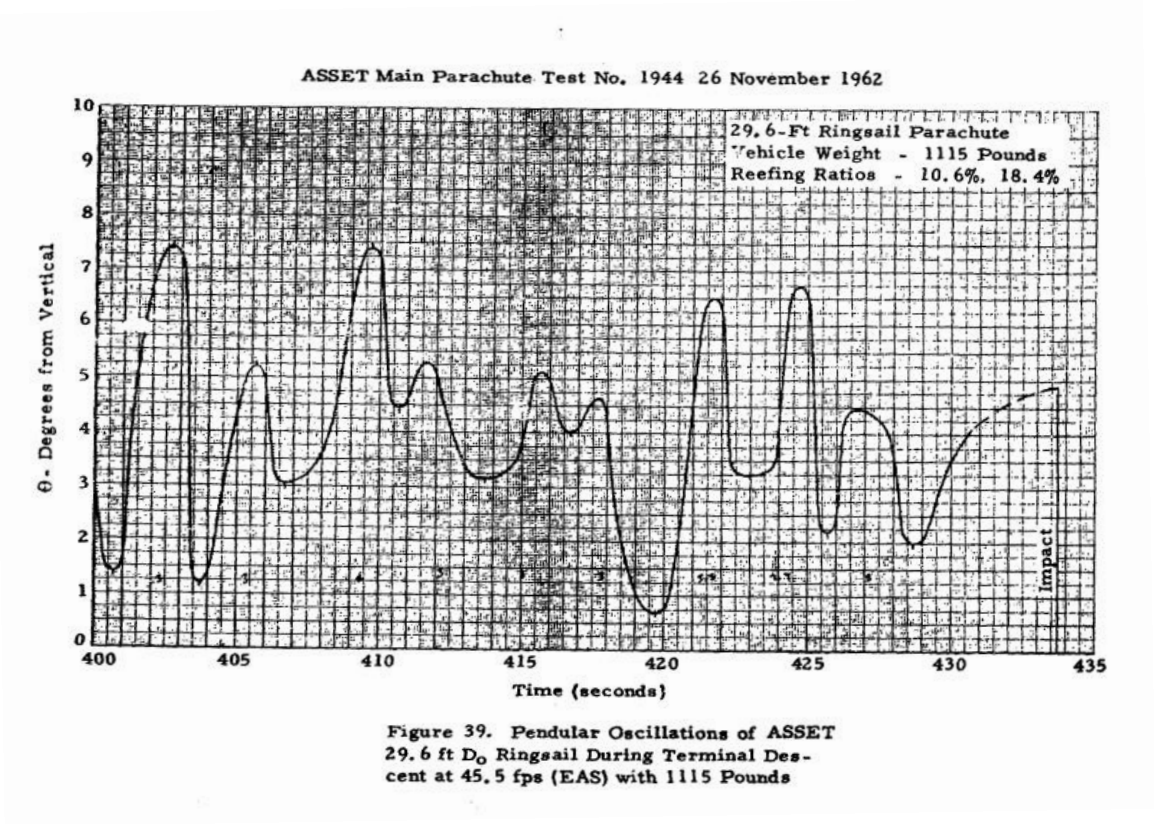

Figure 50: Observed Oscillations of "ASSET" Parachute [53]

These observed oscillations show that the coupled parachute-load system only varied by ±~4°. This represents a coning angle motion which is unable to be captured using the 2D model. It is possible that the model can be expanded to 3 dimensions to explore effects such as this.

The average updrafts over the tropical Pacific Ocean and the Amazon are approximately 1-2m/s at 1000m altitude [54]. It is therefore assumed that no up- or downdrafts are experienced for the duration of descent, as increased drafts only occur at higher altitudes and the Craft is being modelled in near ground scenarios.

Unevenly Distributed Tension

It is currently assumed that all cords are in tension to the same degree. This may not be the case in reality. This may cause damping of Craft oscillations, not dependent on the rotational velocity as forced damping is, but instead on the relative angle of the parachute and Craft. The red cords in Figure 51 represent those which are expected to be in tension, depending on the relative angle of the Craft and parachute. This cause of damping will be accentuated if the parachute lines have several connection points on the Craft, as any time the parachute and Craft are not aligned, one side of the lines will be in tension and the other slack.

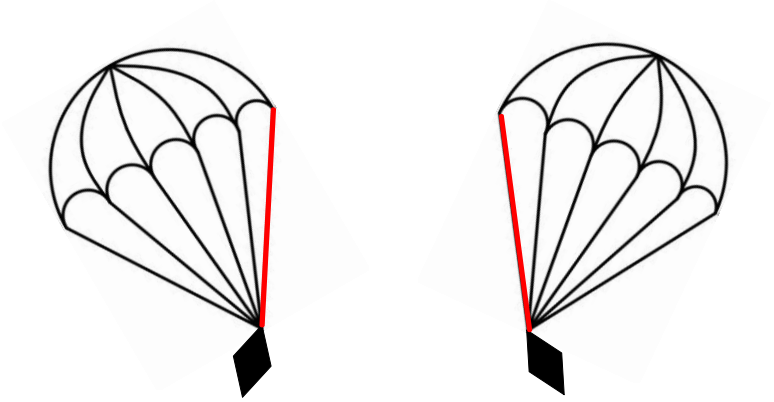

Figure 51: Cords in Tension

The Craft may tip on impact if the horizontal velocity or swinging motion of the Craft is too great. The limits for tipping are not yet known, and tipping may lead to further injury to the pilot or damage to the Craft depending on the terrain. It could be rocky and dangerous. Impact scenarios have not been considered in this model, though this may be an area of future research.

Altering the Spring Constant, *k*

The difference between the accelerations and maximum tension forces in test data and the simulated model may be caused by a differing cord spring constant. Therefore the sensitivity of the peak tension force and acceleration to a changing spring constant was modelled. These variables have been examined for the two different initiation points discussed (at the attachment point and at full cord extension).

Figure 52 shows that the maximum tension increases at a decreasing rate with an increase in the total spring constant value, k. The peak acceleration is sensitive to the cord spring constant below spring constant values of $2x10^6$ N/m.

Beyond k = $4x10^6$ N/m the peak acceleration does not increase significantly for initiation at full extent. If the physical model used a cord with a spring constant more than $4x10^6$ N/m, it is unlikely that the spring constant is the cause of discrepancies between the simulation and experimental tests based on peak acceleration.

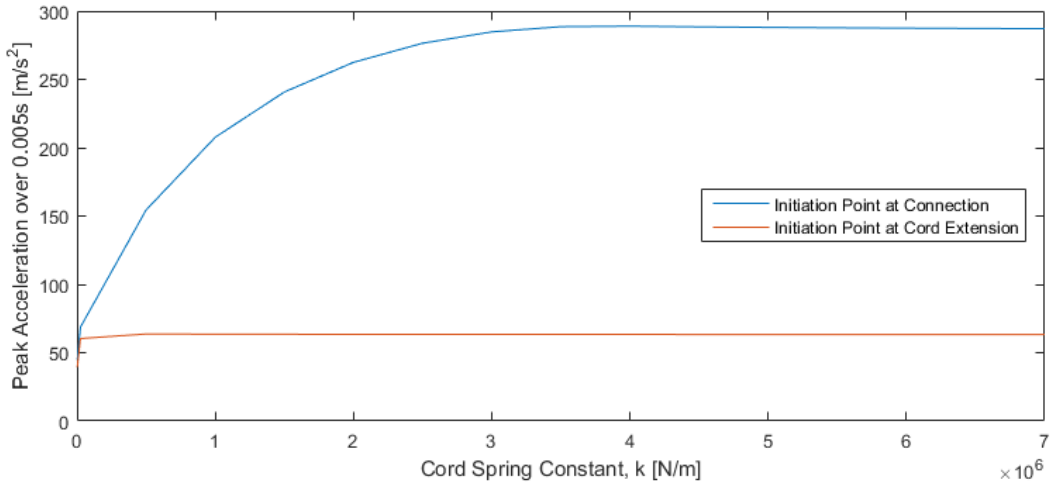

Figure 52: Maximum Acceleration as a Function of Cord Spring Constant

Figure 53 shows that the peak tension force is sensitive to the cord spring constant to values in excess of $7x10^6$ N/m (28x 550 Paracord). The simulated peak tension force changes 0.97 kN between k values of $2.5x10^4$ and $7x10^6$ N/m if the parachute is initiated at full extension.

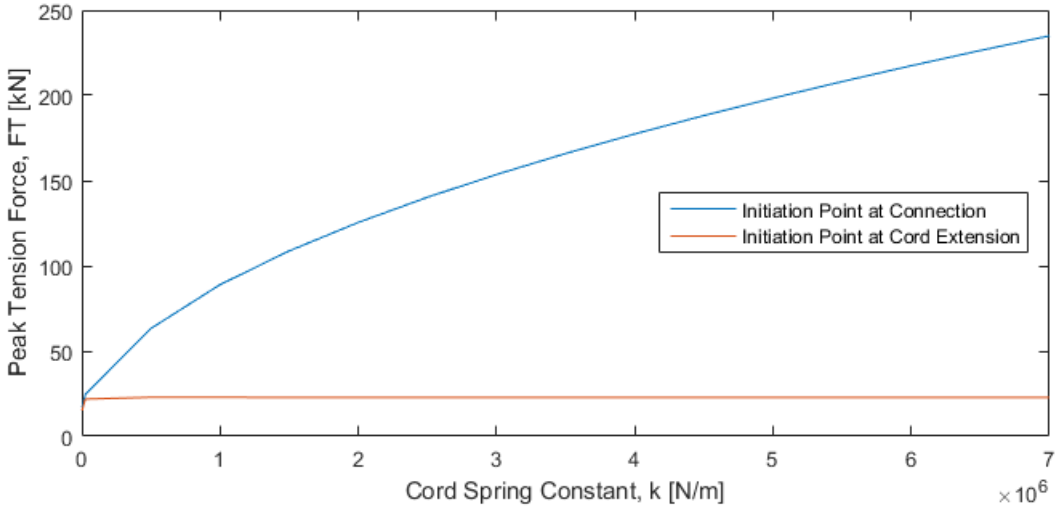

Figure 53: Peak Tension Force as a Function of Cord Spring Constant

Rotational Drag

Rotational drag was added into the model to test how much it affected the rotation. Figure 54 shows that the rotational drag has a negligible effect on the orientation profile of the Craft.

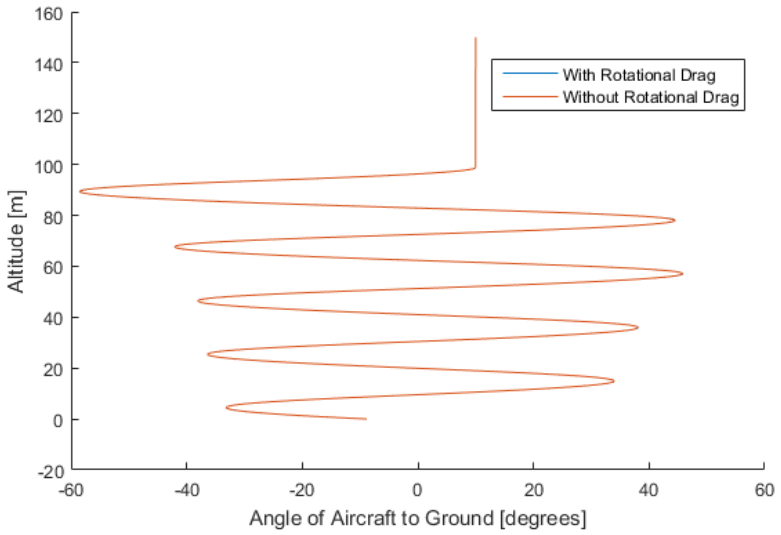

Figure 54: Orientation Profile of Craft - With and Without Rotational Drag

The mass of the parachute canopy may weigh less than the assumed 9.5kg if the total parachute mass is distributed between the canopy, cords and deployment module. 9.5kg is the mass of the entire parachute system, however all of the mass of the parachute has been assumed to be transferred to the COM of the parachute canopy upon inflation.

The Effects of Zero Initial Instantaneous Drag Area

The Drag Area Ratio is zero at the instant of parachute initiation. This means that there is initially no drag on the parachute. As it is assumed that the parachute is launched from the Craft at zero velocity relative to the Craft, gravity is initially the only force acting on the parachute until the instantaneous drag area is no longer zero. This results in the simulation predicting that the parachute falls in front of the Craft for approximately 0.1m before a drag force is applied to the parachute and the parachute begins to deploy in the opposite direction to the Craft. Figure 55 captures this effect.

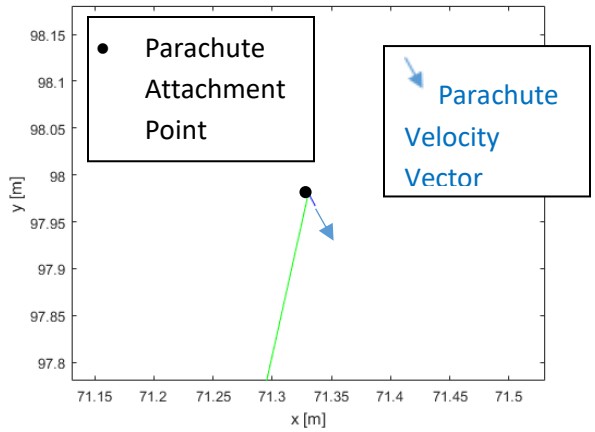

(a) The only force acting on the parachute is gravity. It begins moving in the direction of Craft velocity as a result of having no drag area

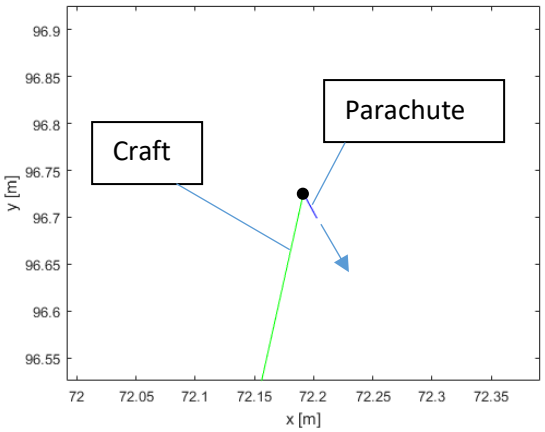

(b) Velocity of parachute is greater than Craft. No drag means parachute moves in direction of Craft motion

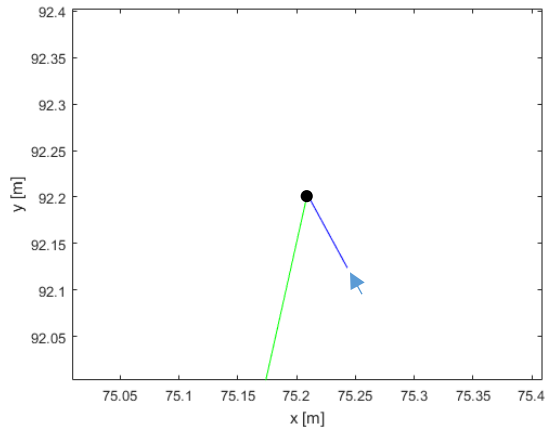

(c) Drag increases on parachute to provide sufficient force for it to move in opposing direction to oncoming velocity.

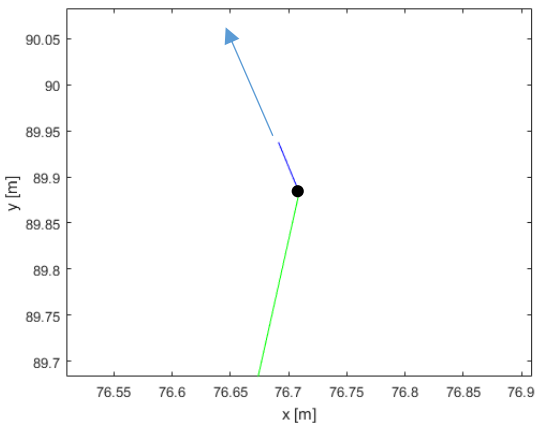

(d) Parachute deploys in opposing direction to oncoming velocity.

Figure 55(a-d): The position of the parachute attachment point and parachute for 93ms (Top Left), 149ms (Top Right), 297ms (Bottom Left) and 372ms (Bottom Right) after deployment

Simulations show that even with an instantaneous drag area of 0.04 at a time of 0.01s after deployment, the parachute has sufficient drag to deploy immediately in the opposing direction to the Craft velocity, as per Figure 55d.

Figure 56 is a graph of the absolute distance between the Craft and parachute during the first stages of initiation. If the Drag Area Ratio is 0.04 after 0.01s, then the parachute travels away from the Craft at an exponential rate, as per the blue line. The orange line shows that if the Drag Area Ratio is zero for the first 0.3s of deployment, the parachute begins to travel in front of the Craft, before changing direction and travelling in the opposing direction to the velocity of the Craft at 0.28s. The inflection point at 0.28 seconds in represents the change in direction of the parachute seen in Figure 55c.

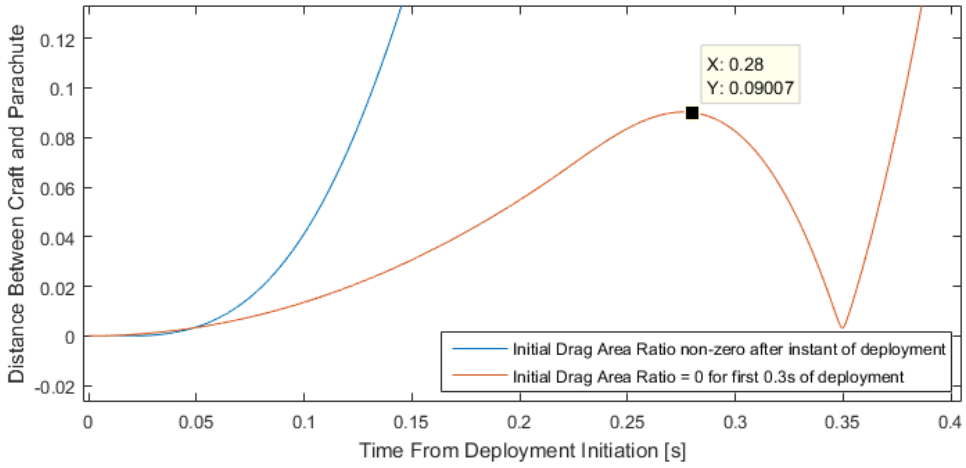

Figure 56: Distance between Craft and Parachute assuming initial drag area ratios of 0 and 0.01m²

The 1D model predicts that there will be no UDZ if the PRT is sufficiently low. The 2D model predicts that the UDZ is present regardless of the PRT. One factor influencing this is the assumed launch point. In the 2D model the parachute is launched from the craft attachment point, while the 1D model assumes a fixed-distance parachute-Craft system. Other factors include the rotation of the Craft around the parachute and the addition of wind conditions in the 2D model.

Conclusions

A model for the descent of the Martin Jetpack under emergency descent conditions was created. This included modelling the freefall of the Craft as well as the dynamic interaction between the parachute and Craft after the parachute had been deployed.

A range of initial velocities pilot reaction times were considered and simulated. From this, the impact velocity of the Craft has been determined for these initial conditions and compared to known impact velocity limits. The minimum height needed for the parachute to decelerate the Craft for each scenario was recorded as the UDZ (Unsafe Deployment Zone) upper limit.

The UDZ upper limit starts at ~40m under most circumstances when the PRT is 0s. The simulated UDZ upper limit was approximately halved for PRTs under 0.5s if the parachute diameter is increased to 12m. This indicates that even with a larger parachute, the upper limit of the UDZ cannot be completely eliminated. The effect of different wind conditions and the assumed initiation point in space of the parachute were simulated. The effects of an 8m/s wind changed the UDZ upper limit by up to 19.2m while the assumed initiation point had little effect.

In the initial model the Craft oscillations relative to the parachute were undamped. Two methods were compared to simulate more closely to observations of how parachuting objects behave. In one simulation a damping constant was added and in another the parachute and Craft were assumed to remain in alignment once they were aligned. There was a maximum variation of the simulated UDZ upper limit of 1.1m at a PRT of 3.5s.

While the model may be reliable at predicting the fall velocity and position profiles, as well as the orientation of the Craft, it does not accurately predict the maximum acceleration and cord tension in the current setup, based on comparisons to experimental data.

Department of Mechanical Engineering
University of Canterbury
Te Whare Wānganga o Waitaha
Private Bag 4800
Christchurch 8020, New Zealand

Telephone: +64-3-366 7001
Facsimile: +64-3-364 2078
Website: www.mech.canterbury.ac.nz

UNIVERSITY OF CANTERBURY
Te Whare Wānanga o Waitaha
CHRISTCHURCH NEW ZEALAND

Mathematical Modelling of Craft Landing Gear

Abstract

This model simulates the impact of the landing gear. The system is modelled as a mass-spring model, with the craft body as the mass and the legs as cantilever tubes. The maximum accelerations were assumed to last the duration of the impact until the craft reaches zero velocity. These accelerations and the durations were compared with known human tolerance limits.

Steel alone is not ideal for absorbing compressive impact forces on an infinitely hard surface. In bending the landing is much more tolerable as shown by the difference in maximum acceleration at a leg angle of 0° versus 90°.

Adding damping into the model may decrease stress in the members and allow higher drop heights to be simulated before yield stress is exceeded. This is yet to be included.

Introduction

The aim of this model is to simulate the impact of the craft. This was done by simulating the impact of four legs modelled by hollow steel cantilever tubes.

MATLAB Model

Assumptions

- The legs are the only mechanism decelerating the pilot.
- The leg material is structural steel
- The parachute is not deployed in any fall scenario, therefore the legs are the only part of the craft that cause deceleration.
- The pilot is rigidly attached to the craft.
- The craft lands on 1 leg when calculating the spring constant of an individual leg (i.e. the 1 leg is the entire system). The mass of the craft on one leg is therefore $m/4$
- The legs are independent of each other and can be modelled as cantilever tubes
- $\mu_{ground} = 0$. The ground is infinitely slippery.
- The ground is infinitely hard and offers no damping effects
- All stresses above the yield point are ignored because the spring constant will change above this point.
- The maximum deflection is the deflection that is to be used in the governing equation.
- The legs follow Simple Harmonic Motion (SHM) and can be simulated as a mass-spring system.
- The SHM of the legs is undamped
- The craft lands on all 4 legs simultaneously, therefore giving the highest spring constant.
- The craft lands perfectly vertically, and any horizontal force caused by the legs acting as springs is cancelled out by an equal and opposite force from an opposing leg.
- The efficiency of the impact, η, is 1; all of the energy from the fall is converted into spring potential energy in the legs.
- Force is spread equally throughout the tubes. There are no stress concentrations.

The datum of $h = 0$ is at the COM of the craft. Refer Figure 58.

Craft Layout

Figure 57 shows the simplified craft used in the model. This consists of steel tubes rigidly attached to a mass. Figure 58 shows the resulting ground reaction forces. There will be a compressive component and a bending component. The geometry of the legs will determine the amount of force which results in each. The drops are being modelled in freefall, and the drop heights are the heights above the ground from where the craft is released into freefall, without a parachute.

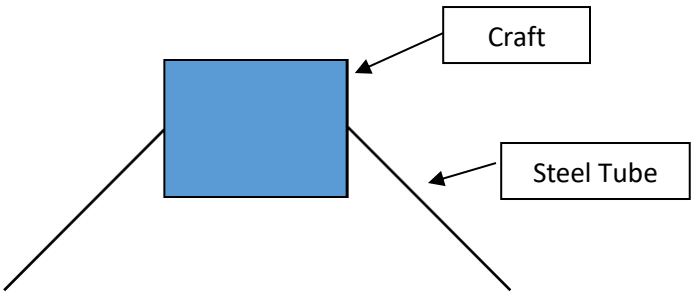

Figure 57: Craft Model Used

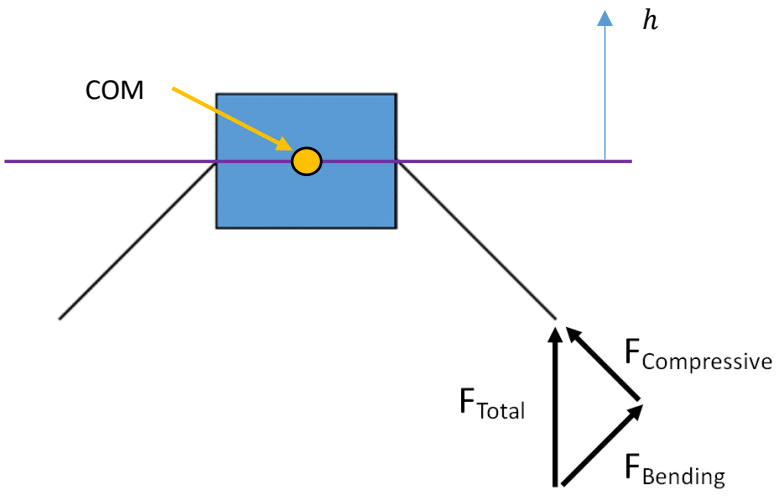

Figure 58: Ground Reaction Forces on the Craft

VARIABLES

Variable Name	Description	Value [Units]	Notes/References (if applicable)
θ	Angle of legs to vertical axis of craft	45 [°]	(assumed)
L	Length of leg	1 [m]	(assumed)
ΔL	Change of length of leg due to static compression	~	*Varies*
E	Young's Modulus of material of landing gear leg	200e9 [Pa]	Steel
		69e9 [Pa]	Aluminium
OD	Outer Diameter of tube	0.060 [m]	(assumed)
ID	Inner Diameter of tube	0.050 [m]	(assumed)
A	Cross sectional area of member	8.64×10^{-4} [m^2]	$A = \frac{\pi}{4}(OD^2 - ID^2)$
I	Second Moment of Area of material of landing gear leg	3.29×10^{-7} [m^4]	$I = \frac{\pi}{64}(OD^4 - ID^4)$
m	Total Mass of Craft	330 [kg]	[36]
g	Acceleration due to gravity	9.81 [m/s^2]	-
d	Damping constant of dynamic system	N/A	Assumed no damping
k	Spring constant of craft leg	~ [N/m]	*Varies with θ*
$\ddot{x}$	Acceleration craft experiences	~ [m/s^2]	*Varies with drop height*
$\dot{x}$	Velocity of mass in dynamic system relative to resting point	~ [m/s]	*Varies*
x	Position of mass in dynamic system relative to resting point	~ [m/s]	*Varies*
x_d	Deflection of tube	~ [m]	*Varies*
x_{static}	Tip deflection of tube resulting from static bending force	~ [m]	*Varies*
x_{vert}	Vertical component of x_{static}	~ [m]	*Varies*

x_c	Change in length of tube due to compression	~ [m]	*Varies*
$x_{c,vert}$	Vertical component of x_c	~ [m]	*Varies*
$x_{c,max}$	Maximum change in length of tube due to compression	~ [m]	*Varies*
$x_{b,max}$	Maximum tip deflection of tube due to bending	~ [m]	*Varies*
F	Total external force (weight force of Craft)	3237 [N]	$F = mg$
k_b	Spring coefficient of leg in bending	1.97×10^5 [N/m]	-
k_c	Spring coefficient of leg in compression	1.73×10^8 [N/m]	-
σ	Compressive stress through tube	~ [MPa]	*Varies*
σ_{max}	Max bending stress in tube	~ [MPa]	*Varies*
ϵ	Strain in tube	~ [m/m]	*Varies*
n	Impact load factor for bending	~	*Varies with drop height*
F_v	Vertical impact force on each leg	~ [N]	*Varies*
F_b	Bending force on each leg from impact load	~ [N]	*Varies*
F_c	Impact force tube experiences lengthwise	~ [N]	*Varies*
P	Bending force in 1 leg with no impact	~ [N]	*Varies*
P_c	Compressive force in 1 leg with no impact	~ [N]	*Varies*
$F_{spring,b}$	Vertical spring force caused by bending of leg	~ [N]	*Varies*
$F_{spring,c}$	Vertical spring force caused by compression of leg	~ [N]	*Varies*
h	Drop height of Craft	~ [m]	0.001 m – 6 m
η	Efficiency of impact	1	(Assumed)

V_{impact}	Impact velocity of craft	[m/s]	*Varies with fall height*
HIC	Head Injury Criterion Value	$[s][m/s^2]^{2.5}$	*Varies with max acceleration*
t_2	Head Injury Criterion – end time of acceleration affecting head. Taken to be when craft reaches zero velocity after impact	[s]	*Varies*
t_1	Head Injury Criterion – start time of acceleration affecting head. Taken to be when craft initially impacts ground	0 [s]	-
t	Time of deceleration from impact velocity to zero	[s]	*Varies*
F_{buckle}	Minimum force required to buckle the tube in first mode bending	162.4 [kN]	-
n_{end}	Buckling factor which accounts for end conditions	0.25 [unitless]	fixed-free configuration
Z	Section Modulus	$1.10x10^{-5}$	Refer Eq. 33

Governing Equation

The governing equation of motion for damped and forced dynamic motion is:

$$m\ddot{x} + d\dot{x} + kx = F \tag{1}$$

Eq. 1 will be solved for the maximum acceleration by rearranging it into (2)

$$\max(\ddot{x}) = \left[\frac{F - d\dot{x} - kx}{m}\right]_{max} \tag{2}$$

For a mass-spring system, no force is applied by the spring when the amplitude is zero. Therefore when the amplitude is zero, the acceleration is also zero. The highest acceleration that the craft experiences will be at maximum deflection, hence $\dot{x} = 0$. Future work may involve analyzing an ANSYS model or similar for determining the validity of this assumption – it may be that a non-zero product combination of x and

$\dot{x}$ gives the highest value of acceleration. Refer Appendix 3 for a possible method of damping constant attainment.

Equation 3 is the altered form of the Governing Equation, rearranged for acceleration.

$$\max(\ddot{x}) = \left[\frac{F - kx}{m}\right]_{max} \tag{3}$$

It is assumed that the maximum deflection is the deflection that is to be used in the governing equation.

Spring Constant Attainment

The spring constants of the leg under bending and compressive forces were derived separately.

Bending Spring Constant, k_b

A mathematical model of the craft and legs system was developed. It uses a free body diagram and the assumption of a steel tube to represent the leg (Figure 57).

A bending spring constant for the legs was attained by applying a static force and simulating the static deflection. The application of the force is shown in Figure 59.

Figure 59 (Left) shows the total force that the leg experiences. Figure 59 (Right) shows the force which will result in bending of the tube.

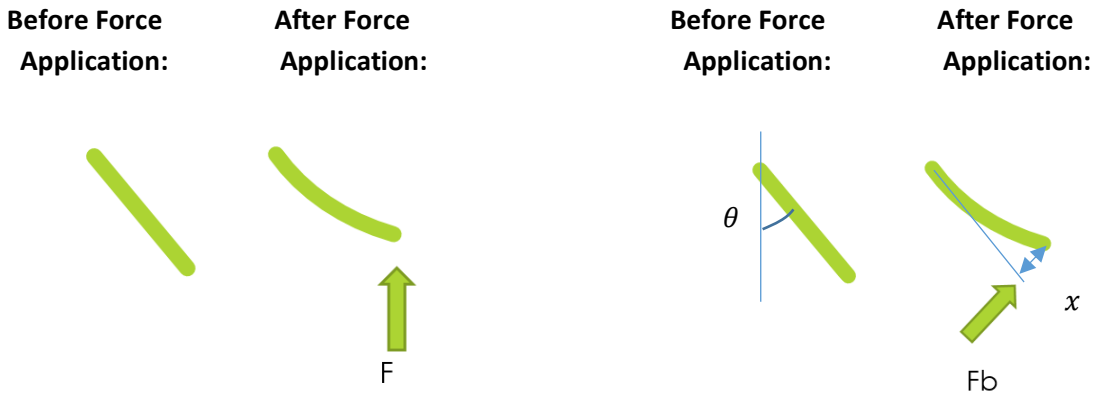

Figure 59: Total (Left) and Bending (Right) Forces Applied to the Leg

The total force was varied from 0 N to 3924 N in order to obtain a slope in the F_b vs. x_d curve (Figure 60). x_d is the deflection of the tube relative to the no-load position, in the direction perpendicular to the tube.

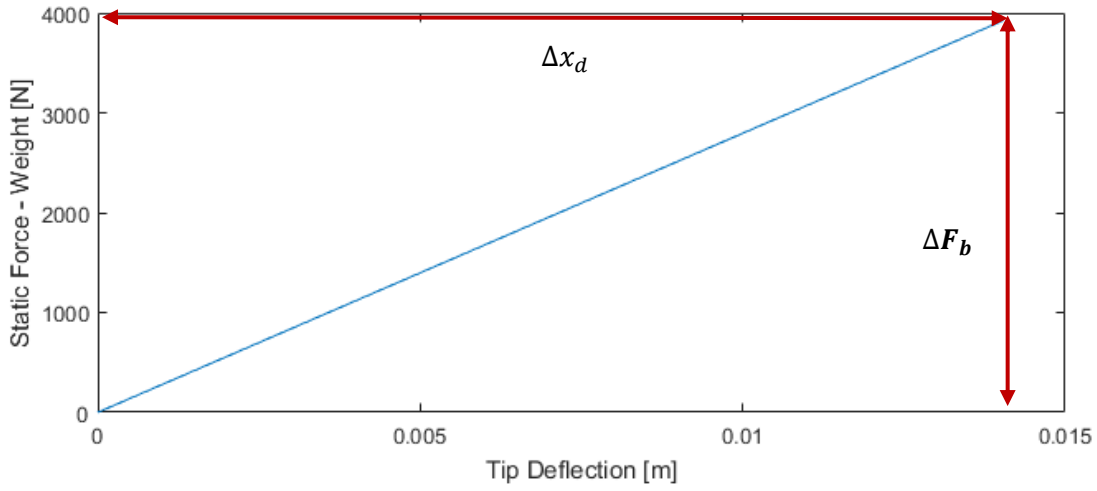

Figure 60: Increasing force and the Resulting Tip Deflection

The proportion of the force which results in bending of the leg, F_b, is calculated using Equation 4.

$$F_b = Fsin(\theta) \tag{4}$$

The deflection of the tube (x_d) is calculated using Equation 5, the equation for the tip deflection for a cantilever tube.

$$x_d = \frac{F_b L^3}{3EI} \tag{5}$$

Hooke's Law can be rearranged into Equation 6 to determine the spring constant, 'k_b'.

$$k_b = \frac{F_b}{\Delta x_d} \tag{6}$$

The bending spring constant of all four legs acting together will be 4*k_b.

Compressive Spring Constant, k_c

The compressive spring constant was determined using stress/strain relations (Eqs. 7 and 8) and the properties of the leg material. Eq. 9 relates stress and strain:

$$\sigma = \frac{F_c}{A} \tag{7}$$

$$\epsilon = \frac{\Delta L}{L} \tag{8}$$

$$E = \sigma/\epsilon \tag{9}$$

Eq. 7 - 9 can be combined and rearranged to form Eq. 10.

$$\Delta L = \frac{F_c L}{EA} \tag{10}$$

Eq. 10 can be combined with Hooke's Law (Eq. 6) to form an equation for the spring constant for the member in compression (Eq. 11). This case substitutes the following variables from Eq. 6: k for k_c, F for F_c, and Δx_d for ΔL.

$$k_c = \frac{F_c}{\Delta L} = \frac{EA}{L} \tag{11}$$

K_c is 870x larger than K_b (172x10^6 vs. 197x10^3 N/m). The deflection from compression is negligible compared to the deflection caused by bending at higher leg angles. If the leg angle is near zero then most of the force will be along the length of the leg and must be accounted for.

Calculating Tip Deflection

The craft was simulated to be dropped from a range of heights. The maximum vertical deflection of the cantilever tube was calculated using an impact factor and deflection equations.

The static bending and compression forces through one leg, P and P_c, respectively, were taken to be ¼ of what they would be under static Craft weight. The distribution of Craft weight into bending or compressive forces is dependent on the angle of the craft leg. Refer Figure 61. Eqs. 12 and 13 are used to calculate the bending and compression forces, respectively, through one member of the landing gear.

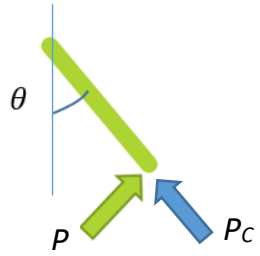

Figure 61: Static Bending and Compression Forces

$$P = \frac{mgsin(\theta)}{4} \tag{12}$$

$$P_c = \frac{mgcos(\theta)}{4} \tag{13}$$

Eq. 14 calculates tip deflection as a result of the bending force under static craft weight. Eq. 15 describes the change of length of one member. This is Eq. 10 with ΔL substituted for x_c and F_c for P_c.

$$x_{static} = \frac{PL^3}{3EI} \tag{14}$$

$$x_c = \frac{P_c L}{EA} \tag{15}$$

Eq. 16 is used to find the vertical distance that the Craft moves as a result of the static weight. Eq. 17 describes the change of length in the vertical direction of 1 member. This is the vertical distance over which the craft will come to a stop.

$$x_{vert} = x_{static} sin(\theta) \tag{16}$$

$$x_{c,vert} = x_c \cos(\theta) \tag{17}$$

An impact load factor is calculated using Eq. 18. This factor can be multiplied by the resting force to obtain the impact force that a member experiences [55]. The impact factor changes with the simulated drop height, h.

$$n = 1 + \sqrt{1 + \frac{2h\eta}{x_{vert} + x_{c,vert}}} \tag{18}$$

The impact factor is multiplied by the weight force that one leg experiences to calculate the vertical impact force on each leg using Eq. 19.

$$F_v = \frac{m}{4} gn \tag{19}$$

The bending and compression impact forces are calculated using Eqs. 20 and 21.

$$F_b = F_v \sin(\theta) \tag{20}$$

$$F_c = F_v \cos(\theta) \tag{21}$$

The tip deflections perpendicular to the tube and tube compression as a result of the impact force are calculated using Eqs. 22 and 23.

$$x_{b,max} = \frac{F_b L^3}{3EI} \tag{22}$$

$$x_{c,max} = \frac{F_c L}{EA} \tag{23}$$

Calculating Total Vertical Spring Force

Eqs. 24 and 25 calculate the vertical spring force caused by bending and compression of the leg. Both are scaled forms of Hooke's Law. They account for the spring force from four legs by multiplying through by a factor of 4. The compression and bending proportions of the spring force are multiplied by $\cos(\theta)$ and $\sin(\theta)$, respectively, in order to calculate the proportion of each force in the vertical.

$$F_{spring,c} = 4k_c x_{c,max} \cos(\theta) \tag{24}$$

$$F_{spring,b} = 4k_b x_{b,max} \sin(\theta) \tag{25}$$

These forces are combined with the Governing Equation to calculate the acceleration which the craft experiences in the vertical as a result of the spring forces and its own weight. g is taken to be positive, hence the " $[\text{negative}]mg$ " term in Eq. 26.

$$\ddot{x} = \frac{-mg + F_{spring,c} + F_{spring,b}}{m} \tag{26}$$

Impact Velocity

The impact velocity of the craft is calculated using Eq. 27.

$$V_{impact} = \sqrt{2gh} \tag{27}$$

Assuming constant deceleration at the value calculated in Eq. 26, the impact duration can be calculated using Eq. 28.

$$t = \frac{V_{impact}}{\ddot{x}} \tag{28}$$

The Criteria for a safe landing

Three measures used to quantify a safe impact in this study are the HIC [56] and estimates given in Eiband Curves [57] and Ernstings [58]. All three use average acceleration and average acceleration duration to predict likelihood of injury. The HIC is used for accelerations applied directly to the head, and the other two limits assume the subject to be in a seated position when a negative inertial force is applied to them (acceleration in the positive, +Gz direction – Refer Figure 65)

HIC (Head Injury Criterion)

A HIC value is calculated for each fall height based on the magnitude and duration of the average acceleration that the craft and rigidly attached pilot experiences.

The formula for the HIC is:

$$HIC = max\left[(t_2 - t_1)\left(\frac{1}{t_2 - t_1}\int_{t_1}^{t_2} \ddot{x}\, dt\right)^{2.5}\right] \quad (31)\ [56]$$

This takes the average acceleration over the interval which that acceleration affects the occupant, $t_2 - t_1$ (in this model, the peak acceleration and time taken for the craft to completely decelerate at the peak acceleration) and raises the average acceleration to a factor of 2.5. This value of 2.5 is chosen for head impacts based on experiments [56]. This value is multiplied by the time interval.

Yield Stresses

Eq. 3 only holds true for the elastic bending zone of a material, and therefore the yield limit of the material must be checked. If the yield limit is exceeded the spring constant will change and the deformation will become permanent.

4140 Q&T steel has a yield stress of 1640 MPa [59]. The maximum stress in the member can be calculated using Eqs 32 and 33 [60].

$$\sigma_{max} = \frac{F_b L}{Z} \quad (32)$$

$$Z = \frac{\pi(OD^4 - ID^4)}{32 \times OD} \quad (33)$$

For bending stresses under 1640 MPa, the legs will remain in the elastic region. The maximum stress simulated is 1641 MPa from a fall height of 0.95m for four 1m legs at 45°. With a 2m leg length, the yield stress is exceeded from a drop height of 1.77m.

Buckling Calculation

It is possible that the tube will buckle if the craft lands on one of the legs vertically. Eq. 34 is used to calculate the force necessary for the buckling of a member.

$$F_{buckle} = \frac{n_{end}\pi^2 EI}{L^2} \quad (34)$$

$$F_{buckle} = \frac{(0.25)(\pi^2)(200 \times 10^9)(3.29 \times 10^{-7})}{1^2}$$

$$F_{buckle} = 162.4\ kN$$

The simulation is ended if either the buckling limit or yield limit is exceeded.

Results

Worst Case Impact

The worst case acceleration is endured when the craft lands on all 4 legs, because the combined spring constant of all of the legs will be largest in this scenario. It is also possible that the craft lands on 1 leg, with the craft tilted over such that the impact is transmitted along the length of the leg, and only compressive forces act on the pilot. The difference in maximum acceleration experienced as a result of these two scenarios is shown in Figure 62. The maximum acceleration experienced from one leg increases at a much larger rate with increasing drop height than if all four legs simultaneously impacted the ground.

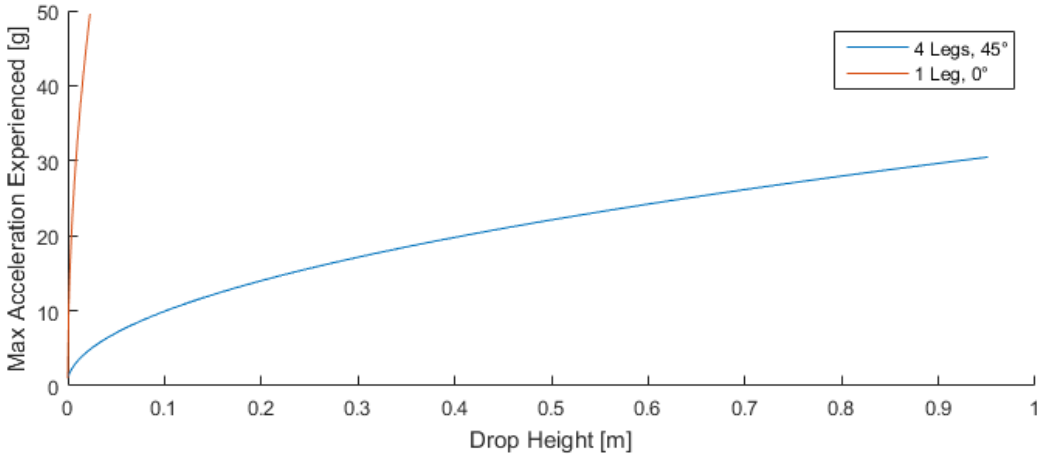

Figure 62: Landing Vertically on 1 Leg vs. 4 Legs at 45°

Figure 43 of the previous chapter shows that even when the craft is travelling at cruise speed, a craft angle of 40° is seldom exceeded with the exception of the outer bounds of the first 2-3 oscillations. The landing case of all 4 legs is a more likely scenario, as this is the equilibrium position of the craft with the parachute. This landing scenario (modelled without the parachute) is the focus of this report.

Comparison of Results to Known Limits

The simulated magnitude of the acceleration that the craft may experience is compared to known toleration and survival limits. Head and spinal injuries are two ways of measuring survival limits.

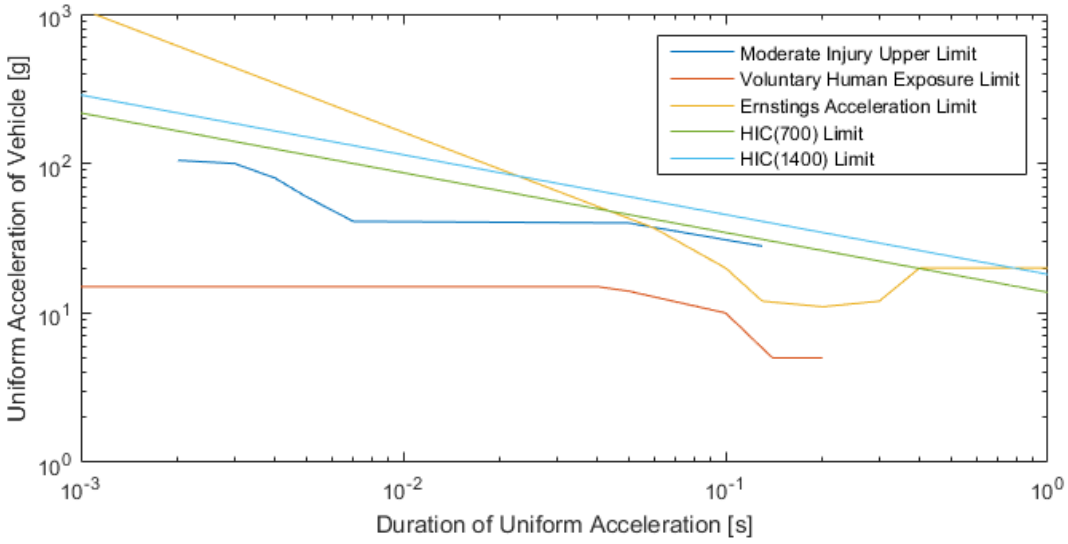

Figure 63: Comparison of Known Acceleration Limits

Figure 63 shows a comparison of limits of acceleration. A HIC value of 700 gives a 5% chance of life threatening brain injury, and HIC = 1400 gives a 50% chance [61]. Limits from Eiband curves (upper and voluntary exposure limits) [62] and Ernstings [58] are also included.

Spinal Injury Limits

Yoganandan [63] states that a vertical loading of 3.7 kN or above has a 50% chance in causing a spinal fracture. Figure 64 shows that the impact force rapidly increases with drop height. From a simulated height of 0.09m, the vertical force that the craft and rigidly attached pilot will be subjected to is 627 kN. This is 170x larger than the 50% probability threshold. The 3.5kN limit is surpassed from a drop height of 0.32mm.

From a drop height of 1mm off the ground, the total force on the craft/pilot is 66 kN and the impact factor is 21.7. This is largely due to the rigidity of the tube. If the same static force resulted in increased deflection, the impact factor and peak force experienced would also be lower.

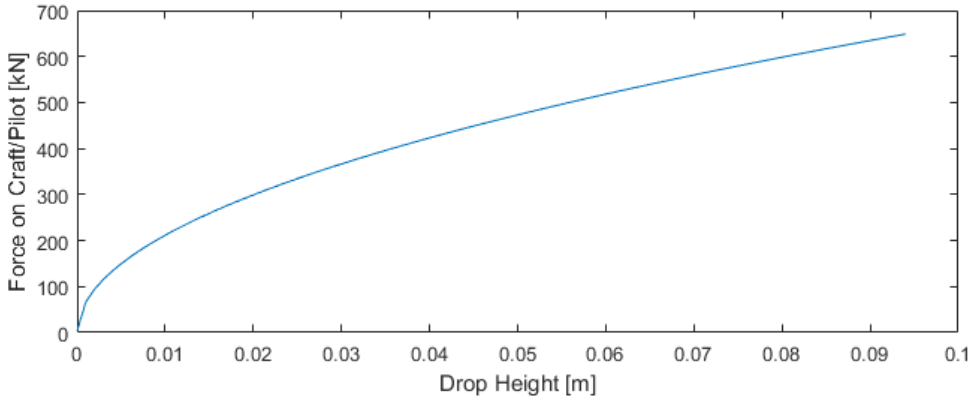

Figure 64: Force Craft and Rigidly Attached Pilot Experience from a Range of Fall Heights

Vertical (+Gz) Full Body Limits

The human tolerance and survivability to an acceleration is measured in [58] and [62] by average peak acceleration and its duration. This study assumes that the peak acceleration is the average acceleration, and the duration of the acceleration the time taken for the craft to decelerate from impact velocity to zero at the peak acceleration.

Figure 65 compares the known tolerable and survivable limits presented in [58] and [62] to the values obtained through simulated drop test simulations. One simulation translates to one data point on Figure 65, and a series of simulations from a range of heights makes up a line for one leg angle.

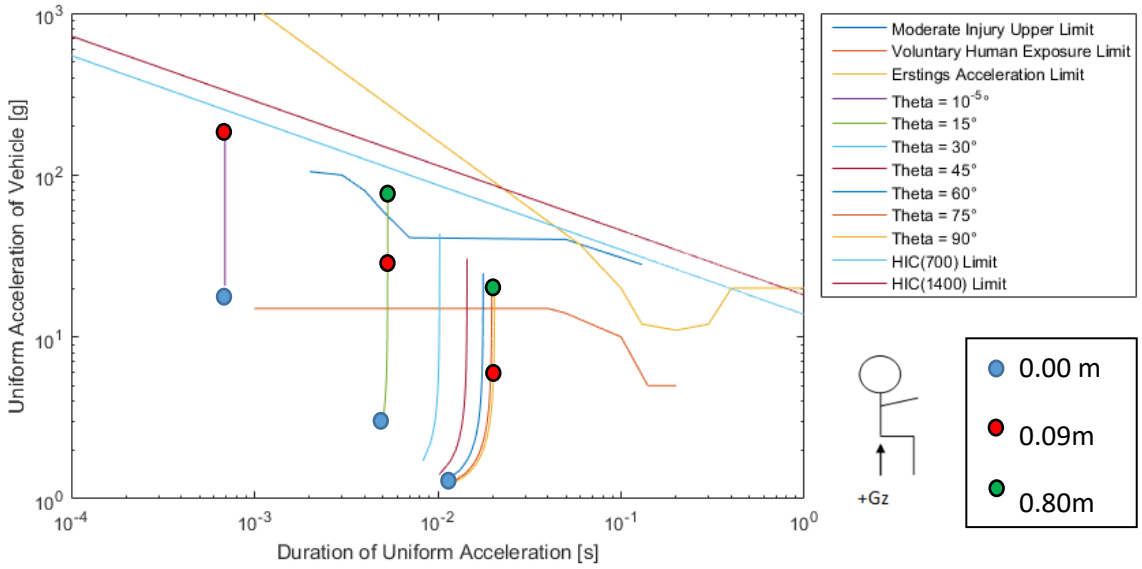

Figure 65: Simulated Acceleration Exposure against Known Limits. Material – Steel.

Table 8 summarizes where the known human limits are intersected on Figure 65. None of the simulated exposures cross the acceleration limit presented in [58].

Leg Angle [°]	Failure Mode	Fall Height at Failure [m]	Drop Height Exceeding Voluntary Human Exposure [m]	Drop Height Exceeding Moderate Injury [m]	Time Max Acceleration Endured [ms]
$1x10^{-5}$	Buckle	0.093	-	0.035	0.7
15	Yield	1.005	0.031	0.423	5.3
30	Yield	0.971	0.115	0.905	10.2
45	Yield	0.95	0.229	-	14.5
60	Yield	0.934	0.344	-	17.7
75	Yield	0.925	0.428	-	19.7
90	Yield	0.922	0.458	-	20.4

Table 8: Relevant Drop Heights and Heights where Thresholds are crossed

The moderate injury upper limit is not exceeded for leg angles of 45° and above, as the yield strength of the tube is exceeded before this limit. The limit estimated by Ernstings is also not reached before the yield stress is exceeded.

At a leg angle of $1x10^{-5}$ °, the acceleration duration is shorter than any estimate on the Eiband plot. Therefore the moderate injury limit has been extrapolated and may not be correct, hence highlighted in red.

Figure 66 suggests that the maximum acceleration that the craft experiences from a fall height of 0.95m into an infinitely hard surface is 31g's with the legs at 45°. This does not include damping of the ground which may have significant effects. The yield stress is exceeded at a drop height of 0.9-1m for angles of 15° and above.

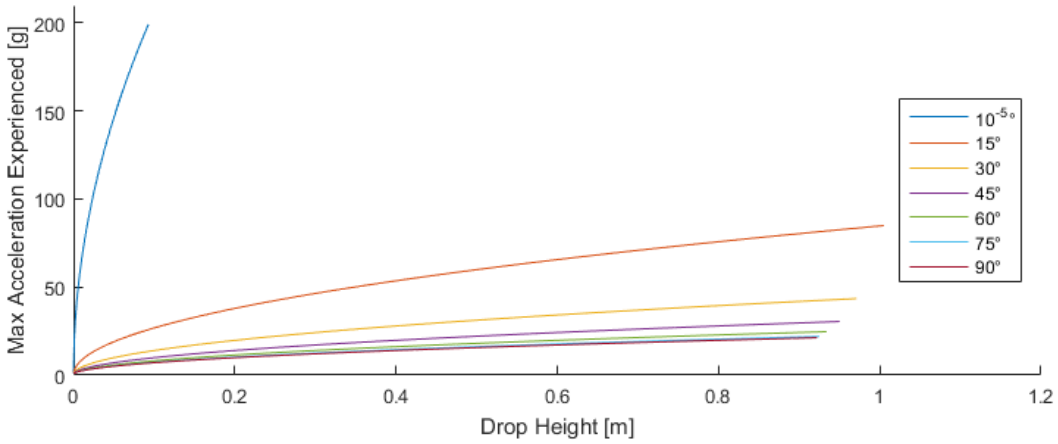

Figure 66: Maximum Acceleration for each Drop Height

The peak acceleration that the craft experiences from a drop height of zero is $+9.81m/s^2$. This is because the impact factor is 2 if dropped from 0m. There is 2g reaction force in the positive vertical, and 1g in the negative, hence a net maximum acceleration of +1g.

Figure 67 shows the peak acceleration and its duration for a leg angle of 45°

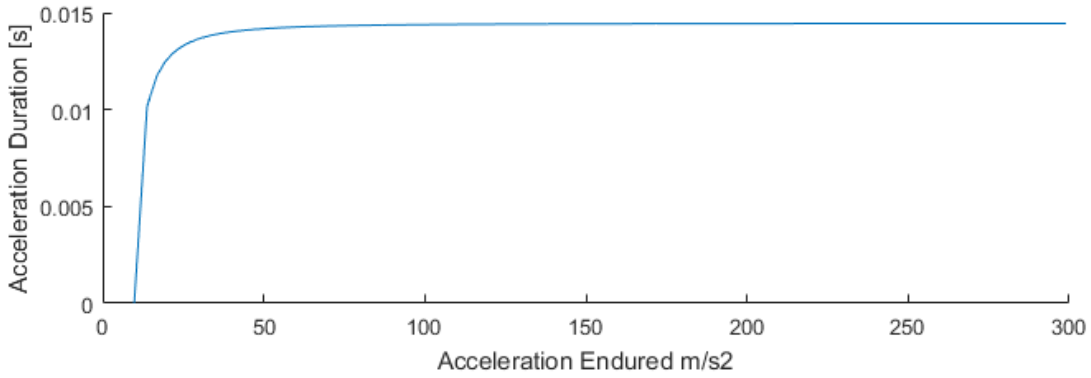

Figure 67: Peak acceleration and duration.

The acceleration duration increases negligibly with drop height above a critical height. This suggests that above this critical height the peak acceleration and impact velocity increase with drop height at a similar rate.

Head Injury Limits

Figure 68 and Figure 69 show the estimated HIC value for increasing drop height.

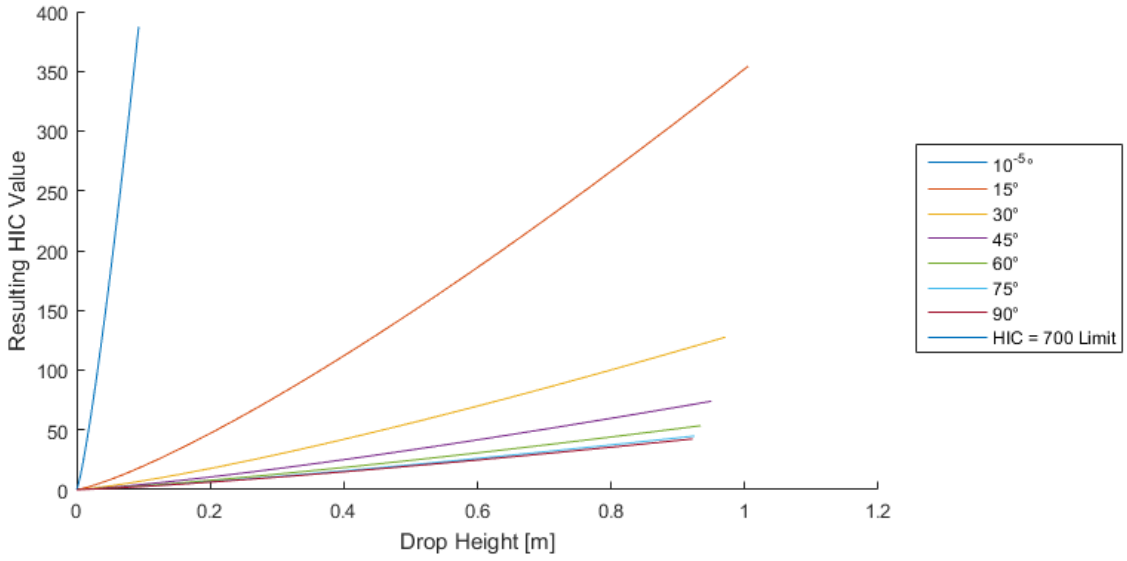

Figure 68: HIC Values for varying Drop Heights and Leg Angle

The HIC remains extremely low for all drop heights. This is likely due to the extremely large stress in the members. Lower angles cause the HIC to increase as the angle gets smaller, because of the large difference in the spring constants.

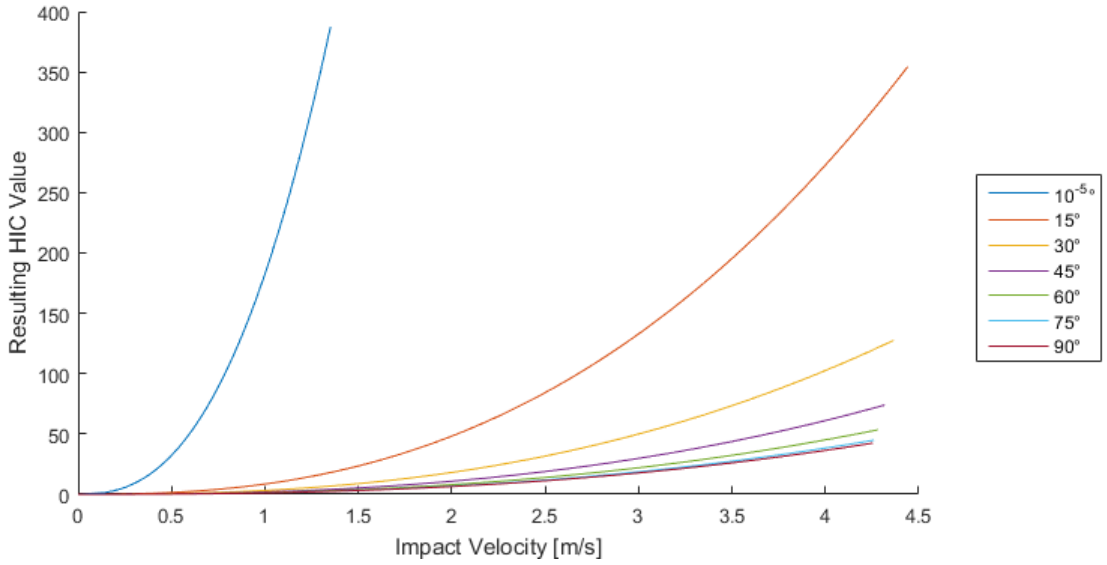

Figure 69: HIC vs. Impact Velocity for Different Leg Angles to Craft

For 15° and above, the impact velocity required to yield the material decreases. This is because the increase in angle increases the bending force, which is what the bending stress relies upon.

Figure 69 shows that the HIC values are very sensitive to the angle of the legs to the craft. At an angle of 90° (i.e. the legs are directly parallel to the ground and would only prevent the craft body from impacting the ground over a crevasse) the HIC increases at a much lower rate with increasing impact velocity than if the legs were at a lower angle.

The acceleration limits compared against rely on accurate data for the average acceleration and impact duration. The simulated accelerations and their durations are estimated based on the assumptions that the peak acceleration is also the average acceleration and that the acceleration is constant. The HIC relies on $\bar{a}^{2.5}$. Any error in the acceleration will be magnified. The Eiband and Ernstings limits do not need an altered acceleration value, and therefore will be a more accurate comparison to reality as errors are not magnified.

Discussion

The critical failure limit of the material was assumed to be the yield limit. In reality this will be the UTS, however the spring constant of the material will change if stresses beyond the yield limit are applied. The model must be expanded in order to explore the effects of a changing spring constant.

If a member is assumed to take ¼ of the crafts weight, the static bending stress at a leg angle of 45° is 52.3 MPa from Eqs 19, 32 and 33. This means that an impact factor of 31.4 is needed to exceed the 1640 MPa yield limit. It is possible to lower the impact factor at each drop height by adding damping in the system. All of the energy is assumed to be absorbed in the steel legs as opposed to the ground or other damping methods. If a rubber end or a more flexible tube was used, or the ground was assumed to be not infinitely hard, the static deflection would increase and therefore the impact factor would decrease. Another

method of decreasing the maximum stress in the member is to add a spring between the tube connection points on the craft.

Despite the large stresses, the accelerations and their durations are relatively low compared to known limits. This is likely because the craft is not dropped from a particularly large height when the yield stress is exceeded, meaning that the impact velocity is relatively low.

Changing the Leg Material

If the rod is modelled to be less rigid, static deflection would increase and impact factor would decrease as they are inversely related. The craft would decelerate over a longer time interval, which results in a lower HIC value. Figure 70 shows that aluminium produces a lower HIC value than steel from the same drop height.

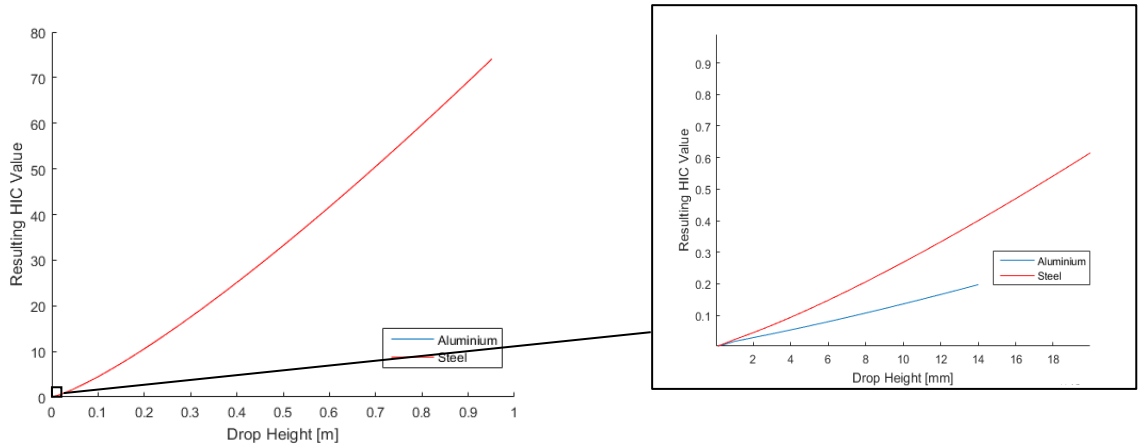

Figure 70: HIC Value if Steel (Left) or Aluminium (Right) Legs used.

The yield limit for the steel and aluminium legs is exceeded from drop heights of 0.951m and 0.014m, respectively. The HIC predicted for both steel and aluminium from these drop heights seems very small, though these are for low drop heights.

Figure 71 shows the accelerations and their durations for changing leg angles for different drop heights when the leg material is aluminium. The acceleration time for aluminium is longer than steel because of its lesser rigidity, and the peak accelerations which result from impact are much lower than those of steel. For example, at a 45° leg angle, the peak acceleration and duration from a drop height of 0.014m (the drop height from which aluminium yield stress is exceeded) is 23.4 m/s^2 for 22.4 ms for aluminium, compared with 37.6 m/s^2 for 14.0 ms for steel. These differences result in a HIC value of approximately 2x less for aluminium than steel for equivalent drop heights – 0.2 vs. 0.4 in this example.

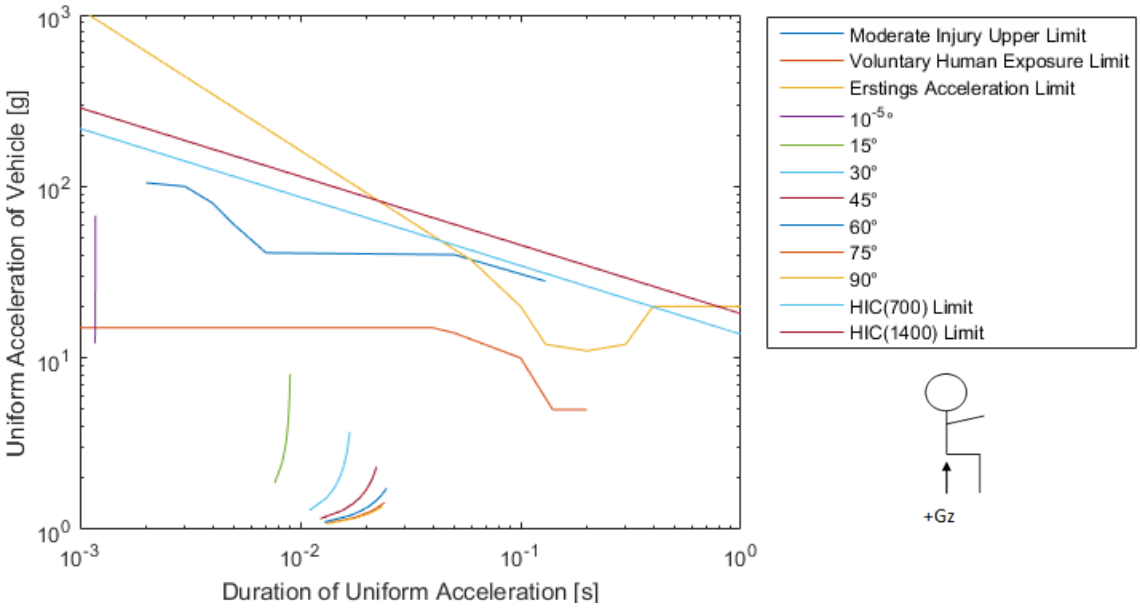

Figure 71: Accelerations and Durations for Changing Leg Angle for Aluminium

Yield Strength Comparison

Figure 72 shows the stresses in the legs from each drop height (onto all 4 legs) if steel or aluminium is assumed for the material. Refer Table 9 for yield stress limits.

Material	Yield Strength (MPa)
Steel (4140, Q&T)	1640 [59]
Aluminium – 335.0 sand casted	175 [59]

Table 9: Yield Strength of Materials used

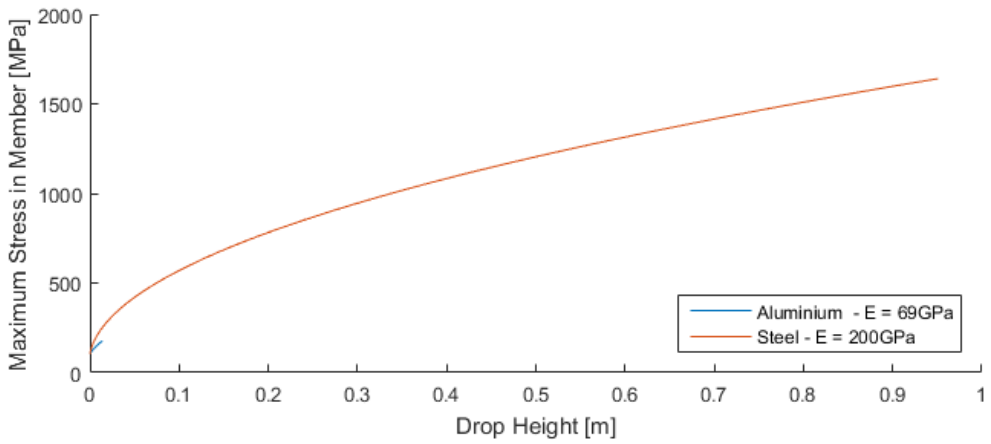

Figure 72: Stress that one Aluminium or Steel leg experiences.

The yield strength is exceeded above drop heights of 0.032m and 0.951m for aluminium and steel, respectively. One does not expect a metal tube of its size to reach its yield point from such a low fall height, however it is more understandable under the assumption of an infinitely hard surface and no other compliance in the system.

The member would certainly break under these scenarios. The steel tube would require a yield limit of 4.04 GPa to not yield from any drop height below 6m.

Fall onto One Leg

The craft can be modelled to fall onto 1 leg as one worst case scenario. Aluminium was not modelled as the maximum stress in the aluminium exceeded the yield limit even at a drop height of 0.001m.

Figure 73 shows the stress that a steel tube would experience if falling onto infinitely hard ground.

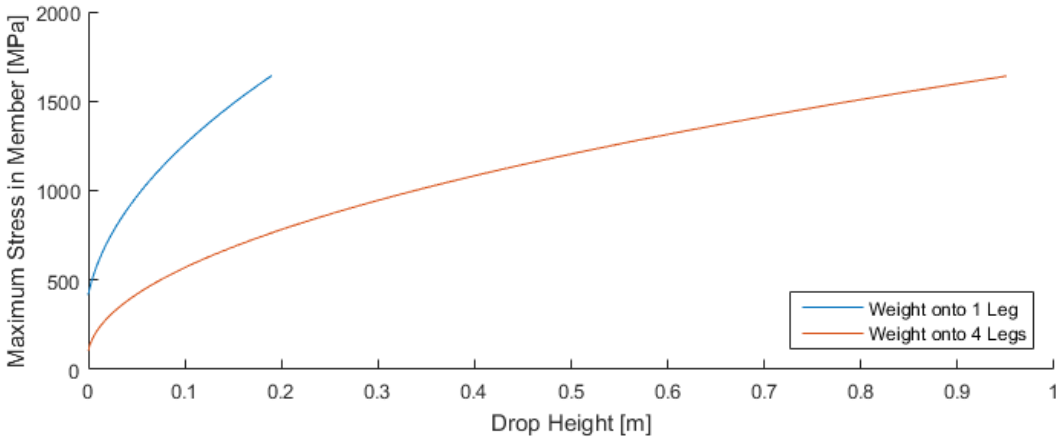

Figure 73: Modelled Fall onto Steel Leg, Theta = 45°

Buckling Comparison

Buckling occurs before the yield limit is exceeded at angles under 6° and 1° for steel and aluminium, respectively. Table 10 summarizes the buckling limits for the steel and aluminium tubes.

Material	Buckling Limit [kN]
Steel	162
Aluminium	56

Table 10: Buckling Limits

Figure 74 shows the differences in compression force for near vertical leg angles.

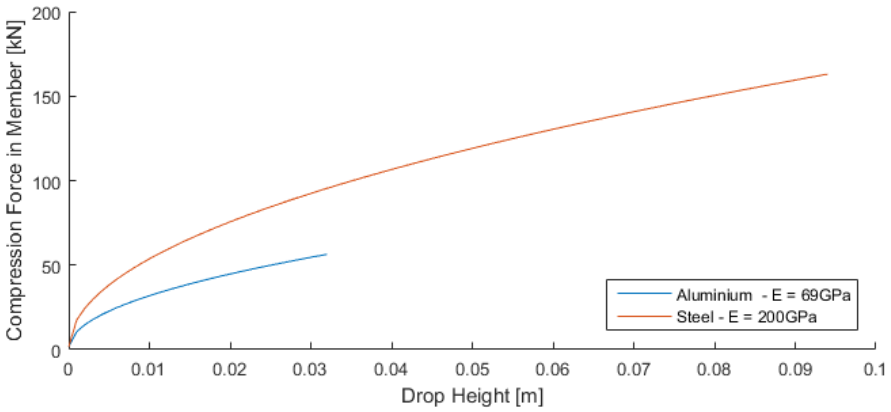

Figure 74: Buckling of Steel and Aluminium Member, Theta = 10^{-5} °.

The legs may buckle at small non-zero angles at a relatively lower compressive force when a bending force is present. The extent which the tube bends and compresses are assumed to be independent of one another. The bending of the tube may have effects on the compression limits and vice versa.

Altering Acceleration Values

The assumptions of infinitely hard ground and zero compliance in the leg mounts, airframe or pilots harness ensure that the peak acceleration is overestimated. Additionally, the average acceleration may not be the peak acceleration in reality. If the duration and average acceleration from test data were used, then the HIC value may be different.

Figure 75 shows that when the average acceleration is half peak acceleration (and the acceleration duration is therefore doubled), the HIC value decreases by a factor of 2.8 when compared to the assumption that the craft experiences the peak acceleration for the duration of the deceleration.

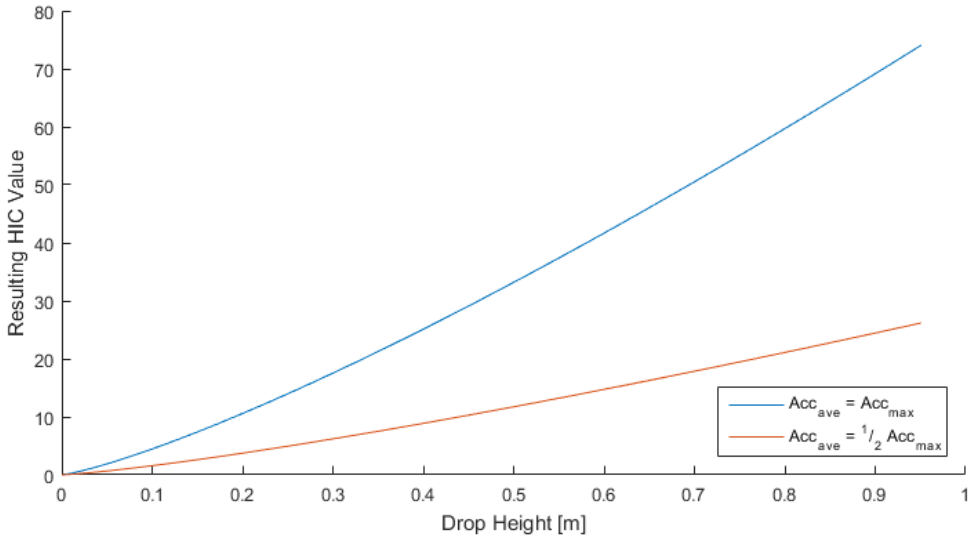

Figure 75: Comparison of HIC Experienced assuming full and half peak acceleration as the average.

Limitations and Future Impact Modelling

Onset rate of acceleration is not considered in this model. Eiband [57] states that the onset rate affects human tolerance and injury levels. Onset rates should therefore be investigated.

This model only considers the impact of a rigid body with rigidly attached legs impacting an infinitely hard surface. The accuracy of this model can be improved by accounting for damping and absorption of energy from factors such as the ground, damping systems on the Craft, and the pilot's body.

Conclusions

The impact of the craft onto all 4 legs from a vertical craft orientation was simulated. The leg angle was shown to have a large difference in accelerations and acceleration durations in changes of smaller angles, but the same changes at larger angles had less influence. This is because of the difference in the spring constants for the bending and compression of the leg.

The peak accelerations and estimated duration of the accelerations were modelled for leg angles of 10^{-5} (effectively zero) through to 90°. The peak acceleration caused by the reaction force from the legs on impact at a leg angle of 45° was modelled to be 299 m/s^2 from a drop height of 0.95m. If this acceleration is assumed to be the average deceleration which slows the craft from its impact velocity, then the duration of this acceleration would be 14.5ms. This combination is below the survivable limit by all 3 measures used – Ernstings, Eiband and HIC estimates.

The acceleration resulting from leg bending and compression for leg angles of 45° and above was shown to be below the limits given by Ernstings, the Eiband upper limit for moderate injury and the HIC from the drop heights where the yield stresses were exceeded. The maximum stress as a result of impact loading was shown to exceed the yield limit of 4140 steel from a drop height of 0.951m.

Steel is more rigid than aluminium, and therefore the accelerations experienced with a steel member are higher. The yield stress of aluminium is lower, therefore the yield stress for aluminium is exceeded from a lower drop height than steel.

Halving the assumed average acceleration and doubling the deceleration time was shown to decrease the HIC value by a factor of 2.8.

The forces upon impact were shown to be extremely high (98.7 kN from a drop height of 0.951m for a 45° leg angle). It is likely that injury will result from this simulated impact via spinal fracture. Introducing damping, such as a rubber foot, damper between the craft and pilot, or ground deformation may decrease the forces the pilot and craft are subjected to.

Other Research

Airbags

Different airbag mechanisms were considered. The motorcycle "Safety Sphere" [64] is a suit which the pilot wears with a built in airbag. If the rider is disconnected from their motorcycle, the suit inflates into a ball around them, shielding them from impact. This device may only be useful if the pilot is disconnected from the craft, which may not be possible due to the safety harness.

An airbag which surrounds the craft like on the Mars Curiosity rover may protect the pilot and craft, although the landing and bounce characteristics upon impact are not known, and may result in extra damage to surrounding people and objects.

An airbag vest or airbags built into the straps supporting the pilot may decrease the impulse that the pilot experiences. However, the lesser space between themselves and the strap may mean that if they are tightly strapped into the craft before the Airvest is activated they may be crushed.

Objective 2 – Requirements Setting via Functional and Safety Analysis

Since an automatic deployment system is likely needed, an initial concept is designed and detailed. The parachute system will be easier to certify if the automatic deployment system is completely separate from the rest of the Craft, because the systems will be separate.

Design of a Parachute Automatic Deployment System

The design of an automatic deployment system is an iterative process. The requirements of the system are to deploy the parachute when desired, and alert the pilot of error within the system

It is desired that the deployment system is made independently to the rest of the Craft. This means that the system can be removed from the Craft and still function without the need of any information that the Craft systems provide. It may be that only a system design which is dependent on other Craft signals (such as engine power or speed) can enable the parachute to be safely deployed.

The standard 14 CFR 23.1309 describes the rules under which equipment must be designed and installed. For example, “Information concerning unsafe system operating condition(s) must be provided in a timely manner to the crew to enable them to take appropriate corrective action.” [22] The notification of the failure of the automatic deployment system (before the system is needed) is accounted for with the inclusion of an LED or other means of warning.

MIL-HDBK-217F was constructed in 1991, so does not capture the failure rates of more modern circuit boards. The permissible failure rate for a component depends on the failure consequences of the system within which it is contained. If the component is part of a system where the consequences of failure are catastrophic (potentially the case for the CPU in Version 6 of the automatic deployment system), the failure rate of that system must not exceed 10^{-6} failures per flight hour for Class I aircraft. [21]. Versions 5b and 6 are described as they are the most recent.

Version 5b

Version 5b includes an automatic deployment system and a manual deployment system.

The GIS (Ground Isolation Switch) closes when the craft is in flight. This closes the battery powered test circuit. A resistor restricts the current through the circuit so that the cutter and ignitor do not activate, and to not blow out the LED. The LED indicates whether the test circuit is completed.

The manual deployment system requires the pilot to press the Parachute Activation Switch. The automatic deployment system uses inputs from accelerometers and gyroscopes to detect the acceleration of the craft in three dimensions. The FCS decides whether the acceleration or position is outside the acceptable flight envelope. If they are, a signal is sent through a relay which closes the circuit. Once the circuit has been manually or automatically closed the resistor is bypassed and the full current of the battery is able to pass through the circuit. This activates the CYPRES cutter which stops the engine in the case it is still operating by cutting the engine wire, and initiates the ignitor.

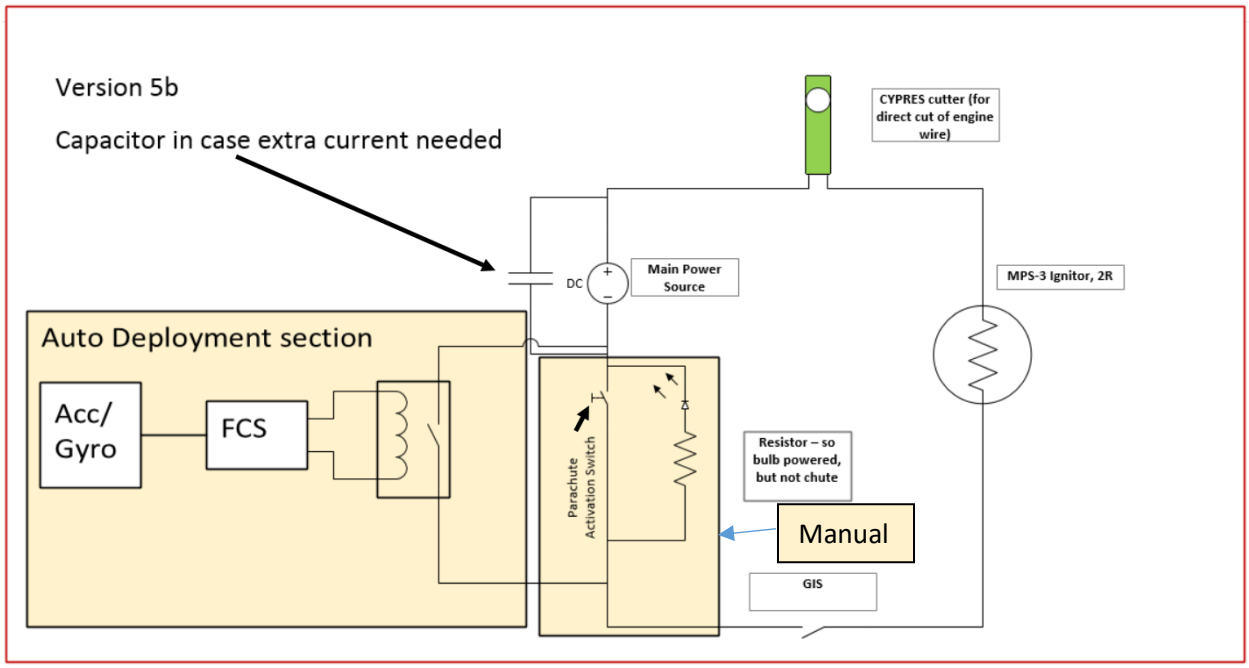

Figure 76: Automatic Deployment System – Version 5b

Version 6

Version 6 is the same as version 5b, with the changes being that a CPU is used to control the current through the circuit, and to test the battery. There are two LEDs, the active one depending on battery voltage. If the battery has charge, but not enough charge to fire the parachute then the red LED attached to the CPU will light, indicating to the pilot that the battery has low voltage. Otherwise the green LED will be active.

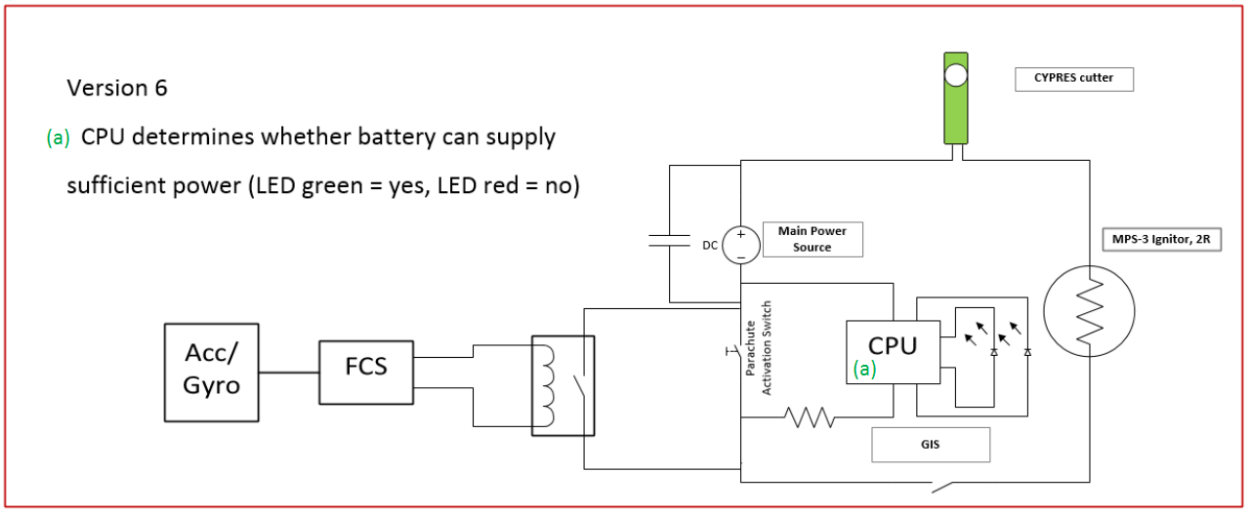

Figure 77: Automatic Deployment System – Version 6

If the cutter and detonator were in parallel instead of series, the exclusive failure of one item may be less or more hazardous depending on which item failed. For example, if the two components were in parallel and the cutter failed, the ignitor would still activate and the parachute would still deploy. However, if the ignitor failed and the cutter was successfully initiated the craft may be left in a perilous position.

The function of the CPU is to measure the voltage and output a signal to the LED which is dependent on whether the battery has sufficient voltage to fire the parachute.

This does bring a CPU into the system, which is something that has been attempted to be avoided in order to keep the components as simple as possible, and also the failure rates of these components are readily available through MIL-HDBK -217F.

The capacitor will hold a charge at the same voltage as the battery, so if the battery voltage is low, the capacitor voltage will be as well.

CYPRES Cutter [65]

One of the requirements of the parachute deployment mechanism is that it needs to send a cease engine command when activated. This command is important if the fans are still operating but are providing insufficient thrust to keep the craft airborne. Different methods of the engine cease command were explored, with an emphasis on physical means to break the engine circuit, as opposed to electronic signals. The motivation of physically breaking the engine wire was to ensure that independence of the system is maintained, i.e. it is impossible for the engine to influence the operation of the parachute deployment system. It is now likely that an electronic means will be used to send the cease engine command.

The most promising physical means to cease the engine upon parachute deployment was the CYPRES cutter, an Automatic Activation Device (AAD). Figure 78 shows the cutter.

Figure 78: CYPRES Cutter, adapted from [65]. Official website: https://www.cypres.aero.

The intended use for the CYPRES cutter is in a skydiver's automatic deployment system, although alternative uses of the cutter are permitted [65]. The CYPRES cutter can cut 7x7 aircraft cable (structure) up to 2.6mm thick (2.6mm>3/32 inches).

It is possible that the CYPRES system can assist in determining whether the parachute should deploy. The CYPRES system activates if the user is i) Below a given altitude and ii) travelling beyond a given vertical velocity limit. This means that it is likely that this type of automatic deployment system will not be ideal for the Craft as it could be falling from a low height, thereby not activating until the aircraft gains sufficient speed. The CYPRES system will be useful for automatic deployment if the Craft loses power at a significant height, but it is desired that engine power loss is detected as soon as possible.

Inertial Measurement Unit

An Inertial Measurement Unit (IMU) will almost certainly be required to accurately and reliably detect whether the position, orientation, travel path and velocity of the Craft are within the limits of the normal flight envelope. Further research and optimization of the correct IMU is required.

Estimates as per MIL-HDBK-217F [66] suggest that the relay is the most likely component to fail. The option of adding redundant systems is possible so long as they don't inadvertently activate the automatic deployment system or interfere with one another. Refer Appendix 6 for values and equations used for failure rate calculations.

Component Failure Rates

As the various versions of the deployment circuit were developed, fault trees for each of them were created to identify the possible ways of failure. Refer Appendix 5 for FTAs constructed for Version 5b. FTAs are based on industry FHAs.

The "failure rates of the system" means the failure rate for a given failure condition, as identified in the FHA. Quantitative data for the failure rates of the system were obtained using MIL-HDBK-217F [66]. Table 11 summarizes these failure rates as calculated assuming the conditions highlighted in Appendix 6. Note that "wires and cables are assumed to have a zero failure rate", and the failure probability of some components of the circuit are currently unknown.

Component	Failure Rate (Failures/flight hour)	Number of Component (in Version 5b)	Overall Failure Rate (Failures/flight hour)
Accelerometer/Gyro/IMU	(No Data)	1	-
FCS/CPU1	(No Data)	1	-
Relay	**2.97E-08**	1	**2.97E-08**
Parachute Activation Switch	**2.20E-08**	1	**2.20E-08**
Resistor	**1.77E-10**	1	**1.77E-10**
Ground Isolation Switch	**2.20E-08**	1	**2.20E-08**
LED	**7.39E-08**	2	**1.48E-07**
MPS-3 Ignitor 2R	(No Data)	1	-
CYPRES Cutter	(No Data)	1	-
Capacitor	**2.00E-08**	1	**2.00E-08**
Battery	(No Data)	1	-
Connections	**5.60E-11**	40	**2.24E-09**
SYSTEM		51	(Insufficient Data)

Table 11: estimated failure rates of Version 5b components and System

Overall Failure Rate Calculation

The probabilities can be inserted into the fault trees as basic events and their probability of failure summed at "OR", however this does not account for "the overall hybrid function, π_F, screening level, π_Q, and maturity π_L" as mentioned in §5.5, MIL-217F. This is the recommended procedure for determining the failure rate of hybrid circuits. The failure rates of "No Data" items in Table 11 have not been estimated nor assumed, and thus a failure rate for the overall system has not yet been identified.

The probability of failure of the deployment of the parachute system may by multiplied. "For example, the deployment system might fail 1/100 times resulting in fatality. But if the probability of the aircraft requiring the parachute is once every 10000 flight hours, then overall probability of requiring a parachute and it failing is 1/1,000,000 which might be OK" [7]. Another consideration is that "some failure modes [may] only lead to injury (e.g partial deployment), hence are allowed to have a higher probability [in accordance with the] safety objective"

Future Work on Parachute Auto Deployment System

Extra calculations may be required in order to assess the system as a whole (and obtain a failure rate for it) as opposed to each individual component.

Patent Review - Auto Deployment System

The following patents may include material of interest when designing an automatic deployment system or parachute system. These include a method of parachute initiation which may be similar to future developments of the system in question and a method of releasing the parachute upon impact.

"Method for deploying a parachute release on a drone"
http://www.google.com/patents/US6471160

"Parachute release apparatus"
https://www.google.com/patents/US2843416

Conclusions

The Martin Jetpack is an aircraft whose type has not yet been fully certified under civil aviation law. Clear grounds do not currently exist for its full type certification. One path to certification involves understanding all systems of the Craft through quantitative and qualitative analysis. This can be achieved under the guidance of standards such as ARP4761 and ARP4764A.

Three systems were studied – the parachute during emergency descent, the landing gear and the parachute automatic deployment system. The dynamics of the parachute and Craft during the emergency descent phase are modelled. A range of initial conditions were tested to gain an understanding of under which scenarios the pilot is likely to survive impact, based on known limits. Simulations using the assumed parameters suggest that an ø8.4m parachute will not be sufficient to eliminate the UDZ, regardless of the pilot/system reaction time. A larger (>ø12m) parachute may be sufficient, assuming a similar deployment time to the ø8.4m parachute.

Simulated factors which affected the UDZ included whether wind conditions were present, the crafts initial vertical velocity and whether the craft was travelling at cruise speed or had zero horizontal velocity at power loss. The UDZ upper limit starts at ~40m under most circumstances when the PRT is 0s, and increases with increasing reaction time.

The addition of an 8m/s wind increases the UDZ upper limit by 19.2m for the descending case and a reaction time of 0s. At a PRT of 3s, the difference in UDZ upper limit between initial vertical velocities of +2m/s and -2m/s is 12.9m. If the PRT is decreased to zero, this decreases to 4.2m. The effects of initial horizontal velocity conditions on the UDZ upper limit were noticeable, though not as significant as changing the parachute diameter when the craft was at cruise speed. Changing the parachute diameter from 8.4m to 12m decreased the UDZ upper limit by up to 24.5m. Reducing the PRT from 3s to zero decreases the UDZ upper limit from 102.4m to 40.5m for an ø8.4m parachute when the Craft has zero initial vertical velocity.

An automatic deployment system may be necessary (albeit a more advanced one than the one developed here), but not sufficient to eliminate the Unsafe Deployment Zone if it can send the deployment signal faster than a manual system. FTAs were carried out after identifying the ways in which the system could fail, and the failure rates were calculated based on estimates and assumptions. An automatic deployment system will be useful certain power loss heights, the range of which dependent on factors such as craft initial conditions and wind speed. The values of these heights depend on factors such as the parachute diameter.

Rudimentary modelling of the landing gear was performed. This model needs further developments such as the addition of damping before results will be useful.

Future Modelling Work

The resources of this project do not allow the model to be investigated further, however the following changes and scenarios can be considered in future.

Changes in the model

The 2D model could be expanded into a 3D model to account for aircraft roll and yaw. This will be especially useful for modelling the craft if the parachute is launched when the roll or yaw is non-zero, as the oscillations of the craft will no longer be restricted to one plane.

The damping properties of the craft oscillations relative to the parachute may need to be revised. This will determine whether the oscillatory behaviour of the craft in reality matches other objects in descent, or whether the damping factor used in the model is not necessary.

This model only considers a single point where the parachute attaches to the craft. In reality there may be more attachment points. Modelling this will be possible in both 2D and 3D simulations. The forces in the individual risers could be modelled in future. Figure 79 shows how a model might look with this change.

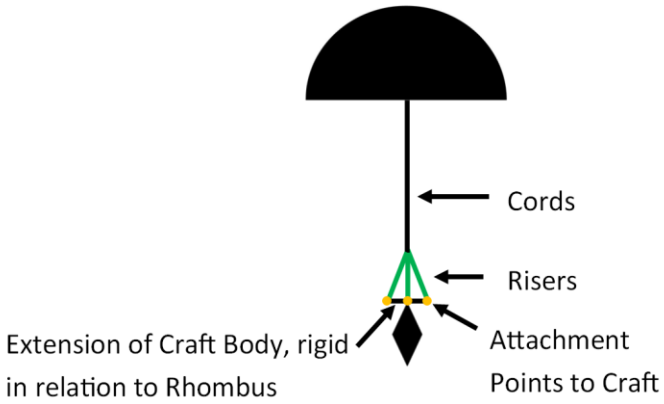

Figure 79: Possible Future Model

Future modelling could allow for change of craft orientation during freefall. This would involve using the relative positions of the COP and COM to calculate a torque on the aircraft. This torque can be used to find a new craft angle.

The parachute has been assumed to remain at full inflation for the duration of the descent. Future research may involve determining whether this is true for the majority of emergency descent conditions.

This model does not account for the ballistic nature of the parachute. Future simulations could assume an initial non-zero parachute velocity relative to the Craft. Data for the area of the parachute exposed to the oncoming air will be required for drag force calculations as opposed to force measurements.

The behaviour of the parachute may depend on the pitch and roll of the craft. Testing may need to be performed to determine how the parachute acts in each scenario.

Scenario Testing

Parachute Drawn into Fans

It is possible that the parachute could get drawn into the fans if they are still rotating at the time of deployment. If it does not get drawn in, then the successful deployment of the parachute could still be delayed. Further modelling or testing will be required to determine how the rotating fans affect the deployment of the parachute.

Unsafe Parachute Deployment Angle

The parachute has been assumed to successfully deploy independent of the angle it is launched at. Future testing may include identifying if there are scenarios where the parachute will not successfully deploy.

Impact Modelling - Analysis of Orientation Impacts

Impact orientation effects have not been extensively considered. The orientation may be a significant factor of impact damage. Future work may need to be performed in this area.

Impact Modelling – Spring-Damper Model of Ground and Systems

The assumption of infinitely hard ground has been used, with no damping systems modelled. A more accurate model should consider the damping of the ground and Craft systems. This may decrease peak stress in the members from each drop height.

Impact Modelling – Model for Composite Material

Only steel and aluminium have been modelled and compared. Future modelling should involve the analysis of a composite material and a more realistic geometry of the legs.

This Modelling Work and Certification

The impact conditions predicted by the dynamic descent model can be used as input data for a model simulating craft impact. The forces and acceleration on the pilot and craft can be simulated and compared to known limits. A more complex impact model than that presented in this thesis will be required to assess this data.

The scenarios which may cause catastrophic failure (loss of craft and pilot) can be determined. If there are scenarios which result in catastrophic failure, then the architecture of the systems designed to protect against high velocity impact will need to be reassessed.

Future Automatic Deployment systems:

Future systems may need to have a timer (such as a 555 timer) or a micro controller in order to restrict the current to pulse it through the circuit.

It was not recommended that a constant current be allowed to run through the circuit continuously. CYPRES [67] recommended a test current be sent every 5 minutes as a continuous test current “will dissolve the guncotton … due to the constant heat”. Version 6 begins to explore methods of allowing an intermittent test current through the system.

Appendix 1 – Survivable Impact Velocities for a Human

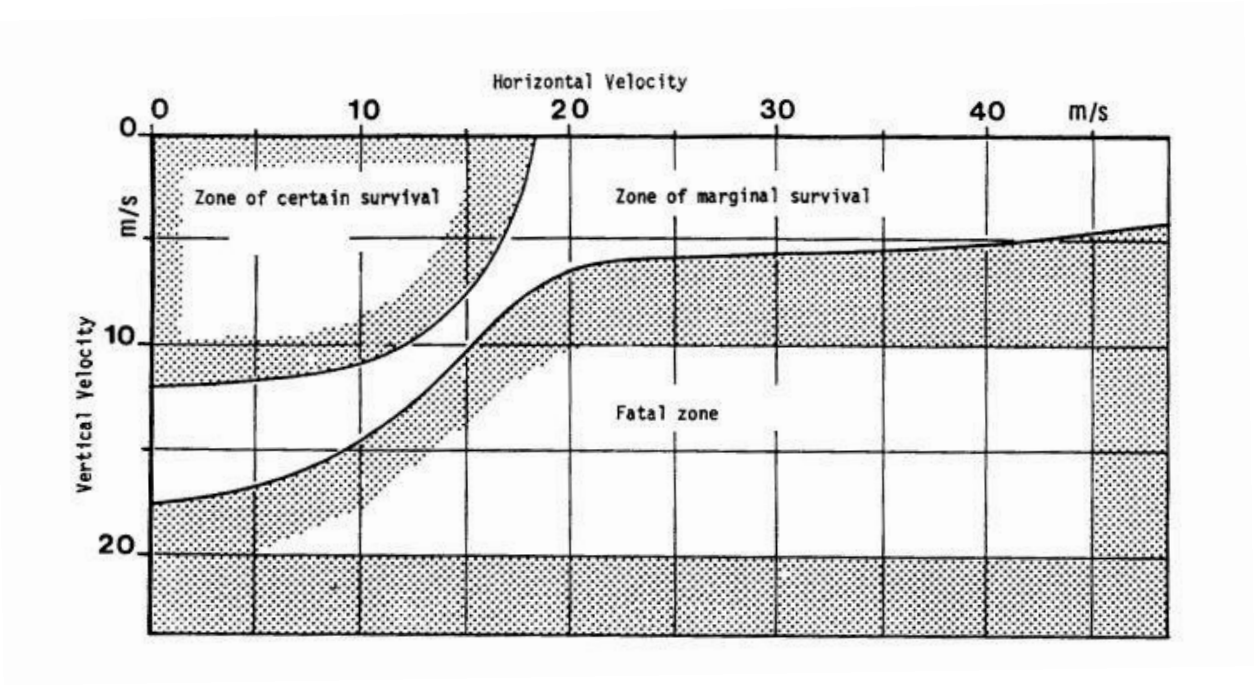

Figure 80: Human Tolerance to Impact Velocities [4]

Appendix 2 –Convergence Study Values

For Simulated Descent Time and Horizontal Distance Travelled					
Spring Constant, k	Timestep [s]	Simulated Descent Time [s]	Difference	Horizontal Distance Travelled [m]	Difference
k=28*250000	0.0005	12.751	4.02E-01	127.713	2.96E+00
k= $7x10^6$ N/m	0.0004	12.349	3.45E-01	124.756	2.46E+00
	0.0003	12.004	2.67E-01	122.298	2.06E+00
	0.0002	11.737	1.66E-01	120.234	1.30E+00
	0.0001	11.572	1.93E-02	118.932	1.48E-01
	0.00008	11.553	7.68E-03	118.784	6.00E-02
	0.00007	11.545		118.724	
For Measuring Tension Force, FT					
Spring Constant, k	Timestep [s]	Max FT [N]	Difference	Max du [m]	Difference
k=28*250000	0.00005	2.72E+05	3.46E+03	0.03881	4.95E-04
k= $7x10^6$ N/m	0.00004	2.68E+05	3.37E+03	0.03832	4.82E-04
	0.00003	2.65E+05	3.33E+03	0.03784	4.76E-04
	0.00002	2.62E+05	3.28E+03	0.03736	4.69E-04
	0.00001	2.58E+05	1.62E+03	0.03689	2.32E-04
	0.000005	2.57E+05		0.03666	
k=10*250000	0.00005	1.60E+05	1.15E+03	0.06386	4.61E-04
k= $2.5x10^6$ N/m	0.00004	1.58E+05	1.13E+03	0.06340	4.50E-04
	0.00003	1.57E+05	1.12E+03	0.06295	4.48E-04
	0.00002	1.56E+05	1.11E+03	0.06250	4.44E-04
	0.00001	1.55E+05	5.50E+02	0.06206	2.20E-04
	0.000005	1.55E+05		0.06184	

Table 12: Convergence Study Values

Appendix 3 – Method for Damping Constant Attainment [68]

One method of obtaining the damping constant is determining how the system responds to a pulse/step input and observing how it responds. The response will likely take a similar form to that illustrated in Figure 81.

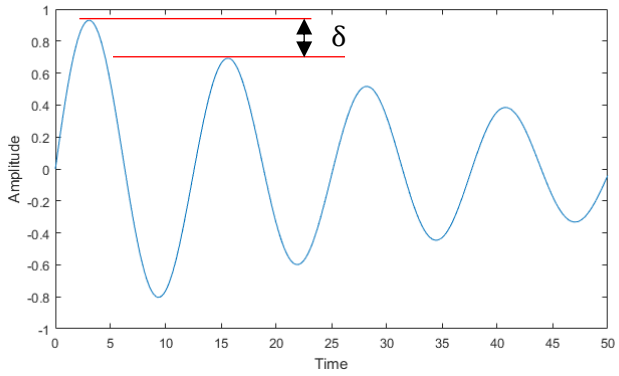

Figure 81: Damped Oscillation

From the difference in the peaks over one oscillation it will be possible to determine the damping constant. This can be done by using the logarithmic decrement, which is the "natural logarithm of the ratio of any two successive amplitudes" [68] (Equation A1)

$$\delta = \frac{1}{n}\ln\left(\frac{x(t)}{x(t+nT)}\right) \tag{A1}$$

Where:

δ = difference in amplitude between the 2 peaks
$x(t)$ = amplitude of first peak examined
$x(t+nT)$= amplitude of second peak examined
n = Number of oscillations between peaks analyzed.
T = Period of oscillatory motion

From this the damping ratio, ζ, can be determined by Equation A2

$$\zeta = \frac{1}{\sqrt{1+\left(\frac{2\pi}{\delta}\right)^2}} \tag{A2}$$

From the damping ratio, the damping constant can be determined using Equation A3

$$d = \zeta 2\sqrt{mk} \tag{A3}$$

Appendix 4 – Iterative design of the deployment mechanism

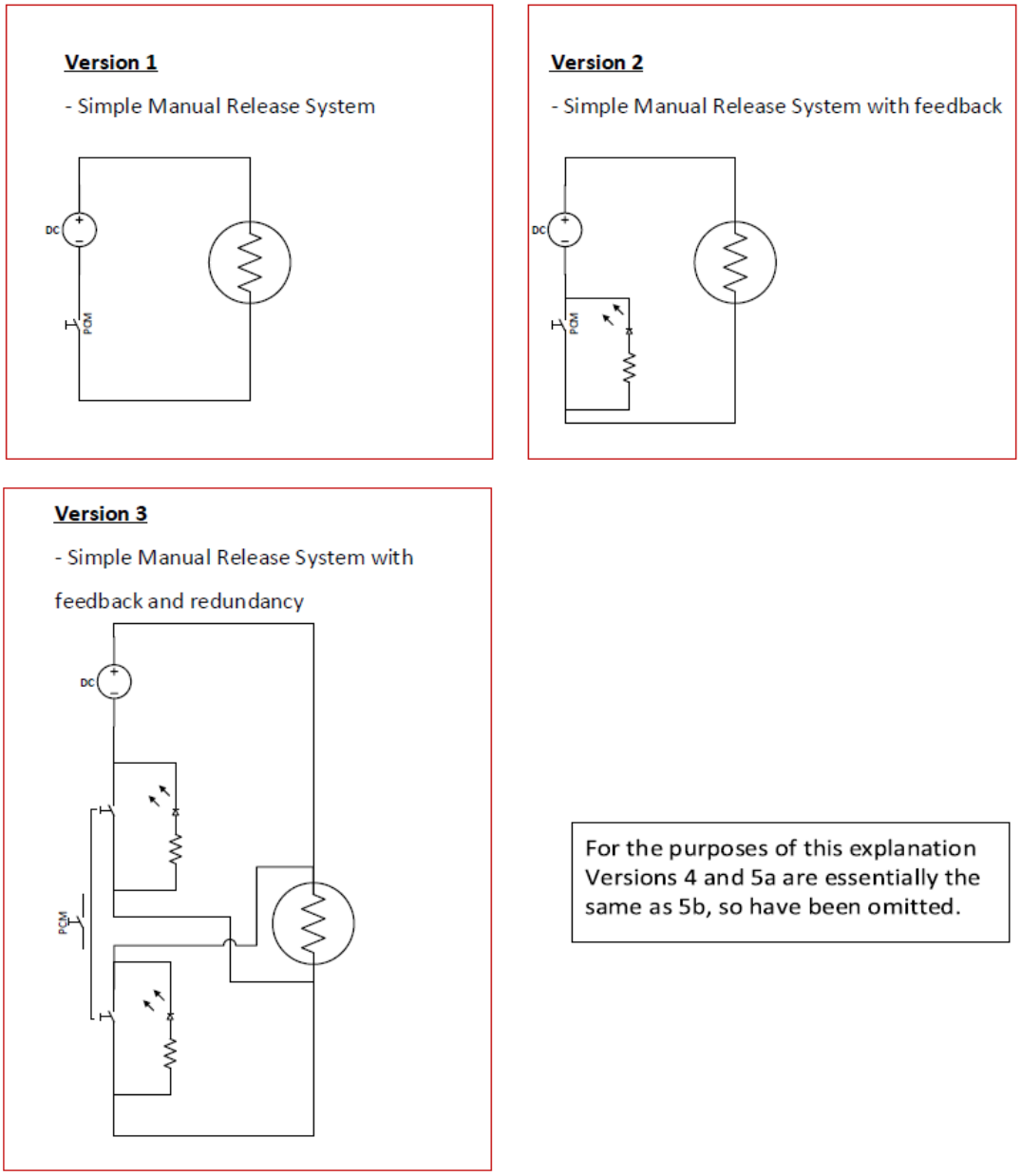

Figure 82: First Three Versions of Automatic Deployment System

Appendix 5 – FTAs for Version 5b

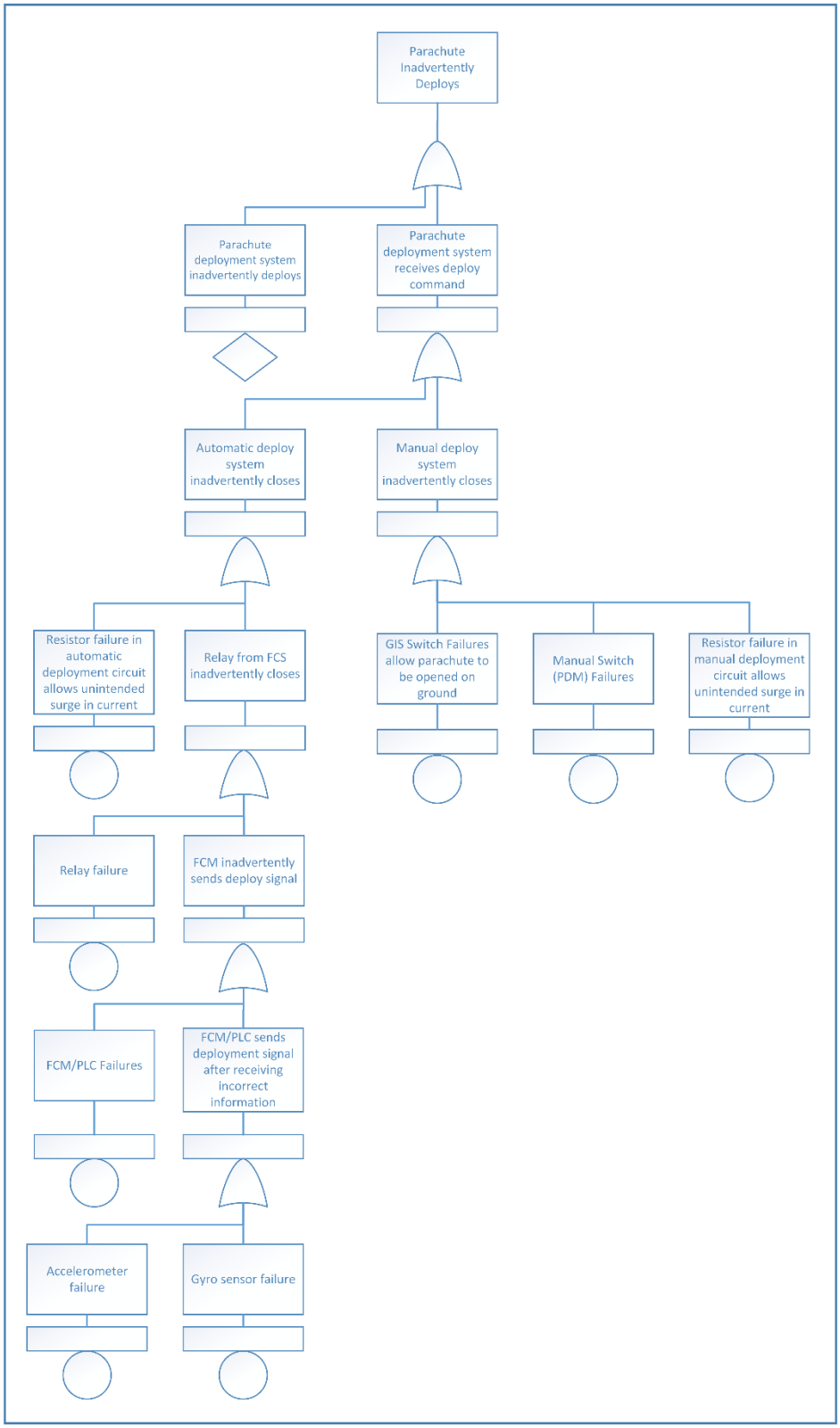

Figure 83: FTA for Inadvertent Parachute Deployment

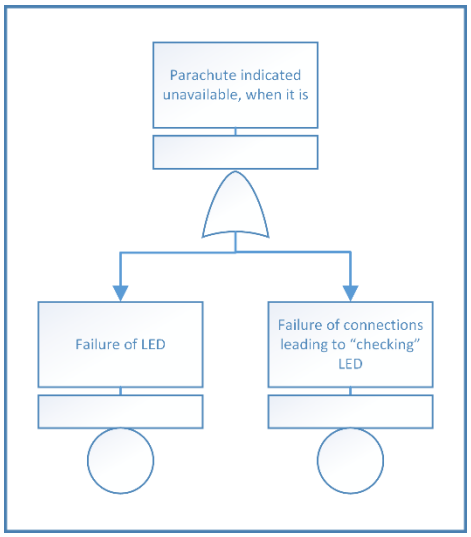

Figure 84: FTA for Parachute Availability Indication

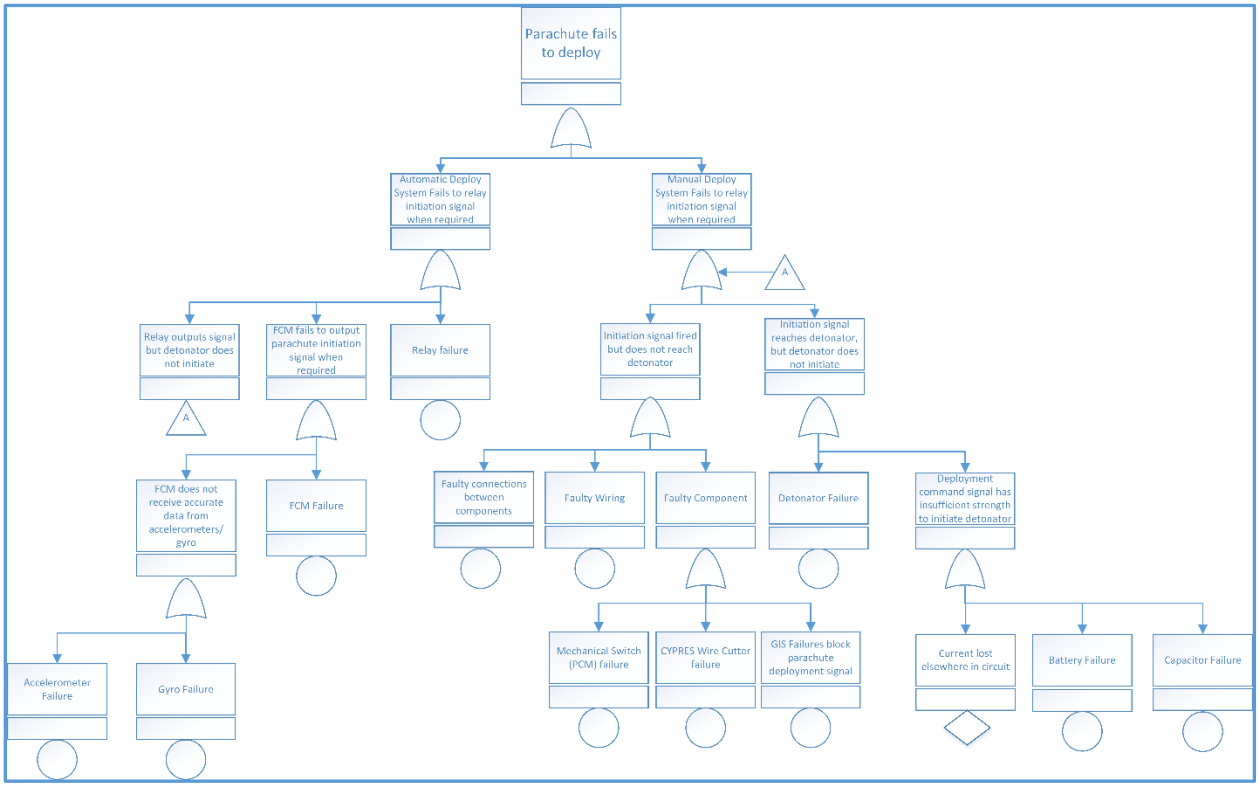

Figure 85: FTA for Failed Parachute Deployment

FCM – Flight Control Module
GIS – Ground Isolation Switch
PCM – Pilot Control Module
PDM – Power Distribution Module

Appendix 6 – Failure Rate Calculations – Assumed Factors

NOTE: These values by no means represent the conditions and quality of the components used on the craft. The chosen values in the following tables and calculated failure rates are intended to provide an estimate only and a process of predicting failure rates. Reasoning to the selection of values has been given where possible.

Determining Junction Temperature, T_J

Assume one layer substrate of Beryllium Oxide. Assume Die Power Dissipation of 1 Watt. Assume 47 Die Active Wire Terminals, because same number of connections. **NOTE**: Number of terminals and connections may be different.

MIL-HDBK-217F

5.12 MICROCIRCUITS, T_J DETERMINATION, (FOR HYBRIDS)

This section describes a method for estimating junction temperature (T_J) for integrated circuit dice mounted in a hybrid package. A hybrid is normally made up of one or more substrate assemblies mounted within a sealed package. Each substrate assembly consists of active and passive chips with thick or thin film metallization mounted on the substrate, which in turn may have multiple layers of metallization and dielectric on the surface. Figure 5-1 is a cross-sectional view of a hybrid with a single multi-layered substrate. The layers within the hybrid are made up of various materials with different thermal characteristics. The table following Figure 5-1 provides a list of commonly used hybrid materials with typical thicknesses and corresponding thermal conductivities (K). If the hybrid internal structure cannot be determined, use the following default values for the temperature rise from case to junction: microcircuits, 10°C; transistors, 25°C; diodes, 20°C. Assume capacitors are at T_C.

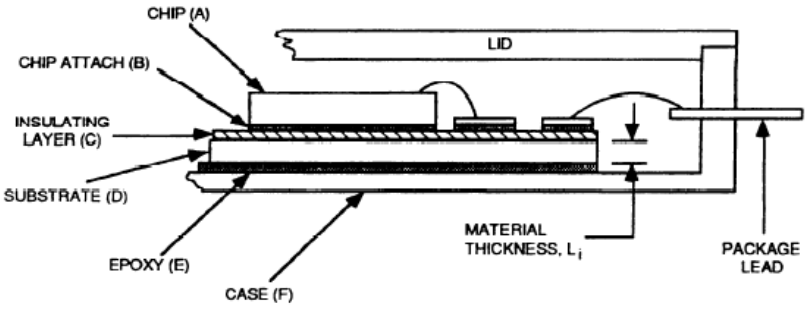

Figure 5-1: Cross-sectional View of a Hybrid with a Single Multi-Layered Substrate

5-18

Figure A 1: Junction Temperature Determination, Part I

5.12 MICROCIRCUITS, T_J DETERMINATION, (FOR HYBRIDS)

Typical Hybrid Characteristics

Material	Typical Usage	Typical Thickness, L_i (in.)	Feature From Figure 5-1	Thermal Conductivity, K_i $\left(\frac{W/in^2}{°C/in}\right)$	$\left(\frac{1}{K_i}\right)(L_i)$ $\left(in^2\ °C/W\right)$
Silicon	Chip Device	0.010	A	2.20	.0045
GaAs	Chip Device	0.0070	A	.76	.0092
Au Eutectic	Chip Attach	0.0001	B	6.9	.000014
Solder	Chip/Substrate Attach	0.0030	B/E	1.3	.0023
Epoxy (Dielectric)	Chip/Substrate Attach	0.0035	B/E	.0060	.58
Epoxy (Conductive)	Chip Attach	0.0035	B	.15	.023
Thick Film Dielectric	Glass Insulating Layer	0.0030	C	.66	.0045
Alumina	Substrate, MHP	0.025	D	.64	.039
Beryllium Oxide	Substrate, PHP	0.025	D	6.6	.0038
Kovar	Case, MHP	0.020	F	.42	.048
Aluminum	Case, MHP	0.020	F	4.6	.0043
Copper	Case, PHP	0.020	F	9.9	.0020

NOTE: MHP: Multichip Hybrid Package, PHP: Power Hybrid Package (Pwr: ≥ 2W, Typically)

$$\theta_{JC} = \frac{\sum_{i=1}^{n}\left(\frac{1}{K_i}\right)(L_i)}{A}$$

n = Number of Material Layers

K_i = Thermal Conductivity of i^{th} Material $\left(\frac{W/in^2}{°C/in}\right)$ (User Provided or From Table)

L_i = Thickness of i^{th} Material (in) (User Provided or From Table)

A = Die Area (in^2). If Die Area cannot be readily determined, estimate as follows:
$A = [\ .00278\ (\text{No. of Die Active Wire Terminals}) + .0417]^2$

Estimate T_J as Follows:

$$T_J = T_C + .9\ (\theta_{JC})\ (P_D)$$

T_C = Hybrid Case Temperature (°C). If unknown, use the T_C Default Table shown in Section 5.11.

θ_{JC} = Junction-to-Case Thermal Resistance (°C/W) (As determined above)

P_D = Die Power Dissipation (W)

Figure A 2: Junction Temperature Determination, Part II

5.11 MICROCIRCUITS, T_J DETERMINATION, (ALL EXCEPT HYBRIDS)

Ideally, device case temperatures should be determined from a detailed thermal analysis of the equipment. Device junction temperature is then calculated with the following relationship:

$$T_J = T_C + \theta_{JC}P$$

T_J = Worst Case Junction Temperature (°C).

T_C = Case Temperature (°C). If not available, use the following default table.

Default Case Temperature (T_C) for all Environments

Environment	G_B	G_F	G_M	N_S	N_U	A_{IC}	A_{IF}	A_{UC}	A_{UF}	A_{RW}	S_F	M_F	M_L	C_L
T_C (°C)	35	45	50	45	50	60	60	75	75	60	35	50	60	45

θ_{JC} = Junction-to-case thermal resistance (°C/watt) for a device soldered into a printed circuit board. If θ_{JC} is not available, use a value contained in a specification for the closest equivalent device or use the following table.

Package Type (Ceramic Only)	Die Area > 14,400 mil^2 θ_{JC} (°C/W)	Die Area ≤ 14,400 mil^2 θ_{JC} (°C/W)
Dual-In-Line	11	28
Flat Package	10	22
Chip Carrier	10	20
Pin Grid Array	10	20
Can	–	70

P = The maximum power dissipation realized in a system application. If the applied power is not available, use the maximum power dissipation from the specification for the closest equivalent device.

Figure A 3: Junction Temperature Determination, Part III

Environmental Definition

Rotary wing (RW) environment closest to Craft operating conditions.

Table 3-2: Environmental Symbol and Description (cont'd)

Environment	π_E Symbol	Equivalent MIL-HDBK-217E, Notice 1 π_E Symbol	Description
Airborne, Inhabited, Cargo	A_{IC}	A_{IC} A_{IT} A_{IB}	Typical conditions in cargo compartments which can be occupied by an aircrew. Environment extremes of pressure, temperature, shock and vibration are minimal. Examples include long mission aircraft such as the C130, C5, B52, and C141. This category also applies to inhabited areas in lower performance smaller aircraft such as the T38.
Airborne, Inhabited, Fighter	A_{IF}	A_{IF} A_{IA}	Same as A_{IC} but installed on high performance aircraft such as fighters and interceptors. Examples include the F15, F16, F111, F/A 18 and A10 aircraft.
Airborne, Uninhabited, Cargo	A_{UC}	A_{UC} A_{UT} A_{UB}	Environmentally uncontrolled areas which cannot be inhabited by an aircrew during flight. Environmental extremes of pressure, temperature and shock may be severe. Examples include uninhabited areas of long mission aircraft such as the C130, C5, B52 and C141. This category also applies to uninhabited area of lower performance smaller aircraft such as the T38.
Airborne, Uninhabited, Fighter	A_{UF}	A_{UF} A_{UA}	Same as A_{UC} but installed on high performance aircraft such as fighters and interceptors. Examples include the F15, F16, F111 and A10 aircraft.
Airborne, Rotary Winged	A_{RW}	A_{RW}	Equipment installed on helicopters. Applies to both internally and externally mounted equipment such as laser designators, fire control systems, and communications equipment.
Space, Flight	S_F	S_F	Earth orbital. Approaches benign ground conditions. Vehicle neither under powered flight nor in atmospheric reentry; includes satellites and shuttles.

Figure A 4: Environmental Factor Description

Switches

Assume MIL-SPEC snap action as gives lowest failure rate. Deployment switch is single use, single input and output (pull and throw), assumed 1 cycle/hour max. Lamp load assumed at lowest stress. Rotary wing (RW) environment closest to Craft operating conditions.

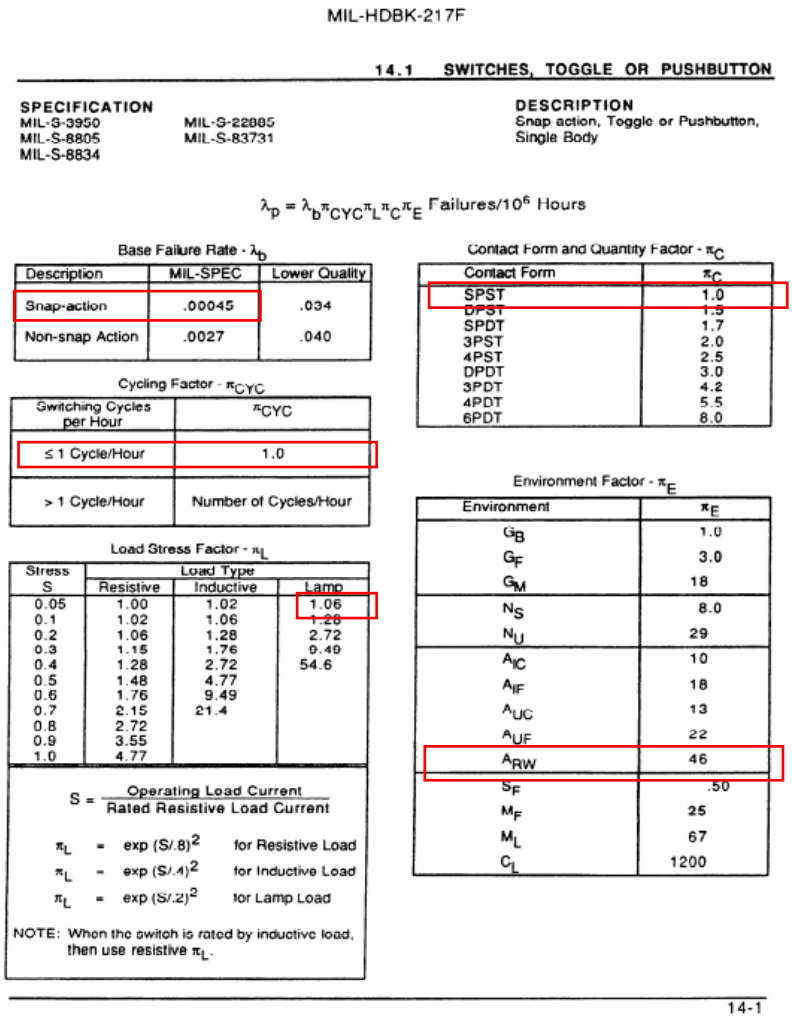

MIL-HDBK-217F

14.1 SWITCHES, TOGGLE OR PUSHBUTTON

SPECIFICATION
MIL-S-3950
MIL-S-8805
MIL-S-8834
MIL-S-22885
MIL-S-83731

DESCRIPTION
Snap action, Toggle or Pushbutton, Single Body

$\lambda_p = \lambda_b \pi_{CYC} \pi_L \pi_C \pi_E$ Failures/10^6 Hours

Base Failure Rate - λ_b

Description	MIL-SPEC	Lower Quality
Snap-action	.00045	.034
Non-snap Action	.0027	.040

Cycling Factor - π_{CYC}

Switching Cycles per Hour	π_{CYC}
≤ 1 Cycle/Hour	1.0
> 1 Cycle/Hour	Number of Cycles/Hour

Load Stress Factor - π_L

Stress S	Load Type Resistive	Inductive	Lamp
0.05	1.00	1.02	1.06
0.1	1.02	1.06	1.28
0.2	1.06	1.28	2.72
0.3	1.15	1.76	9.49
0.4	1.28	2.72	54.6
0.5	1.48	4.77	
0.6	1.76	9.49	
0.7	2.15	21.4	
0.8	2.72		
0.9	3.55		
1.0	4.77		

$$S = \frac{\text{Operating Load Current}}{\text{Rated Resistive Load Current}}$$

$\pi_L = \exp(S/.8)^2$ for Resistive Load
$\pi_L = \exp(S/.4)^2$ for Inductive Load
$\pi_L = \exp(S/.2)^2$ for Lamp Load

NOTE: When the switch is rated by inductive load, then use resistive π_L.

Contact Form and Quantity Factor - π_C

Contact Form	π_C
SPST	1.0
DPST	1.5
SPDT	1.7
3PST	2.0
4PST	2.5
DPDT	3.0
3PDT	4.2
4PDT	5.5
6PDT	8.0

Environment Factor - π_E

Environment	π_E
G_B	1.0
G_F	3.0
G_M	18
N_S	8.0
N_U	29
A_{IC}	10
A_{IF}	18
A_{UC}	13
A_{UF}	22
A_{RW}	46
S_F	.50
M_F	25
M_L	67
C_L	1200

14-1

Figure A 5: Assumed Factors for Calculating Failure Rate of Switches

Connections

Assume solderless wrap and automated crimp type as lowest failure rate.

MIL-HDBK-217F

17.1 CONNECTIONS

DESCRIPTION
Connections Used on All Assemblies Except Those Using Plated Through Holes (PTH)

APPLICATION NOTE: The failure rate model in this section applies to connections used on all assemblies except those using plated through holes. Use the Interconnection Assembly Model in Section 16 to account for connections to a circuit board using plated through hole technology. The failure rate of the structure which supports the connections and parts, e.g., non-plated-through hole boards and terminal straps, is considered to be zero. Solderless wrap connections are characterized by solid wire wrapped under tension around a post, whereas hand soldering with wrapping does not depend on a tension induced connection. The following model is for a single connection.

$$\lambda_p = \lambda_b \pi_Q \pi_E \text{ Failures}/10^6 \text{ Hours}$$

Base Failure Rate - λ_b

Connection Type	λ_b (F/10^6 hrs)
Hand Solder, w/o Wrapping	.0026
Hand Solder, w/Wrapping	.00014
Crimp	.00026
Weld	.00005
Solderless Wrap	.0000035
Clip Termination	.00012
Reflow Solder	.000069

Quality Factor - π_Q

Quality Grade	π_Q	Comments
Crimp Types		
Automated	1.0	Daily pull tests recommended.
Manual		
Upper	1.0	Only MIL-SPEC or equivalent tools and terminals, pull test at beginning and end of each shift, color coded tools and terminations.
Standard	2.0	MIL-SPEC tools, pull test at beginning of each shift.
Lower	20.0	Anything less than standard criteria.
All Types Except Crimp	1.0	

Environment Factor - π_E

Environment	π_E
G_B	1.0
G_F	2.0
G_M	7.0
N_S	4.0
N_U	11
A_{IC}	4.0
A_{IF}	6.0
A_{UC}	6.0
A_{UF}	8.0
A_{RW}	16
S_F	.50
M_F	9.0
M_L	24
C_L	420

17-1

Figure A 6: Assumed Factors for Calculating Failure Rate of Connections

Resistors

Assume hot operating conditions on hot day, 40°C ambient temperature. Assume 0.1 stress factor. Assume "S" quality factor as lowest failure rate.

MIL-HDBK-217F

9.1 RESISTORS, FIXED, COMPOSITION

SPECIFICATION	STYLE	DESCRIPTION
MIL-R-39008	RCR	Resistors, Fixed, Composition (Insulated), Established Reliability
Mil -R-11	RC	Resistors, Fixed, Composition (Insulated)

$$\lambda_p = \lambda_b \pi_R \pi_Q \pi_E \text{ Failures/}10^6 \text{ Hours}$$

Base Failure Rate - λ_b

T_A (°C)	Stress .1	.3	.5	.7	.9
0	.00007	.00010	.00015	.00020	.00028
10	.00011	.00015	.00021	.00030	.00043
20	.00015	.00022	.00031	.00045	.00064
30	.00022	.00031	.00046	.00066	.00096
40	.00031	.00045	.00067	.00098	.0014
50	.00044	.00066	.00098	.0014	.0021
60	.00063	.00095	.0014	.0021	.0032
70	.00090	.0014	.0021	.0032	.0048
80	.0013	.0020	.0031	.0047	
90	.0018	.0029	.0045		
100	.0026	.0041	.0065		
110	.0038	.0060			
120	.0054				

$$\lambda_b = 1.5 \times 10^{-9} \exp\left(12\left(\frac{T+273}{343}\right)\right) \exp\left(\frac{S}{.6}\left(\frac{T+273}{273}\right)\right)$$

T = Ambient Temperature (°C)

S = Ratio of Operating Power to Rated Power

Quality Factor - π_Q

Quality	π_Q
S	.03
R	0.1
P	0.3
M	1.0
MIL-R-11	5.0
Lower	15

Resistance Factor - π_R

Resistance Range (ohms)	π_R
< .1 M	1.0
> .1 M to 1 M	1.1
> 1.0 M to 10 M	1.6
> 10 M	2.5

Environment Factor - π_E

Environment	π_E
G_B	1.0
G_F	3.0
G_M	8.0
N_S	5.0
N_U	13
A_{IC}	4.0
A_{IF}	5.0
A_{UC}	7.0
A_{UF}	11
A_{RW}	19
S_F	.50
M_F	11
M_L	27
C_L	490

9-2

Figure A 7: Assumed Factors for Calculating Failure Rate of Resistors

LEDs

Assume switching application. Junction temperature calculated as per Figure A 1 to Figure A 3. Assume JANXTV quality. “The applicable MIL specification for transistors, and optoelectronic devices is MIL-S-19500. The quality levels (JAN, JANTX, JANTXV) are as defined in MIL-S-19500.” [66]

6.11 OPTOELECTRONICS, DETECTORS, ISOLATORS, EMITTERS

SPECIFICATION
MIL-S-19500

DESCRIPTION
Photodetectors, Opto-isolators, Emitters

$$\lambda_p = \lambda_b \pi_T \pi_Q \pi_E \quad \text{Failures/}10^6 \text{ Hours}$$

Base Failure Rate - λ_b

Optoelectronic Type	λ_b
Photodetectors	
Photo-Transistor	.0055
Photo-Diode	.0040
Opto-Isolators	
Photodiode Output, Single Device	.0025
Phototransistor Output, Single Device	.013
Photodarlington Output, Single Device	.013
Light Sensitive Resistor, Single Device	.0064
Photodiode Output, Dual Device	.0033
Phototransistor Output, Dual Device	.017
Photodarlington Output, Dual Device	.017
Light Sensitive Resistor, Dual Device	.0086
Emitters	
Infrared Light Emitting Diode (IRLD)	.0013
Light Emitting Diode (LED)	.00023

Quality Factor - π_Q

Quality	π_Q
JANTXV	.70
JANTX	1.0
JAN	2.4
Lower	5.5
Plastic	8.0

Environment Factor - π_E

Environment	π_E
G_B	1.0
G_F	2.0
G_M	8.0
N_S	5.0
N_U	12
A_{IC}	4.0
A_{IF}	6.0
A_{UC}	6.0
A_{UF}	8.0
A_{RW}	17
S_F	.50
M_F	9.0
M_L	24
C_L	450

Temperature Factor - π_T

T_J (°C)	π_T	T_J (°C)	π_T
25	1.0	75	3.8
30	1.2	80	4.3
35	1.4	85	4.8
40	1.6	90	5.3
45	1.8	95	5.9
50	2.1	100	6.6
55	2.4	105	7.3
60	2.7	110	8.0
65	3.0	115	8.8
70	3.4		

$$\pi_T = \exp\left(-2790\left(\frac{1}{T_J + 273} - \frac{1}{298}\right)\right)$$

T_J = Junction Temperature (°C)

Figure A 8: Assumed Factors for Calculating Failure Rate of LEDs, Part I

Capacitors

Assume ambient temperature 40°, Ratio of operating to rated voltage = 0.1, assume 1700μF capacitor required, assume "S" quality grade.

MIL-HDBK-217F

10.14 CAPACITORS, FIXED, ELECTROLYTIC, ALUMINUM

SPECIFICATION	STYLE	DESCRIPTION
MIL-C-39018	CUR and CU	Electrolytic, Aluminum Oxide, Est. Rel. and Non-Est. Rel.

$$\lambda_p = \lambda_b \pi_{CV} \pi_Q \pi_E \text{ Failures}/10^6 \text{ Hours}$$

Base Failure Rate - λ_b
(T = 85°C Max Rated)
(MIL-C-39018 Style 71)

T_A (°C)	Stress .1	.3	.5	.7	.9
0	.0095	.011	.019	.035	.064
10	.012	.015	.024	.046	.084
20	.017	.020	.033	.062	.11
30	.023	.028	.046	.087	.16
40	.034	.042	.068	.13	.23
50	.054	.065	.11	.20	.36
60	.089	.11	.18	.33	.60
70	.16	.19	.31	.58	1.1
80	.29	.35	.58	1.1	2.0

$$\lambda_b = .00254\left[\left(\frac{S}{.5}\right)^3 + 1\right]\exp\left(5.09\left(\frac{T+273}{358}\right)^5\right)$$

T = Ambient Temperature (°C)

S = Ratio of Operating to Rated Voltage

Operating voltage is the sum of applied D.C. voltage and peak A.C. voltage.

Base Failure Rate - λ_b
(T = 105°C Max Rated)
(MIL-C-39018 Styles 16 and 17)

T_A (°C)	Stress .1	.3	.5	.7	.9
0	.0070	.0084	.014	.026	.047
10	.0085	.010	.017	.031	.057
20	.011	.013	.021	.040	.072
30	.014	.017	.027	.051	.094
40	.019	.022	.037	.069	.13
50	.026	.031	.052	.097	.18
60	.038	.046	.076	.14	.26
70	.059	.071	.12	.22	.40
80	.095	.11	.19	.35	.64
90	.16	.20	.32	.61	1.1
100	.30	.36	.59	1.1	2.0

$$\lambda_b = .00254\left[\left(\frac{S}{.5}\right)^3 + 1\right]\exp\left(5.09\left(\frac{T+273}{378}\right)^5\right)$$

T = Ambient Temperature (°C)

S = Ratio of Operating to Rated Voltage

Operating voltage is the sum of applied D.C. voltage and peak A.C. voltage.

Base Failure Rate - λ_b
(T = 125°C Max Rated)
(All MIL-C-39018 Styles Except 71, 16 and 17)

T_A (°C)	Stress .1	.3	.5	.7	.9
0	.0055	.0067	.011	.021	.030
10	.0065	.0078	.013	.024	.044
20	.0077	.0093	.015	.029	.052
30	.0094	.011	.019	.035	.064
40	.012	.014	.023	.044	.080
50	.015	.019	.030	.057	.10
60	.021	.025	.041	.077	.14
70	.029	.035	.057	.11	.20
80	.042	.050	.083	.16	.28
90	.064	.077	.13	.24	.43
100	.10	.12	.20	.38	
110	.17	.21	.34	.63	
120	.30	.37	.60	1.1	

$$\lambda_b = .00254\left[\left(\frac{S}{.5}\right)^3 + 1\right]\exp\left(5.09\left(\frac{T+273}{398}\right)^5\right)$$

T = Ambient Temperature (°C)

S = Ratio of Operating to Rated Voltage

Operating voltage is the sum of applied D.C. voltage and peak A.C. voltage.

10-24

Figure A 9: Assumed Factors for Calculating Failure Rate of Capacitor, Part I

10.14 CAPACITORS, FIXED, ELECTROLYTIC, ALUMINUM

Capacitance Factor - π_{CV}

Capacitance, C (μF)	π_{CV}
2.5	.40
55	.70
400	1.0
1700	1.3
5500	1.6
14,000	1.9
32,000	2.2
65,000	2.5
120,000	2.8
$\pi_{CV} = .34C^{0.18}$	

Environment Factor - π_E

Environment	π_E
G_B	1.0
G_F	2.0
G_M	12
N_S	6.0
N_U	17
A_{IC}	10
A_{IF}	12
A_{UC}	28
A_{UF}	35
A_{HW}	27
S_F	.50
M_F	14
M_L	38
C_L	690

Quality Factor - π_Q

Quality	π_Q
S	.030
R	.10
P	.30
M	1.0
Non-Est. Rel.	3.0
Lower	10

Figure A 10: Assumed Factors for Calculating Failure Rate of Capacitors, Part II

Relays (Mechanical)

Assume 40° ambient temperature, assume lamp load at lowest stress, assume single throw and pull, assume → zero cycles per hour average. Assume "R" (best possible) quality, assume MIL-SPEC mercury wetted.

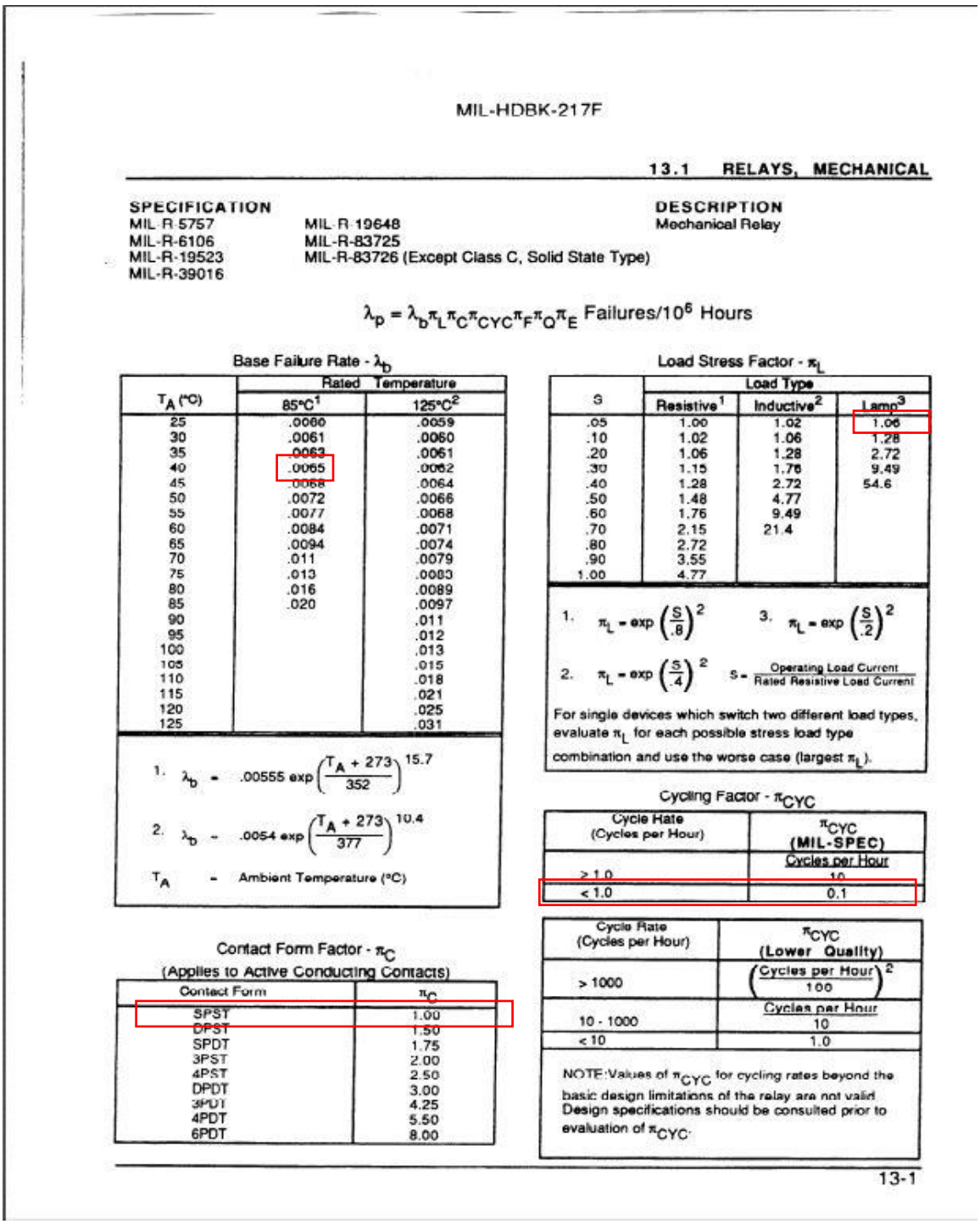

MIL-HDBK-217F

13.1 RELAYS, MECHANICAL

SPECIFICATION
MIL-R-5757, MIL-R-6106, MIL-R-19523, MIL-R-39016, MIL-R-19648, MIL-R-83725, MIL-R-83726 (Except Class C, Solid State Type)

DESCRIPTION
Mechanical Relay

$$\lambda_p = \lambda_b \pi_L \pi_C \pi_{CYC} \pi_F \pi_Q \pi_E \text{ Failures}/10^6 \text{ Hours}$$

Base Failure Rate - λ_b

T_A (°C)	Rated Temperature 85°C[1]	125°C[2]
25	.0060	.0059
30	.0061	.0060
35	.0063	.0061
40	.0065	.0062
45	.0068	.0064
50	.0072	.0066
55	.0077	.0068
60	.0084	.0071
65	.0094	.0074
70	.011	.0079
75	.013	.0083
80	.016	.0089
85	.020	.0097
90		.011
95		.012
100		.013
105		.015
110		.018
115		.021
120		.025
125		.031

1. $\lambda_b = .00555 \exp\left(\frac{T_A + 273}{352}\right)^{15.7}$

2. $\lambda_b = .0054 \exp\left(\frac{T_A + 273}{377}\right)^{10.4}$

T_A = Ambient Temperature (°C)

Load Stress Factor - π_L

S	Load Type Resistive[1]	Inductive[2]	Lamp[3]
.05	1.00	1.02	1.06
.10	1.02	1.06	1.28
.20	1.06	1.28	2.72
.30	1.15	1.76	9.49
.40	1.28	2.72	54.6
.50	1.48	4.77	
.60	1.76	9.49	
.70	2.15	21.4	
.80	2.72		
.90	3.55		
1.00	4.77		

1. $\pi_L = \exp\left(\frac{S}{.8}\right)^2$

2. $\pi_L = \exp\left(\frac{S}{.4}\right)^2$

3. $\pi_L = \exp\left(\frac{S}{.2}\right)^2$

$S = \frac{\text{Operating Load Current}}{\text{Rated Resistive Load Current}}$

For single devices which switch two different load types, evaluate π_L for each possible stress load type combination and use the worse case (largest π_L).

Contact Form Factor - π_C
(Applies to Active Conducting Contacts)

Contact Form	π_C
SPST	1.00
DPST	1.50
SPDT	1.75
3PST	2.00
4PST	2.50
DPDT	3.00
3PDT	4.25
4PDT	5.50
6PDT	8.00

Cycling Factor - π_{CYC}

Cycle Rate (Cycles per Hour)	π_{CYC} (MIL-SPEC)
	Cycles per Hour / 10
≥ 1.0	
< 1.0	0.1

Cycle Rate (Cycles per Hour)	π_{CYC} (Lower Quality)
> 1000	$\left(\frac{\text{Cycles per Hour}}{100}\right)^2$
10 - 1000	Cycles per Hour / 10
< 10	1.0

NOTE: Values of π_{CYC} for cycling rates beyond the basic design limitations of the relay are not valid. Design specifications should be consulted prior to evaluation of π_{CYC}.

13-1

Figure A 11: Assumed Factors for Calculating Failure Rate of Relays, Part I

13.1 RELAYS, MECHANICAL

Quality Factor - π_Q

Quality	π_Q
R	.10
P	.30
X	.45
U	.60
M	1.0
L	1.5
Non-Est. Rel.	3.0

Environment Factor - π_E

Environment	π_E MIL-SPEC	π_E Lower Quality
G_B	1.0	2.0
G_F	2.0	5.0
G_M	15	44
N_S	8.0	24
N_U	27	78
A_{IC}	7.0	15
A_{IF}	9.0	20
A_{UC}	11	28
A_{UF}	12	38
A_{RW}	46	140
S_F	.50	1.0
M_F	25	72
M_L	66	200
C_L	N/A	N/A

Application and Construction Factor - π_F

Contact Rating	Application Type	Construction Type	π_F MIL-SPEC	π_F Lower Quality
Signal Current (Low mv and ma)	Dry Circuit	Armature (Long)	4	8
		Dry Reed	8	18
		Mercury Wetted	1	3
		Magnetic Latching	4	8
		Balanced Armature	7	14
		Solenoid	7	14
0-5 Amp	General Purpose	Armature (Long)	3	6
		Balanced Armature	5	10
		Solenoid	6	12
	Sensitive (0 - 100 mw)	Armature (Long and Short)	5	10
		Mercury Wetted	2	6
		Magnetic Latching	6	12
		Meter Movement	100	100
		Balanced Armature	10	20
	Polarized	Armature (Short)	10	20
		Meter Movement	100	100
	Vibrating Reed	Dry Reed	6	12
		Mercury Wetted	1	3
	High Speed	Armature (Balanced and Short)	25	NA
		Dry Reed	6	NA
	Thermal Time Delay	Bimetal	10	20
	Electronic Time Delay, Non-Thermal		9	12
	Latching, Magnetic	Dry Reed	10	20
		Mercury Wetted	5	10
		Balanced Aramture	5	10
5-20 Amp	High Voltage	Vacuum (Glass)	20	40
		Vacuum (Ceramic)	5	10
	Medium Power	Armature (Long and Short)	3	6
		Mercury Wetted	1	3
		Magnetic Latching	2	6
		Mechanical Latching		
		Balanced Armature	3	6
		Solenoid	2	6
			2	6
25-600 Amp	Contactors (High Current)	Armature (Short)	7	14
		Mechanical Latching	12	24
		Balanced Armature	10	20
		Solenoid	5	10

Figure A 12: Assumed Factors for Calculating Failure Rate of Relays, Part II

References

1. *The Martin Jetpack - Fly the Dream*. [cited 2016; Available from: http://www.martinjetpack.com/.
2. *ASX June Newsletter Final v3.pdf*. 2016; Available from: http://www.martinjetpack.com/dam/jcr:b4014c1c-5a2f-4301-9301-ed651603c11c/ASX%20June%20Newsletter%20Final%20v3.pdf.
3. *OPHAVs*. [cited 2017 27th February]; Available from: http://www.martinjetpack.com/sales/manned-jetpack0.html.
4. *Flying Colours*. 2016; Available from: https://www.youtube.com/watch?v=5TBmOiLgYSQ.
5. NZCAA. *Bilateral Aviation Safety Agreement (BASA)*. 2002 [cited 2016 3 May]; Available from: https://www.caa.govt.nz/publicinfo/BASA-EA.htm.
6. Dominique, B., F. Christian, and T. Pascal, *Electrical Flight Controls, From Airbus A320/330/340 to Future Military Transport Aircraft*, in *Digital Avionics Handbook, Second Edition - 2 Volume Set*. 2000, CRC Press.
7. Dumbleton, H. 2016., *Flight Structures Limited,* Personal Communication
8. Airbus, *Fly-by-wire (1980-1987)*, in *airbus.com*.
9. *UNIT II - AIRCRAFT CONTROL SYSTEMS*. SRM University: http://www.srmuniv.ac.in/. p. 26-35.
10. Peter Potocki de, M. and F.B. Gregg, *Fly-By-Wire Flight Controls*, in *Digital Avionics Handbook, Second Edition - 2 Volume Set*. 2000, CRC Press.
11. Bateman, D. *Some thoughts on reducing the risk of aircraft loss of control*. in *AIAA Guidance, Navigation, and Control Conference*. 2010.
12. Niedermeier, D., *Fly-by-wire augmented manual control - basic design considerations*. 2012. p. 3073-3086.
13. Kim, S.K., *The Bell 525 Relentless, the world's first "next generation" fly-by-wire commercial helicopter.* Annual Forum Proceedings - AHS International, 2014. **1**: p. 245-257.
14. Federal Aviation Administration, *System Design and Analysis - AC 25.1309-1A*, in *Discussion*. 1988.
15. Perry, D. *Bell confirms certification delay for 525*. 2017. **2017**.
16. Perry, D. *FARNBOROUGH: AW609 certification slips, but test flights to resume shortly*. 2016.
17. *The FAA and Industry Guide to Product Certification, Second Edition*. 2004, AIA, GAMA, FAA Aircraft Certification Services.
18. SAE International, *Guidelines for Development of Civil Aircraft and Systems*. 2010.
19. Voros, R.E., *Planning for the Application of ARP4754A for New and Modified Aircraft Projects with New, Simple, and Reused Systems.* SAE International journal of aerospace, 2015. **8**(1): p. 72-80.
20. SAE International, *Guidelines and Methods for Conducting the Safety Assessment Process on Civil Airborne Systems and Equipment*. 1996, Society of Automotive Engineers, Inc.: U.S.A.
21. *Advisory Circular 23.1309-1E - System Safety Analysis and Assessment for Part 23 Airplanes*, U.S. Department of Transportation, Editor. 2011.
22. *14 CFR 23.1309 - EQUIPMENT, SYSTEMS, AND INSTALLATIONS*. 2002, U.S. Government Publishing Office: USA.
23. Ginn, J.M., I.G. Clark, and R.D. Braun. *Parachute Dynamic Stability and the Effects of Apparent Inertia*. in *AIAA Atmospheric Flight Mechanics Conference*. 2014.
24. Wolf, D., *Dynamic stability of a nonrigid parachute and payload system.* Journal of Aircraft, 1971. **8**(8): p. 603-609.
25. Doherr, K.-F. and H. Schilling, *Nine-degree-of-freedom simulation of rotating parachute systems.* Journal of Aircraft, 1992. **29**(5): p. 774-781.
26. Gao, X., Q. Zhang, and Q. Tang, *Parachute dynamics and perturbation analysis of precision airdrop system.* Chinese Journal of Aeronautics, 2016. **29**(3): p. 596-607.

27. Guglieri, G., *Parachute-payload system flight dynamics and trajectory simulation.* International Journal of Aerospace Engineering, 2012. **2012**.
28. Tory, C. and R. Ayres, *Computer model of a fully-deployed parachute.* Journal of Aircraft, 1977. **14**(7): p. 675-679.
29. Dobrokhodov, V.N., O.A. Yakimenko, and C.J. Junge, *Six-degree-of-freedom model of a controlled circular parachute.* Journal of Aircraft, 2003. **40**(3): p. 482-493.
30. Tanner, C.L., *Optimization of Earth Flight Test Trajectories to Qualify Parachutes for Use on Mars.*
31. Stein, K.R., R.J. Benney, and E.C. Steeves, *A computational model that couples aerodynamic and structural dynamic behavior of parachutes during the opening process*. 1993, DTIC Document.
32. Accorsi, M., et al., *Structural modeling of parachute dynamics.* AIAA journal, 2000. **38**(1): p. 139-146.
33. Benney, R., et al. *Current 3-D structural dynamic finite element modeling capabilities*. in *14th Aerodynamic Decelerator Systems Technology Conference*. 1997.
34. Tutt, B., et al. *Finite mass simulation techniques in LS-DYNA*. in *21st AIAA Aerodynamic Decelerator Systems Technology Conference and Seminar*. 2011.
35. PURVIS, J. *Numerical prediction of deployment, initial fill, and inflation of parachute canopies*. in *8th Aerodynamic Decelerator and Balloon Technology Conference*. 1984.
36. *Technical Specifications*. 2016; Available from: http://www.martinjetpack.com/dam/jcr:36c3e858-d621-42f4-91a3-2be543161beb/MJP_TechSpec_Series1%20Estimated_2016%20V2.pdf.
37. Delany, N.K. and N.E. Sorensen, *Low-speed drag of cylinders of various shapes.* 1953.
38. *Air Properties Definitions*. 2015 [cited 2017 13th February]; Available from: https://www.grc.nasa.gov/www/k-12/airplane/airprop.html.
39. Parazero. *Parazero | Drone Safety Solutions*. 2016 [cited 2016 26th July]; Available from: http://www.parazero.com/.
40. K. Vasantha Kumar, W.T.N., *Issues on Human Acceleration Tolerance After Long-Duration Space Flights.* NASA Technical Memorandum 104753, 1992: p. 36.
41. Flight Safety Foundation Editorial Staff, *Simulator-based Study of Emergencies Yields Insights into Pilots' Reaction Times.* Helicopter Safety, 1999. **25**(2).
42. Cockrell, D.J. and A.D. Young, *The Aerodynamcis of Parachutes*. 1987, DTIC Document.
43. Hall, N. *Shape Effects on Drag*. 2015 [cited 2016; Available from: https://www.grc.nasa.gov/www/k-12/airplane/shaped.html.
44. Morse, K.M., S; Riley, M; . *Tensegrity payload protection*. 2014 21 July 2014 [cited 2016; Available from: http://www.mindworks.shoutwiki.com/wiki/Tensegrity_payload_protection.
45. *ParaZero Drone Pyrotechnic Parachute Demo*. 2016; Available from: https://www.youtube.com/watch?v=2BP6sBYqT5w.
46. Poole, L.R., *Effect of suspension-line viscous damping on parachute opening load amplification*, in *Journal of Spacecraft and Rockets*. 1973. p. 92-93.
47. Safarik, L. *10 kg load recovery Parachute SKYROB.COM*. 2016; Available from: https://www.youtube.com/watch?v=5iU83ofCK6k.
48. Ferrier, I. *Accidental deployment SIV 2015*. 2015; Available from: https://www.youtube.com/watch?v=bSOMMeOVcgk.
49. UK Airsports. *GIN GLIDERS Yeti 40 reserve parachute load test*. 2015; Available from: https://www.youtube.com/watch?v=T85PooMjMTc.
50. McFaull, S. and M. Lamontagne. *The angular damping coefficient of the in vivo human knee joint*. in *XIV ISB Congress. Paris, France*. 1993.

51. Currie, I., *Applying the Applying the '3 Millisecond Clip Acceleration' Criterion '3 Millisecond Clip Acceleration' Criterion to Playground Safety*. 2010, Alert Property Inspections Winnipeg, Manitoba
52. Jean Potvin, G.P. *Parachute Opening Shock Basics*. in *Parachute Industry Association Symposium*. 2001. San Diego, CA: Parks College Parachute Research Group.
53. Ewing, E.G. and J.R. Vickers, *Ringsail parachute design*. 1972, DTIC Document.
54. Anderson, N.F., C.A. Grainger, and J.L. Stith, *Characteristics of strong updrafts in precipitation systems over the central tropical Pacific Ocean and in the Amazon.* Journal of Applied Meteorology, 2005. **44**(5): p. 731-738.
55. Akin, J.E., *Impact Load Factors for Static Analysis*. 2015, Rice University.
56. Henn, H.-W., *Crash tests and the head injury criterion.* Teaching mathematics and its applications, 1998. **17**(4): p. 162-170.
57. Eiband, A.M., *Human tolerance to rapidly applied accelerations: a summary of the literature.* 1959.
58. Rainford, D.J. and D.P. Gradwell, *Ernsting's aviation medicine*. 2006: Hodder Education.
59. Shigley, J.E., Charles R. Mischke, and Richard G. Budynas. *Mechanical engineering design*. 2011. McGraw-Hill.
60. Oberg, E., et al., *Machinery's handbook*. Vol. 200. 2004: Industrial Press New York.
61. Young, L., et al., *When physics meets biology: low and high-velocity penetration, blunt impact, and blast injuries to the brain.* Front Neurol, 2015. **6**: p. 89.
62. Shanahan, D.F., *Human tolerance and crash survivability.* Pathological Aspects and Associate Biodynamics in Aircraft Accident Investigation, 2004.
63. Yoganandan, N., et al., *Biomechanics of human thoracolumbar spinal column trauma from vertical impact loading.* Annals of advances in automotive medicine, 2013. **57**: p. 155.
64. Procter, G. *Airbag suits? You ain't seen NOTHING yet: 'Safety Sphere'*. 2011.
65. CYPRES, *Technical Data Information Sheet*. 2016, Airtec GmbH & Co.KG Safety Systems.
66. Military Handbook, *MIL-HDBK-217 F.* Dept. of Defense (USA), 1991. **2**.
67. Veltmann, R. 2016. *Airtec GmbH & Co. KG Safety Systems*, Personal Communication
68. *logdecrement*. 2001; Available from: https://www.andrew.cmu.edu/course/24-352/Handouts/logdecrement.pdf.